Copyright

by

B. Logan Spaller

2023

The Dissertation Committee for B. Logan Spaller Certifies that this is the approved version of the following Dissertation:

Pathways to the Proteasome in Yeast

Committee:

Andreas Matouschek, Supervisor

Jon Huibregtse

Tanya Paull

Lulu Cambronne

Jeffrey Barrick

Pathways to the Proteasome in Yeast

by

B. Logan Spaller

Dissertation

Presented to the Faculty of the Graduate School of

The University of Texas at Austin

in Partial Fulfillment

of the Requirements

for the Degree of

Doctor of Philosophy

The University of Texas at Austin

December 2023

Dedication

I dedicate this dissertation to my Grandmother, Nancy Spaller, a woman who has had a profound and lasting impact on my life. Your unwavering belief in me, your unwavering support, and your unwavering love have been the guiding forces that have propelled me forward throughout my journey.

From a young age, you instilled in me a sense of curiosity and a thirst for knowledge. You encouraged me to explore my interests, no matter how unconventional or challenging they might seem. You taught me that there is no limit to what I can achieve if I set my mind to it.

Your example of perseverance and determination has been a constant source of inspiration. You showed me how to overcome obstacles with grace and resilience, and you never gave up on me, even when I doubted myself. Your unwavering support has been the bedrock of my success.

Thank you, Grandmother, for being my cheerleader, my confidante, and my role model. You have taught me the importance of kindness, compassion, and integrity, and you have shown me the true meaning of unconditional love. I miss you and I am forever grateful for the sacrifices you made for me, and I dedicate this dissertation to you, the woman who has helped shape me into who I am today.

Acknowledgements

I would like to express my deepest gratitude to my advisor, Andreas Matouschek, for his unwavering guidance and support throughout my graduate studies. His patience, encouragement, and insightful discussions have been instrumental in shaping me into a thoughtful and creative scientist. I am particularly grateful for his compassion and understanding, especially during challenging times. Andreas has not only taught me the intricacies of scientific research but has also instilled in me the values of integrity, perseverance, and a genuine love for science. I am truly fortunate to have had him as my mentor and role model.

I would also like to thank my dissertation committee members, Tanya Paull, Jeffrey Barrick, Jon Huibregtse, and Lulu Cambronne, for their invaluable advice and support throughout my research journey. Their expertise and insightful feedback have been instrumental in refining my research questions, strengthening my experimental design, and improving my scientific writing. I am deeply grateful for their time and dedication to my success.

My labmates, both past and present, have played a significant role in my graduate experience. Amit Gautam, John Cooper, and Caroline Davis have been wonderful colleagues and friends, providing me with countless hours of stimulating conversations, brainstorming sessions, and technical assistance. Their camaraderie and support have made my research journey all the more enjoyable and rewarding.

I am particularly indebted to Christopher Yellman for his mentorship and guidance in yeast genetics. His expertise and patience have been invaluable in my

development as a researcher. I am also grateful for his unwavering support and encouragement, which have been instrumental in helping me navigate the challenges of graduate school.

Finally, I would like to express my heartfelt gratitude to my family and friends for their unwavering love and support throughout my academic endeavors. My mother, for her unwavering belief in me, my father, for his unwavering enthusiasm and encouragement, and Omar, for being my rock and my unwavering support system. Their love and encouragement have been the driving force behind my success.

The completion of this dissertation would not have been possible without the contributions of these remarkable individuals. I am truly grateful for their support, guidance, and friendship.

Abstract

Pathways to the Proteasome in Yeast

B. Logan Spaller, PhD

The University of Texas at Austin, 2023

Supervisor: Andreas Matouschek

The proteasome is a highly selective and precisely regulated protease that degrades proteins essential for cellular homeostasis. This dissertation explores the molecular mechanisms by which the proteasome selects its substrates from a diverse protein pool First, the interplay between different pathways to the proteasome was investigated, revealing a hierarchy in degradation whereby substrates delivered by ubiquitin-like (UBL) domains may have priority access to the proteasome. Next, the role of spacing between the ubiquitin tag and disordered initiation region in degradation was investigated. The findings reveal another layer to substrate selection by the proteasome, and provide important considerations when determining whether a given protein may be degraded by the proteasome. Overall, this research provides new insights into how the proteasome selects its substrates in a diverse protein pool.

Table of Contents

List of Tables

List of Figures

Chapter 1: Introduction

Proteins, the cellular machines that power life, are essential for every aspect of cell function. DNA encodes proteins, but damaged DNA can lead to imperfect protein expression, which can alter protein activity. To maintain genome integrity, cells have evolved tight regulatory pathways, such as DNA repair pathways. Cellular health also depends on the tight regulation of protein levels and quality. Transcriptional and translational control pathways tightly regulate protein expression, and quality control checks ensure that proteins are expressed correctly. After translation, newly synthesized polypeptides must fold correctly to be functional. Chaperones often catalyze protein folding to ensure that proteins form in their active state, and facilitate their destruction if incapable of folding correctly.

At the other end, protein abundance is also controlled by protein degradation, and degradation is also essential to ensure destruction of misfolded, damaged, or unnecessary proteins. This process is tightly regulated by cellular degradation machinery, including the ubiquitin proteasome system and lysosomal degradation.

THE UBIQUITIN PROTEASOME SYSTEM

Protein degradation in cells is vital to maintain homeostasis. There are two primary protein degradation systems in eukaryotes: the ubiquitin proteasome system (UPS), and autophagic degradation, with most of the regulated protein degradation being carried out by the UPS [1]. At the center of the ubiquitin proteasome system is the 26S proteasome, a large macromolecular machine tasked with regulated intracellular proteolysis. The UPS not only is involved in degrading key proteins in cell cycle control

[2–4], but also degrades misfolded and damaged proteins as a part of maintaining protein quality control [4–6].

Proteins are typically targeted for degradation to the proteasome by the covalent attachment of ubiquitin chains to lysine residues in the target protein by the sequential action of E1, E2, and E3 enzymes [1]. Ubiquitin chains are formed by the covalent attachment of the C-terminus of one ubiquitin to any of the seven lysine residues, or the N-terminus of another ubiquitin [7]. Once a protein has tagged with a ubiquitin chain, it can then bind the proteasome at one of its ubiquitin receptors. Once bound to the proteasome, a substrate is then engaged at a disordered initiation region, where it is pulled into the proteolytic core of the proteasome and degraded (Figure 1.3). The length and composition of amino acids within this disordered region also determines degradation efficiency [8,9].

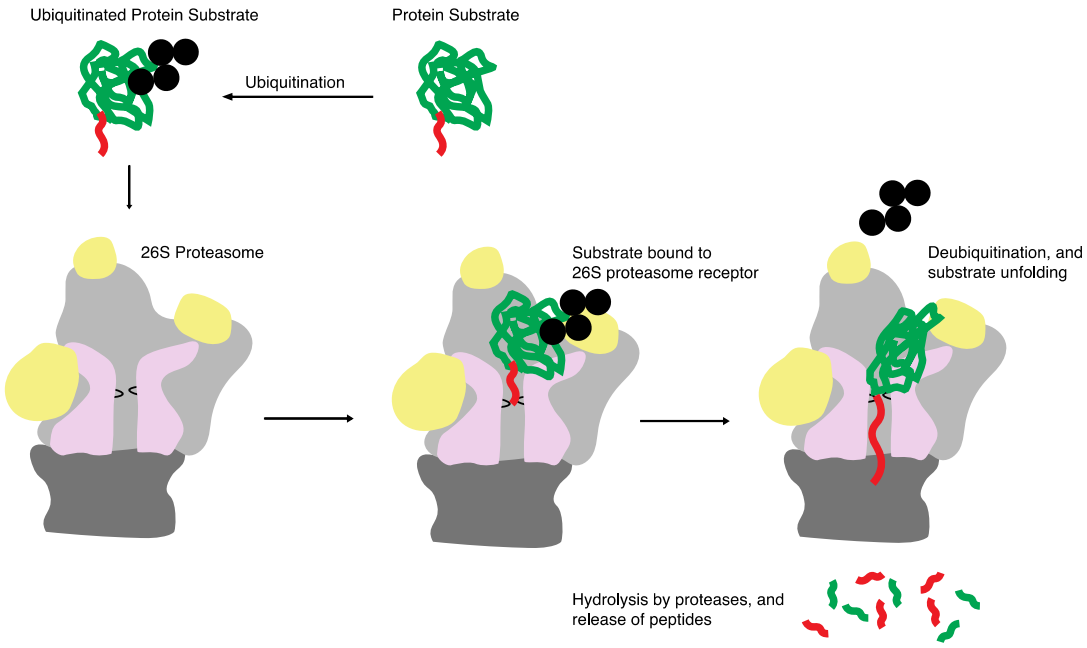

Figure 1.3: Substrate processing by the 26S proteasome.

The past decade has seen a tremendous leap in our understanding of the UPS, both in mechanism and its importance to physiology and disease. Detailed biochemical assays have been performed, demonstrating the kinetic steps in substrate processing [10], while cryo-electron tomography studies have shown how the proteasome interacts with protein aggregates in neurons, demonstrating a connection between the UPS and disease pathology [11–13]. There is still much to be learned about the intricate mechanisms of UPS-mediated protein degradation. The field lacks an understanding of how different substrates are prioritized for degradation. For example, it's unclear how substrates are ordered if they bind different ubiquitin receptors, or how the initiation region composition may impact the ordering of substrate degradation.

Structure and function of the 26S and 30S proteasomes

The proteasome is a 2.5 MDa machine consisting of 33 or more unique subunits. There are two primary complexes: the 20S core particle (CP) and the 19S regulatory particle (RP). The 26S proteasome consists of the 20S CP and the 19S RP (Figure 1.2). There are also 30S proteasomes with C2-symmetry, positioning 19S RPs at both ends of the 20S CP [4]. The mechanism for degradation happens in three steps: recognition, unfolding, and proteolysis.

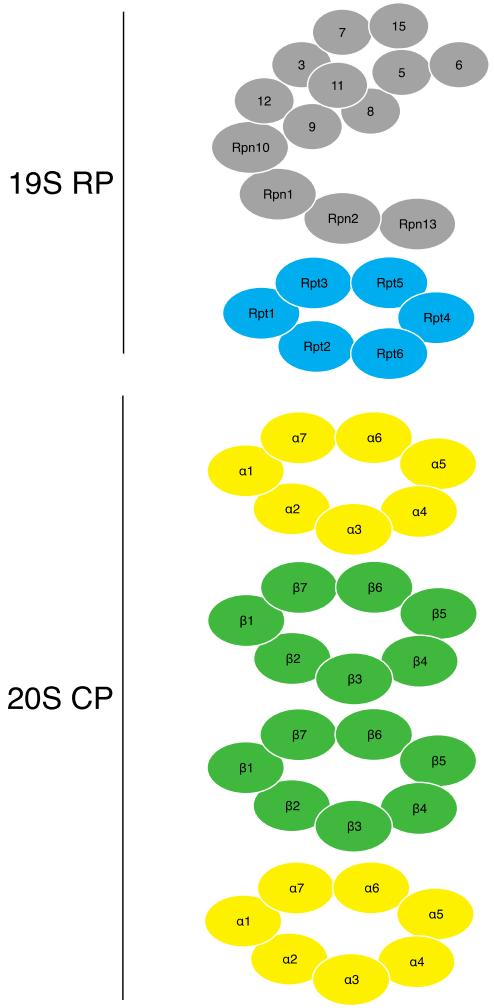

Figure 1.2: Subunits of the 26S proteasome. Adapted from [14].

Recognition happens at the 19S RP. The 19S RP consists of 19 subunits, including six proteasome AAA-ATPases (Rpt1-6) and 13 non-ATPase subunits (**R**egulatory **P**article **N**on-ATPases—RPNs). Ubiquitin chains are recognized by one of three RPN subunits, Rpn10, Rpn13, and Rpn1. Rpn10 is close to the entrance channel, and ubiquitin binds through Rpn10's C-terminal ubiquitin-interacting motif (UIM), which

is connected by a linker to an N-terminal von Willebrand factor type A (VWA) domain. Rpn1 is positioned opposite the entrance channel from Rpn10, and binds ubiquitin by its T1 site, which is in one of the toroidal domains of Rpn1. Finally, Rpn13 is at the top of the RP, and binds ubiquitin at its Pleckstrin-like receptor for ubiquitin (PRU) domain [15].

Arranged in a hexameric ring, Rpt1-6 are positioned just above the α-ring of the 20S CP, and covering the entrance channel for substrates. Unfolding initiates when a disordered initiation region in the substrate is engaged by the conserved pore-1 loops within the ATPases [16]. Substrates are mechanically unfolded and translocated into the CP by repeated cycles of ATP hydrolysis by Rpt1-6 effectively pulling the polypeptide chain into the proteolytic channel. During translocation, Rpn11, which is adjacent to the entrance of the translocation channel, binds to ubiquitin on the substrate and triggers *en bloc* removal of the ubiquitin chain [16–19].

The 20S CP is where the proteolytic activity of the proteasome happens. The 20S CP is shaped like a barrel with four stacked rings consisting of two inner heteroheptameric rings of β-subunits, flanked by an outer heteroheptameric ring of α-subunits on each side [20]. The six proteolytic sites are sequestered in the CP and can cleave almost any protein into small peptides ranging from 3-12 residues in length [15].

Ubiquitination: a complex and diverse proteasome targeting signal

Ubiquitination is a versatile signaling mechanism that regulates many cellular processes, including DNA repair, protein trafficking, kinase activation and proteasome-mediated degradation. Ubiquitin can modify proteins in one of two ways: either as a single unit, or as a chain of multiple ubiquitins linked together. These different ubiquitin modifications have different shapes, and they lead to different effects on the proteins they

are attached to. This is the ubiquitin code. Understanding the ubiquitin code is essential to understanding how ubiquitin fits into diverse cellular processes, including UPS regulation. Ubiquitin is a small, 76-amino acid, globular protein, that can be covalently attached at lysine residues in target proteins.

Proteins can be ubiquitinated by the combined action of ubiquitin-activating enzymes (E1), ubiquitin-transferring enzymes (E2), and ubiquitin ligases (E3). The E1 enzyme activates a ubiquitin in the presence of ATP by covalently ligating the C-terminal carboxyl group to the active cysteine residue in the E1 enzyme. Next, the activated ubiquitin is transferred to the active cysteine residue in an E2 enzyme. The activated ubiquitin is then transferred to a target protein in the presence of an E3 ligase that interacts with the target protein [21–23]. There are two E1 enzymes, dozens of E2 enzymes, and hundred of E3 ligases encoded in the yeast genome to help with conjugating reactions.

E3 ligases are generally classified into three types: HECT (**h**omologous to **E**6-associated protein **C t**erminus) E3s, RING finger E3s, and U box E3s. Generally, HECT E3s function with a cysteine residue in the HECT domain that accepts a ubiquitin from an E2 enzyme before transfer to a substrate. RING and U box E3s, however, do not form intermediates with ubiquitin, but act as a scaffold to position a substrate near an E2 enzyme to facilitate a direct transfer of ubiquitin to the substrate [23–25]. In addition to these enzymes, additional E4 ubiquitin elongating enzymes may lengthen ubiquitin chains further [23].

Substrates are ubiquitinated in a variety of forms. The simplest is monoubiquitination, where a single ubiquitin is covalently attached at a lysine residue on the substrate (Figure 1.1A). Some substrates can also be monoubiquitinated at multiple lysines, leading to multimonoubiquitination (Figure 1.1B). Finally, ubiquitin chains may

be attached to some substrates, and they come in many forms. Ubiquitin contains 7 lysine residues. Ubiquitin chains are formed by the covalent attachment of one ubiquitin at its c-terminus to any of the 7 lysine residues, or the N-terminus of another ubiquitin, leading to eight structurally diverse polyubiquitin chain types (M1-, K6-, K11-, K27-, K29-, K33-, K48-, and K63-linked chains). Polyubiquitin chains can form, and are homogenous if the same residue is used for attachment of the next ubiquitin in the chain (Figure 1.1C). Heterogeneous ubiquitin chains can form when the topology is mixed with different linkage types at different regions of the chain (Figure 1.1D). Finally, branched ubiquitin chains form when a single ubiquitin has multiple ubiquitin attachments (Figure 1.1E) [7].

Ubiquitination plays a critical role in proteasome-targeting. K48-linked chains are the most well understood ubiquitin chain type that targets protein substrates for degradation [26]. Recent studies have demonstrated, though, that K63-, K11-, and other chain-types may be able to target proteins substrates for degradation as well [27]. Branched chains may also play a role in proteasome-mediated degradation targeting. Branched K48/K63 chains increase in abundance in response to proteasome inhibition, suggesting these are also potent degradation signals [28].

Ubiquitination also plays a critical role in processes other than proteasome targeting. For example, the monoubiquitination of K164 in proliferating cell nuclear antigen (PCNA) recruits TLS pols to stalled replication forks, leading to a switch between TLS pols and classical replication pols [29,30]. Another example is the multimonoubiquitination of the epidermal growth factor receptor (EGFR), which acts as a signal for endocytosis and subsequent degradation [31]. Heterogeneous ubiquitin chains also occur in NF-kB signaling, where ubiquitination of NF-kB leads to its activation [7,32–35].

Because ubiquitination can lead to either degradation or other cellular processes, the proteasome must have another layer of substrate selection besides the ubiquitin tag. This additional layer of selection is likely based on the composition and presence of a disordered region, which inserts into the entry channel of the proteasome to initiate degradation.

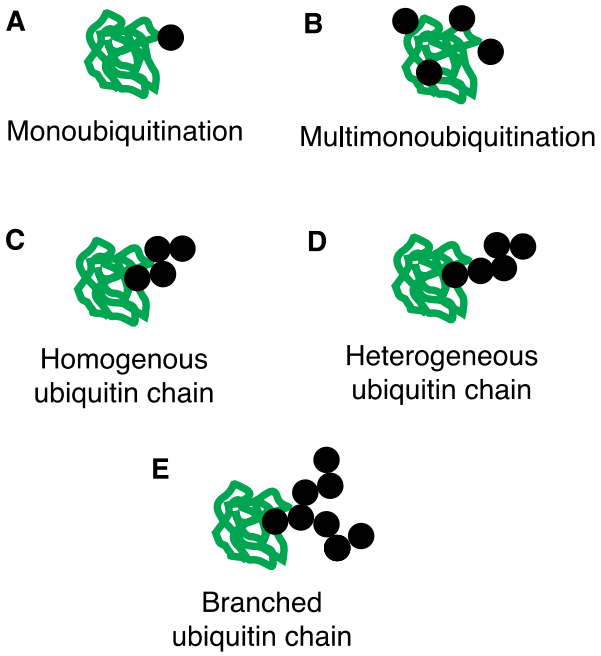

Figure 1.1: Types of ubiquitination

(A) Monoubiquitination at a single lysine residue in the substrate.
(B) Multimonoubiquitination at multiple lysine residues in the substrate.
(C) A homogenous ubiquitin chain with the same linkage type, such as K48-linked ubiquitin chain.
(D) A heterogeneous ubiquitin chain with multiple chain linkage types, such as K48- and K63- linked ubiquitin chain.
(E) A branched ubiquitin chain.

Ubiquitin moieties are removed by deubiquitylating enzymes (DUBs). There are two primary classes of DUBs: metalloproteases and cysteine proteases. Cysteine

proteases, with over 80 known ones in humans, use an active cysteine residue, combined with a histidine, and asparagine or aspartate to catalyze hydrolysis of a ubiquitin linkage [36]. There are six families of cysteine protease DUBs, including: Ubiquitin C-terminal hydrolase (UCH), Ubiquitin-specific protease (USP), Ovarian tumor (OTU), Machado–Josephin domain (MJD), K48 polyubiquitin-specific MINDY domain families, Zinc finger with UFM1-specific peptidase domain [37].

The metalloprotease class of DUBs are zinc dependent enzymes, and six have been identified in humans [36]. A well characterized example is Rpn11, which associated with the proteasome and is important for proteasome-mediated degradation of substrates. Just before degradation, Rpn11 is responsible for cleaving the linkage between the proximal ubiquitin in the chain, and the substrate, which removes the ubiquitin chain *en bloc*. Rpn11 activity is tightly regulated by proteasome interactions, and the ATPase dependent unfolding activity by the AAA ATPases of the 19S RP [2,36].

Specificity in the initiation region for proteasomal degradation

Even though ubiquitination leads to substrates being targeted to the proteasome, there is not always efficient degradation. That is because degradation initiates by binding of the pore-1 loops to a disordered region in the target protein. The protein is then pulled into the proteolytic core of the proteasome and is unfolded and degraded. Early studies of proteasomal unfolding and proteolysis used artificial substrates made from tightly folded domains that can be stabilized against unfolding by ligands [15,38–41]. The proteasome could only degrade these proteins if they also had an unstructured region attached to their C-termini. Stabilization of the core domain by ligands also inhibited degradation because the proteasome was unable to unfold them [42].

Furthermore, there is proteome-wide evidence that proteins with disordered regions may be degraded more by the proteasome. Systematic analysis of sequence, structure, expression, and evolutionary relationships of proteins, combined with their half-lives, has shown that proteins with longer disordered regions, either internally or at the N- or C-termini, have shorter half-lives than proteins lacking these regions [43]. Requirements for length, positioning, and amino acid composition of intrinsically disordered regions have been extensively studied.

Studies have shown that the proteasome has specific sequence and length preferences for the initiation region. Changes in initiation region sequence composition and length can tune degradation of model substrates to the same extent as modifying ubiquitination signals, suggesting its equal importance to the ubiquitin code in proteasome-mediated degradation. These same studies found a negative correlation between sequence complexity (how biased the amino acid composition is) and protein stability. This suggests that initiation regions with biased amino acid compositions are less efficiently degraded by the proteasome. The study also found that hydrophobicity of the initiation region was negatively correlated with stability, while polarity and acidity were positively correlated with stability. This suggests that the proteasome is more efficient at initiating degradation at less hydrophilic and more hydrophobic regions. Sequence dynamics, or how flexible the initiation region is, also plays a role in proteasome initiation. Stiffer initiation regions appear to be better recognized and degraded by the proteasome [9].

Provided that all initiation regions are not created equal, a second layer of proteasome-mediated degradation specificity must exist. Since ubiquitination plays a critical role in other cellular processes, this second layer may help discriminate between

protein substrates that need to be degraded from ones that are ubiquitinated for other purposes.

UPS role in health and disease

All proteins in the cell are continually being recycled to synthesize new proteins, by regulated degradation into amino acids. Proteins of different functions and locations are degraded with varying rates. Regulatory proteins may be degraded in minutes, while long-lived structural/cytoskeletal proteins, like actin, may have a half-life up to days or weeks [44]. The rate of degradation and synthesis of any protein must be strictly balanced to ensure cellular health of a given organism.

The proteasome maintains cellular proteostasis. Is inability to maintain cellular proteostasis may lead to disease phenotypes. For example, the protease sites of the proteasome are capable of digesting almost any polypeptide sequence. However, some proteins are not capable of being degraded by the proteasome, and manifest into neurodegenerative disorders. For example, polyglutamine repeat proteins, which seem to manifest importance in Huntington's disease [45], are poorly degraded. This leads to the formation of toxic intracellular aggregates, leading to a disease phenotype. Another neurodegenerative disorder, Alzheimer's disease, is characterized by the buildup of amyloid-beta plaques and neurofibrillary tangles (NFTs). NFTs are made up of hyperphosphorylated tau protein. The proteasome is essential for the breakdown of amyloid-beta and tau. Recent studies have shown that both protein oxidation and excessive phosphorylation can interfere with the proteasome's ability to break down amyloid-beta and tau in Alzheimer's disease [46].

The proteasome also helps regulate the cell cycle by degrading key regulatory proteins. Cancer cells, such as multiple myeloma, are particularly dependent on NF-kB to

produce growth factors like IL-6. Malignant plasma cells also, for example, produce large amounts of abnormal Ig that get degraded by the proteasome in ER-associated degradation by the proteasome (ERAD). Both multiple myeloma and malignant plasma cells require the functional degradation of proteins by the proteasome for cell proliferation and tumor growth. As a result, proteasome inhibitors have been targets for cancer therapy. Bortezomib, one such proteasome inhibitor, has been successful as a treatment in combination with other chemotherapeutic agents [44]. It has been approved by the US Food and Drug Administration as a treatment against multiple myeloma, and clinical trials are under way for the treatment of other cancers.

In addition to its critical role in cell cycle regulation, and proteostasis, the proteasome is also critical to the immune system [47,48]. Immune cells, such as those found in the spleen and thymus, have developed several adaptive mechanisms to improve antigen presentation. The proteasome is responsible for generating antigenic peptides that can be presented to the immune system. Intracellular proteins resulting from bacterial and viral infections can be degraded by the UPS and trafficked to the ER, where they bind MHC class I molecules and are delivered to the cell's surface and presented to cytotoxic CD8+ lymphocytes. When these peptides are identified as non-native proteins, the presenting cells are promptly killed by T cells [44]. To improve this process, organisms have developed different types of proteasomes, such as immunoproteasomes, that can more effectively generate peptides to bind to MHC class I molecules. Immunoproteasomes differ from standard proteasomes in that they contain three different peptidase subunits. These subunits have different specificities, which allows them to cleave proteins in different ways. This results in more peptides that have the correct features for binding to MHC class I molecules [49].

Tissue mass and protein stores in the body are achieved by a tight balance between synthesis and degradation of cellular proteins. Uremic patients, for example, often experience weight loss due to a loss of protein stores. Patients with uremia generally show the same level of protein synthesis, but degradation is often upregulated [50,51]. The balance between protein degradation and synthesis is fragile, and any upregulation of degradation often leads to huge depletions of protein levels and, ultimately disease phenotype.

Ultimately, the mis regulation of the ubiquitin proteasome system has lead to disease-causing phenotypes in many ways. The proteasome is important because of its broad, yet specific, roles in regulating the cell cycle by degrading cyclins, maintaining proteostasis by degrading misfolded and damaged proteins, and mediating the immune response by degrading foreign proteins from bacteria and viruses. The development of drug interventions, such as proteasome inhibitors, or targeted protein degradation technologies may prove useful in facilitating the treatment of related diseases.

Targeted protein degradation to treat disease

Traditionally, diseases are treated by a drug binding strategy, where inhibitors or antagonists bind to disease-related proteins. The clinical outcome of these interventions, therefore, depends on binding efficiency of the drugs to the target-proteins [52]. Some classes of proteins, like transcription factors, scaffolding proteins, or non-enzymatic proteins that may participate in disease phenotypes remain undruggable. An effective approach to blocking the activity of such proteins is to artificially target them to the proteasome for degradation.

One method of achieving targeted protein degradation is with PROteolysis TArgeting Chimeras (PROTACs) [53]. PROTACs function by binding a target protein

and an E3 ligase to form a ternary complex, followed by subsequent ubiquitination and degradation [54]. This technique has been used to treated immunological disorders, cancer, viral infections, and neurological disorders [52,55]. For example, oncoproteins that are required for tumor growth in cancers are of particular interest for PROTAC targets. With effectively designed PROTACs, oncoproteins may be artificially targeted for degradation, leading to inhibition of cancer cell division. BCR-ABL in chronic myeloid leukaemia and the oestrogen receptor in breast cancer are two proteins that can be targeted for degradation by PROTACs and resolve cancer formation. There exist three versions of BCR-ABL degraders that are used in the clinic to manage myeloid leukaemia. The PROTAC ARV-471 was developed by Arvinas to induce degradation of oestrogen receptor in breast cancer patients. This drug is currently in clinical trials [52].

While PROTACs and targeted protein degradation are a promising path forward, there are still limitations. Many PROTAC designs fail, either because they do not effectively induce ubiquitination of the target protein, or the target protein does not get degraded after ubiquitination. Clearly, we lack some understanding of regulated protein degradation by the proteasome. Understanding in greater detail how the proteasome selects its substrates will inform future targeted protein degradation drug strategies in the future.

PATHWAYS TO THE PROTEASOME

There are many types of ubiquitin modifications that can successfully target a substrate for degradation by the proteasome. The three ubiquitin receptors, Rpn1, Rpn10, and Rpn13 recognizes these diverse signals, and serves as a versatile recognition platform. *In vitro* biochemical assays of model substrates revealed that K-48 linked single ubiquitin chains bind and are targeted almost exclusively by Rpn10, while K-63 and other

chain types can interact cooperatively with Rpn1 and Rpn10. Substrates containing multiple short ubiquitin chains can be targeted for degradation by any of the three receptors. Therefore, it's clear that the three receptors in the 19S RP act as a versatile recognition platform for a diverse range of ubiquitin chains [27].

Substrates can also be targeted for degradation by UBL-UBA proteins, which are hypothesized to act as shuttling factors that deliver ubiquitinated substrates to the proteasome. They do this by binding ubiquitin with their ubiquitin-associating (UBA) domain and to one of the proteasome receptors with their ubiquitin-like (UBL) domain. In yeast, there are three UBL-UBA proteins: Rad23, Dsk2, and Ddi1 [26,56–60].

Finally, some substrates are targeted to the proteasome without ubiquitin tags, and are degraded in a ubiquitin independent manner.

Different ubiquitin tags target to the proteasome

Substrates can be targeted to the proteasome by the covalent attachment of ubiquitin chains. The canonical degradation signal is a K48-linked ubiquitin chain of at least four ubiquitin molecules [61]. Recent advances in the field, however, have demonstrated that other ubiquitin chain types also target substrates for proteasome-mediated degradation. For example, K11 chains have been shown to be important for degradation during mitosis [62]. In addition, K63 chains are important for membrane trafficking, but can also target for degradation [27].

Sometimes, ubiquitin chains can be mixed, where different lysine linkages are contained within the same ubiquitin chain. K29/K48, K48/K63, and K11/K48 mixed chain linkage types have been shown to target for proteasome-mediated degradation [63,64]. Degradation of mitotic proteins, for example, show improved degradation with branched K11/K48 chains compared to K11 or K48 chains alone [62,65].

UBL-UBA shuttling factors target substrates for degradation

Ubiquitinated substrates often bind to the proteasome the one of the three intrinsic ubiquitin receptors, Rpn10, Rpn13, and Rpn1. However, some substrates are targeted to the proteasome through extrinsic receptors in the form of UBL-UBA proteins. UBL-UBA proteins contain an N-terminal ubiquitin-like (UBL) domain that binds to the proteasome receptors, along with a ubiquitin-associating (UBA) domain that binds to ubiquitin chains on substrates. There are three known UBL-UBA proteins in yeast, Rad23, Dsk2, and Ddi1 (Figure 1.4).

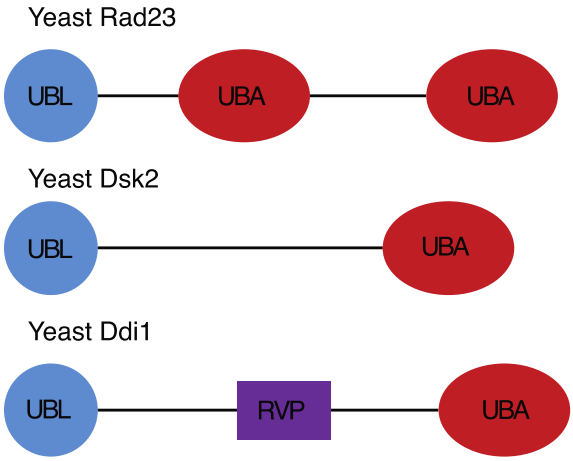

Figure 1.4: The three UBL-UBA proteins in yeast.

UBL-UBA proteins may be important for some proteasome-mediated degradation. When they are dysfunctional, cells, especially neurons, are more likely to be damaged by stress or aging, which can lead to earlier neurodegeneration [66].

The UBL-UBA protein, Rad23, is involved in proteasome-mediated degradation and was first demonstrated by its interaction with Rpn10 [67]. Since then, its role in

proteasome-mediated degradation has been widely studied by yeast two-hybrid screening and co-affinity purification studies. Rad23 contains two UBA domains (Figure 1.4), which bind ubiquitinated substrate proteins, leading to their degradation or stabilization. Previous studies have shown that Rad23 binds to some proteasomal components to move ubiquitylated proteins to the proteasome. It does this by using its N-terminal UBL domain to interact with Rpn1 [59,68], a regulatory subunit of the proteasome. Binding of Rad23 to Rpn1 has also been demonstrated to activate the proteasome's activity, leading to more efficient degradation [69]. Rad23 may provide a versatile recognition platform for substrates, as it has been shown *in vitro* to bind any of the three ubiquitin receptors on the proteasome, including Rpn10, Rpn1, and Rpn13 [27]. Targeting to the proteasome by Rad23 may be regulated by phosphorylation, as it has been demonstrated that phosphorylation of its serine residues may inhibit Rad23 UBL's interaction with the ubiquitin receptors on the proteasome [70], while overexpression leads to inhibition of degradation of substrates [71].

Rad23 has also been demonstrated to be a delivery factor in ER-associated degradation (ERAD) after they are extracted by the Cdc48-Ufd1-Npl4 complex [72]. It may interact directly with Cdc48-Ufd1-Npl4 complex and deliver processed substrates to the proteasome.

UBL-UBA proteins, like Rad23, may serve as an alternative pathway to the proteasome in addition to ubiquitinated substrate binding directly to ubiquitin receptors on the proteasome.

Ubiquitin independent substrate degradation

While many substrates are targeted for degradation by ubiquitination, some substrates do not require ubiquitination at all. It has been difficult to identify these

substrates. Ubiquitin is involved in many cellular processes, and so identifying ubiquitination is not enough to determine if it is required for the degradation of that substrate. Indeed, many substrates have been identified that do not require ubiquitination for their degradation.

One well known example is ornithine decarboxylase (ODC), which is the rate limiting enzyme in polyamine biosynthesis. ODC has been shown to be degraded in a ubiquitin-independent manner, but it requires the cofactor antizyme [73]. Antizyme binds to ODC and induces a conformational change in the protein to expose its C-terminus [74]. The proteasome is thought to recognize and initiate degradation of ODC at its C-terminus [75,76]. The C-terminal degradation region is sufficient for degradation, between it can be fused to other proteins and induce their ubiquitin-independent degradation as well [77].

Another example is Rpn4 which is a transcription factor involved in the expression of proteasome genes. It is also a proteasome substrate itself, which creates a negative feedback loop [78,79]. Rpn4 can be degraded in two ways: with and without ubiquitination. Rpn4 has a ubiquitin-dependent degron, which is recognized by ubiquitinating enzymes like Ubr2 [80]. Rpn4 can also be degraded in a ubiquitin-independent way. The N-terminal region can target Rpn4 to be degraded rapidly, even if all its lysine residues are mutated. This suggests that this region targets degradation in a ubiquitin-independent fashion. This is also supported by the fact that several mutants affecting ubiquitination of Rpn4 do not impair Rpn4 degradation [81].

Ubiquitin-independent degradation may be an alternative pathway to the proteasome even if the ubiquitination machinery is mis regulated. This is important because the ubiquitination system is essential for many cellular processes, and if it is disrupted, it can lead to cell death. Therefore, ubiquitin-independent degradation may

provide degradation mechanisms even under ubiquitination machinery stress as a way of maintaining cellular homeostasis [82].

STATEMENT OF THESIS

The last decade of research on the ubiquitin proteasome system has demonstrated the complexity in substrate selection and processing. Ubiquitination leads to substrate targeting to the proteasome, but ubiquitin is also involved in other cellular processes. What's more, the proteasome has several receptors for binding, and some substrates have been shown to be targeted by extrinsic UBL-UBA proteins, while others seem to bind directly in the pore-1 loops without ubiquitination. Sophisticated biochemical assays have shown the importance of a disordered initiation region for degradation of protein substrates. These studies have also revealed that the length and amino acid composition of this disordered region governs degradation specificity.

The goal of this thesis is to broadly understand how the proteasome selects its substrates. In Chapter 2, I use yeast as a model organism to investigate how the pathways to the proteasome interact. That is, do substrates delivered directly to the proteasome by ubiquitin tags compete with substrates delivered by UBL-UBA shuttling factors or ubiquitin independent substrates? Or, do these pathways occur in parallel? I measure the degradation of fluorescent model substrates integrated into the chromosome of yeast in the presence of dark competitors. I find that substrates with different targeting signals do not compete with one another, and that UBL-UBA shuttling factors may offer a priority path to the proteasome. Using advanced kinetic modeling tools, I have found that my competition results are consistent with a model in which UBL substrates can bind to any of the three receptors, while ubiquitin substrates can only bind to one receptor. This may explain why UBL and ubiquitin substrates do not compete with each other. I have also

found that competition of the initiation regions at the pore-1 loop is modest, suggesting that the primary competition occurs at the level of receptor binding, and not initiation. I further test the degradation of these pathways in the presence of proteotoxic stress, and find that ubiquitinated substrates are sensitive to proteotoxic stress, while UBL and ubiquitin-independent substrates are not.

In Chapter 3, I investigate specific features of quality degradation targets. Specifically, how the spacing between a proteasome-targeting signal, such as a ubiquitin chain or UBL tag, and the initiation region affects the degradation of substrates. I designed model substrates with short initiation regions, and with varying distances from the proteasome-binding signal such as a ubiquitin chain or UBL tag. I find that substrates require specific spacing between the ubiquitin tag and the degradation initiation region.

Recent advances have revealed the complexity of proteasome substrate selection. My findings show that not all substrates are equal, and that the dynamics of proteasome substrate selection depend on the type of targeting signal and its spacing to the initiation region. The proteasome may prioritize substrates targeted by UBL domains and those targeted independently of ubiquitination. Additionally, the spacing between the targeting signal and initiation region must be correct for degradation to occur. My work reveals the strict substrate requirements for proteasomal degradation and how the proteasome prioritizes substrates in the complex degradome pool.

Chapter 2: Ubiquitin-Like Domains Provide a Priority Pathway to the Proteasome

INTRODUCTION

The protein abundance in a cell determines that cell's structural and functional states. There are two major proteolytic pathways in eukaryotic cells: the ubiquitin proteasome system and the lysosome [1,83]. The 26S proteasome is required for the control of cell cycle regulation, protein quality and misfolding control [84]. First the proteasome targets proteins that have been tagged by a small protein, ubiquitin. Usually a ubiquitin tag that can efficiently target a protein for degradation consists of a multi-ubiquitin chain [1,7].

The proteasome also recognizes substrates through extrinsic receptors in the form of UBL-UBA proteins. UBL-UBA proteins contain an N-terminal ubiquitin-like (UBL) domain, which can bind the same receptors on the proteasome as ubiquitin chains, and one or more Ubiquitin-Associating (UBA) domains, which bind polyubiquitin chains. The UBL-UBA protein, Rad23, is involved in proteasome-mediated degradation and was first demonstrated by its interaction with Rpn10 [67]. Since then, its role in proteasome-mediated degradation has been widely studied by yeast two-hybrid screening and co-affinity purification studies. Rad23 contains two UBA domains, which bind ubiquitinated substrate proteins, leading to their degradation or stabilization. Previous studies have shown that Rad23 binds to some proteasomal components to move ubiquitylated proteins to the proteasome. It does this by using its N-terminal UBL domain to interact with Rpn1 [59,68], a regulatory subunit of the proteasome. Binding of Rad23 to Rpn1 has also been demonstrated to activate the proteasome's activity, leading to more efficient degradation

[69]. Rad23 may provide a versatile recognition platform for substrates, as it has been shown in vitro to bind any of the three ubiquitin receptors on the proteasome, including Rpn10, Rpn1, and Rpn13 [27]. Targeting to the proteasome by Rad23 may be regulated by phosphorylation, as it has been demonstrated that phosphorylation of its serine residues may inhibit Rad23 UBL's interaction with the ubiquitin receptors on the proteasome [70], while overexpression leads to inhibition of degradation of substrates [71].

Other substrates are targeted to the proteasome without ubiquitin signals. One well known example is ornithine decarboxylase (ODC), which is the rate limiting enzyme in polyamine biosynthesis. ODC has been shown to be degraded in a ubiquitin-independent manner, but it requires the cofactor antizyme [73]. Antizyme binds to ODC and induces a conformational change in the protein to expose its C-terminus [74]. The proteasome is thought to recognize and initiate degradation of ODC at its C-terminus [75,76]. The C-terminal degradation region is sufficient for degradation, between it can be fused to other proteins and induce their ubiquitin-independent degradation as well [77].

Thus, protein substrates are delivered to the proteasome through multiple pathways. Impairment of proteasome activity is linked to many human health disorders including cardiac dysfunction, cataract formation, neurodegenerative diseases, and cancer [85]. Consequently, understanding the proteasome system could lead to the development of targeted therapies for the associated diseases. However, we still don't know how substrates may compete for degradation.

We designed model substrates with different proteasome targeting signals to explore the interaction of the pathways they take to the proteasome. We found that pathways have a greater impact on themselves than on other pathways. We found that the

nature of proteasome binding tags creates a hierarchy where ubiquitin-like domains compete out ubiquitinated substrates. We also showed that this hierarchy reveals itself in substrate sensitivity to protein misfolding stress where ubiquitinated substrates are sensitive but ubiquitin-like substrates are not.

RESULTS

Rad23 ubiquitin-like fusion substrate does not compete with the other pathways

There are at least three pathways to the proteasome. Proteins are targeted to the proteasome by ubiquitin chains covalently attached to the substrates. The ubiquitin chains are recognized by intrinsic ubiquitin receptors on the proteasome. The proteasome also recognizes substrates through extrinsic receptors in the form of UBL-UBA proteins. UBL-UBA proteins contain an N-terminal ubiquitin-like (UBL) domain, which can bind the same receptors on the proteasome as ubiquitin chains, and one or more Ubiquitin-Associating (UBA) domains, which bind polyubiquitin chains. Other substrates are targeted to the proteasome without ubiquitin signals. Thus, protein substrates are delivered to the proteasome through multiple pathways. We wanted to determine how the 3 pathways to the proteasome compete. To test this, we designed 3 degradation sensors that followed the degradation of the three pathways: ubiquitinated sensor, a ubiquitin-like fusion sensor, and a ubiquitin-independent sensor.

To monitor degradation of ubiquitinated substrates, YFP is expressed with an N-terminal ubiquitin domain that is then cleaved by ubiquitin hydrolases exposing an arginine residue, which acts as an N-end rule degron, causing its ubiquitination [86–88]. To model substrate degradation by a ubiquitin-like domain, we fused the Rad23 UBL to the N-terminus of YFP. To model ubiquitin-independent degradation, we created ODC fusions at the C-terminus of YFP [9]. The substrates were introduced into yeast by

integrating them into the inactive BY4741 strain's HO locus, under the control of a constitutive TPI1 promoter. To induce shutdown of expression, cycloheximide was administered, and the degradation of the sensor was monitored through fluorescence measurements over a time course using flow cytometry.

We wanted to determine how our sensors respond to increased load on the individual pathways. To do this, we co-expressed a set of analogous competitors on 2-micron plasmids, with YFP replaced by a dark core domain, DHFR. DHFR competitors were expressed on estradiol inducible promoters [89], and cells were treated with varying amounts of estradiol to tune the expression level of the competitor. Expression of the competitors in yeast strains expressing the sensors were induced with estradiol at 1nM, 2nM, 5nM, 10nM, and 20nM. Cycloheximide was added and fluorescence of the sensors were monitored over time by flow cytometry. Plots of degradation are shown in Figure 2.1A-C, E-G, and I-K. The initial rate for degradation was determined for each trace, and three total independent experiments. The fold-change in initial rate after induction of competitor is plotted against the fold-change in BFP signal, representing the level of competitor induction. (Figure 2.1D,H,L).

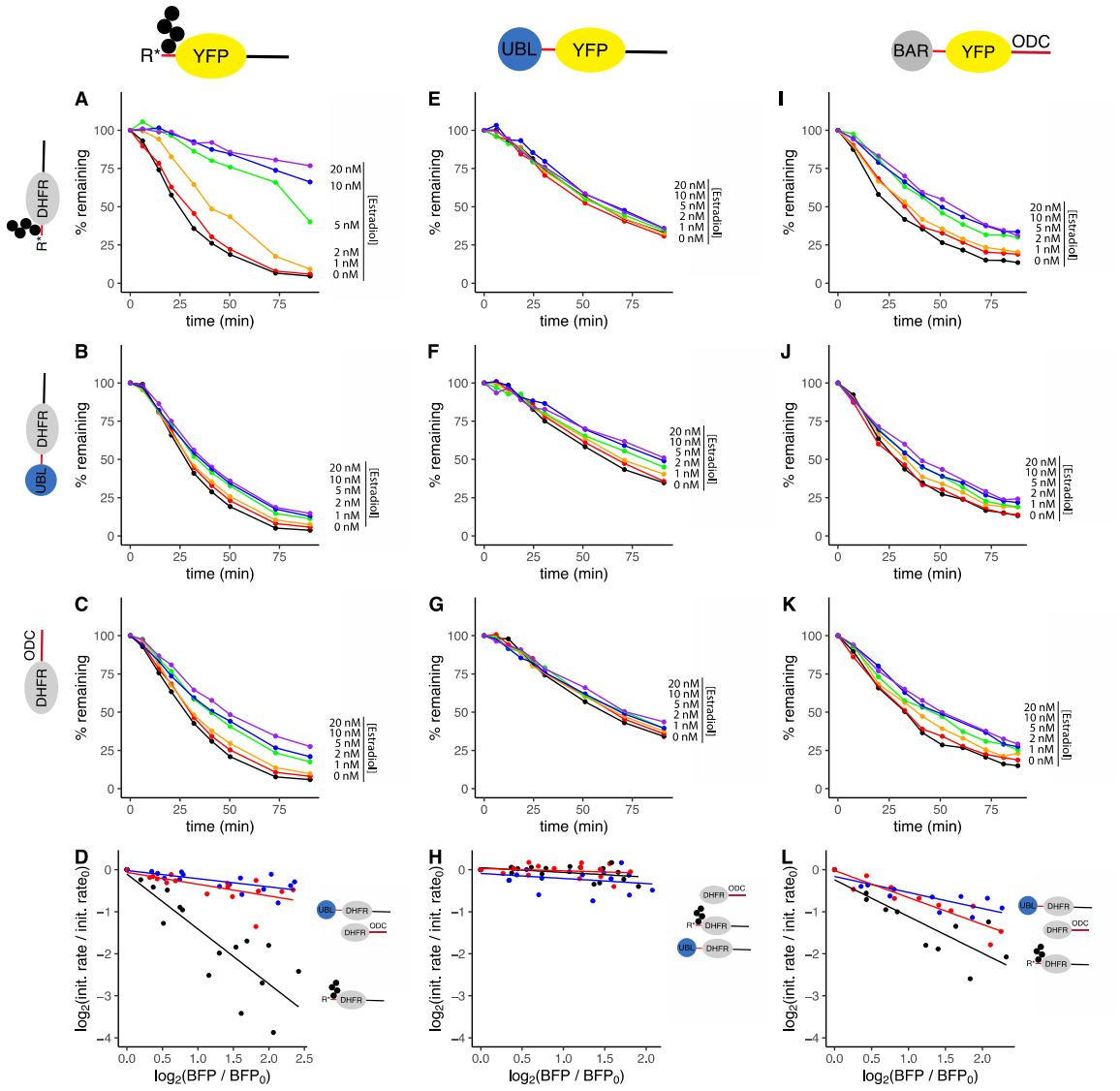

Figure 2.1: Competition of N-end rule, UBL, and ODC substrates.

(A) Normalized time courses of YFP fluorescence illustrating in vivo degradation of ReKK*-YFP-NS construct in the presence of estradiol-inducible ReKK-DHFR-Su9 competitor in the presence of 0nM (black), 1nM (red), 2nM (orange), 5nM (green), 10nM (blue), 20nM (purple) concentrations of estradiol.

(B) Normalized time courses of YFP fluorescence illustrating in vivo degradation of ReKK*-YFP-NS construct in the presence of estradiol-inducible UBL-DHFR-Su9 competitor in the presence of 0nM (black), 1nM (red), 2nM (orange), 5nM (green), 10nM (blue), 20nM (purple) concentrations of estradiol.

(C) Normalized time courses of YFP fluorescence illustrating in vivo degradation of ReKK*-YFP-NS construct in the presence of estradiol-inducible DHFR-ODC competitor in the presence of 0nM (black), 1nM (red), 2nM (orange), 5nM (green), 10nM (blue), 20nM (purple) concentrations of estradiol.

(D) Plots of log2 transformed normalized initial rates of degradation for ReKK*-YFP-NS from A-C as a function of log2 transformed normalized BFP fluorescence, which is expressed 1-to-1 on the same inducible promoter separated by a P2A ribosomal skipping site from the competitor. BFP fluorescence, therefore is a proxy for expression of the competitor.

(E) Normalized time courses of YFP fluorescence illustrating in vivo degradation of UBL-YFP-NS construct in the presence of estradiol-inducible ReKK-DHFR-Su9 competitor in the presence of 0nM (black), 1nM (red), 2nM (orange), 5nM (green), 10nM (blue), 20nM (purple) concentrations of estradiol.

(F) Normalized time courses of YFP fluorescence illustrating in vivo degradation of UBL-YFP-NS construct in the presence of estradiol-inducible UBL-DHFR-Su9 competitor in the presence of 0nM (black), 1nM (red), 2nM (orange), 5nM (green), 10nM (blue), 20nM (purple) concentrations of estradiol.

(G) Normalized time courses of YFP fluorescence illustrating in vivo degradation of UBL-YFP-NS construct in the presence of estradiol-inducible DHFR-ODC competitor in the presence of 0nM (black), 1nM (red), 2nM (orange), 5nM (green), 10nM (blue), 20nM (purple) concentrations of estradiol.

(H) Plots of log2 transformed normalized initial rates of degradation for UBL-YFP-NS construct from E-G as a function of log2 transformed normalized BFP fluorescence, which is expressed 1-to-1 on the same inducible promoter separated by a P2A ribosomal skipping site from the competitor. BFP fluorescence, therefore is a proxy for expression of the competitor.

(I) Normalized time courses of YFP fluorescence illustrating in vivo degradation of Barstar-YFP-ODC construct in the presence of estradiol-inducible ReKK-DHFR-Su9 competitor in the presence of 0nM (black), 1nM (red), 2nM (orange), 5nM (green), 10nM (blue), 20nM (purple) concentrations of estradiol.

(J) Normalized time courses of YFP fluorescence illustrating in vivo degradation of Barstar-YFP-ODC construct in the presence of estradiol-inducible UBL-DHFR-Su9 competitor in the presence of 0nM (black), 1nM (red), 2nM (orange), 5nM (green), 10nM (blue), 20nM (purple) concentrations of estradiol.

(K) Normalized time courses of YFP fluorescence illustrating in vivo degradation of Barstar-YFP-ODC construct in the presence of estradiol-inducible DHFR-ODC competitor in the presence of 0nM (black), 1nM (red), 2nM (orange), 5nM (green), 10nM (blue), 20nM (purple) concentrations of estradiol.

(L) Plots of log2 transformed normalized initial rates of degradation for Barstar-YFP-ODC construct from I-K as a function of log2 transformed normalized BFP fluorescence, which is expressed 1-to-1 on the same inducible promoter separated by a P2A ribosomal skipping site from the competitor. BFP fluorescence, therefore is a proxy for expression of the competitor.

Data information: In (A-C, E-G, and I-K), experiments were performed in triplicate, one representative kinetic experiment shown. In (D, H, and L) data represent the combination of replicates from three experiments. The line is a linear regression fit to the data.

The plasmids used are shown in Appendix Table 2.1. The strains used are BLS 877, BLS 920, BLS 917, BLS 927, BLS 928, BLS 929, BLS 881, BLS 922, BLS 919 and are shown in Table 2.2.

Plasmid ID Number	**Protein**	**Vector**	**Function/Use/purpose**
pBLS183	pZ$_4$EV-tagBFP-P2A-Ub-ReKK-DHFR-Su9-tGAL1	pYES2	ReKK-DHFR-Su9 Competitor
pBLS174	pZ$_4$EV-tagBFP-P2A-UBL(Rad23)-DHFR-Su9-tGAL1	pYES2	UBL-DHFR-Su9 Competitor
pBLS184	pZ$_4$EV-tagBFP-P2A-DHFR-ODC-tGAL1	pYES2	DHFR-ODC Competitor
pBLS175	pZ$_4$EV-tagBFP-P2A-Ub-ReKK-DHFR-Su9-His6-tGAL1	pYES2	ReKK-DHFR-Su9-His Competitor
pBLS176	pZ$_4$EV-tagBFP-P2A-UBL(Rad23)-DHFR-Su9-His6-tGAL1	pYES2	UBL-DHFR-Su9-His Competitor
pBLS177	pZ$_4$EV-tagBFP-P2A-DHFR-ODC-His6-tGAL1	pYES2	DHFR-ODC-His Competitor

Table 2.1: Plasmids used in this study.

Strain Name	**Genotype**
BLS 877	MATa ho::natMX6-pTPI1-DsRed-P2A-ReKK*-sYFP-NS-tADH [pBLS183] his3Δ1 leu2Δ0 met15Δ0 ura3Δ0
BLS 920	MATa ho::natMX6-pTPI1-DsRed-P2A-ReKK*-sYFP-NS-tADH [pBLS174] his3Δ1 leu2Δ0 met15Δ0 ura3Δ0
BLS 917	MATa ho::natMX6-pTPI1-DsRed-P2A-ReKK*-sYFP-NS-tADH [pBLS184] his3Δ1 leu2Δ0 met15Δ0 ura3Δ0
BLS 927	MATa ho::natMX6-pTPI1-DsRed-P2A-UBL(Rad23)-sYFP-NS-tADH

	[pBLS183] his3Δ1 leu2Δ0 met15Δ0 ura3Δ0
BLS 928	MATa ho::natMX6-pTPI1-DsRed-P2A-UBL(Rad23)-sYFP-NS-tADH [pBLS174] his3Δ1 leu2Δ0 met15Δ0 ura3Δ0
BLS 929	MATa ho::natMX6-pTPI1-DsRed-P2A-UBL(Rad23)-sYFP-NS-tADH [pBLS184] his3Δ1 leu2Δ0 met15Δ0 ura3Δ0
BLS 881	MATa ho::natMX6-pTPI1-DsRed-P2A-Barstar-sYFP-ODC-tADH [pBLS183] his3Δ1 leu2Δ0 met15Δ0 ura3Δ0
BLS 922	MATa ho::natMX6-pTPI1-DsRed-P2A-Barstar-sYFP-ODC-tADH [pBLS174] his3Δ1 leu2Δ0 met15Δ0 ura3Δ0
BLS 919	MATa ho::natMX6-pTPI1-DsRed-P2A-Barstar-sYFP-ODC-tADH [pBLS184] his3Δ1 leu2Δ0 met15Δ0 ura3Δ0
BLS 949	MATa ho::natMX6-pTPI1-DsRed-P2A-ReKK*-sYFP-NS-tADH pdr5::KAN^R his3Δ1 leu2Δ0 met15Δ0 ura3Δ0
BLS 948	MATa ho::natMX6-pTPI1-DsRed-P2A-UBL(Rad23)-sYFP-NS-tADH pdr5::KAN^R his3Δ1 leu2Δ0 met15Δ0 ura3Δ0
BLS 946	MATa ho::natMX6-pTPI1-DsRed-P2A-Barstar-sYFP-ODC-tADH pdr5::KAN^R his3Δ1 leu2Δ0 met15Δ0 ura3Δ0
BLS 872	MATa ho::natMX6-pTPI1-DsRed-P2A-ReKK*-sYFP-NS-tADH his3Δ1 leu2Δ0 met15Δ0 ura3Δ0
BLS 926	MATa ho::natMX6-pTPI1-DsRed-P2A-UBL(Rad23)-sYFP-NS-tADH his3Δ1 leu2Δ0 met15Δ0 ura3Δ0
BLS 868	MATa ho::natMX6-pTPI1-DsRed-P2A-Barstar-sYFP-ODC-tADH his3Δ1 leu2Δ0 met15Δ0 ura3Δ0
BLS 933	MATa ho::natMX6-pTPI1-DsRed-P2A-ReKK*-sYFP-NS-tADH [pBLS175] his3Δ1 leu2Δ0 met15Δ0 ura3Δ0
BLS 1001	MATa ho::natMX6-pTPI1-DsRed-P2A-ReKK*-sYFP-NS-tADH [pBLS175] ubr2::KAN^R his3Δ1 leu2Δ0 met15Δ0 ura3Δ0
BLS 934	MATa ho::natMX6-pTPI1-DsRed-P2A-ReKK*-sYFP-NS-tADH [pBLS176] his3Δ1 leu2Δ0 met15Δ0 ura3Δ0
BLS 935	MATa ho::natMX6-pTPI1-DsRed-P2A-ReKK*-sYFP-NS-tADH [pBLS177] his3Δ1 leu2Δ0 met15Δ0 ura3Δ0
BLS 930	MATa ho::natMX6-pTPI1-DsRed-P2A-UBL(Rad23)-sYFP-NS-tADH [pBLS175] his3Δ1 leu2Δ0 met15Δ0 ura3Δ0
BLS 931	MATa ho::natMX6-pTPI1-DsRed-P2A-UBL(Rad23)-sYFP-NS-tADH [pBLS176] his3Δ1 leu2Δ0 met15Δ0 ura3Δ0
BLS 932	MATa ho::natMX6-pTPI1-DsRed-P2A-UBL(Rad23)-sYFP-NS-tADH [pBLS177] his3Δ1 leu2Δ0 met15Δ0 ura3Δ0
BLS 936	MATa ho::natMX6-pTPI1-DsRed-P2A-Barstar-sYFP-ODC-tADH [pBLS175] his3Δ1 leu2Δ0 met15Δ0 ura3Δ0
BLS 937	MATa ho::natMX6-pTPI1-DsRed-P2A-Barstar-sYFP-ODC-tADH [pBLS176] his3Δ1 leu2Δ0 met15Δ0 ura3Δ0
BLS 938	MATa ho::natMX6-pTPI1-DsRed-P2A-Barstar-sYFP-ODC-tADH [pBLS177]

	his3Δ1 leu2Δ0 met15Δ0 ura3Δ0

Table 2.2: Yeast strains used in this study.

As shown in Figure 2.1A, the induction of the N-End rule competitor caused inhibition of degradation of the N-End rule substrate. We quantified that level of inhibition by fitting the cycloheximide chases and calculating the initial rates. A 4-fold increase in competitor expression, represented by an increase in BFP fluorescence, leads to a 9-fold decrease in initial rate of degradation (Figure 2.1D). This effect is consistent in the steady-level of the sensor before the cycloheximide chase. Western blotting showed an accumulation of YFP with an increase in competitor (Figure2.1.2A-D). This increase in steady state levels is also consistent by flow cytometry (Figure 2.1.1A). We confirmed that the inhibition of degradation of the N-End rule substrate in the presence of an N-End rule competitor is not due to the loss of free ubiquitin in the strain by detecting the level of free ubiquitin in the presence and absence of the competitor by western blot. This demonstrated that the level of free ubiquitin did not change based on the addition of competitor (Figure 2.1.5).

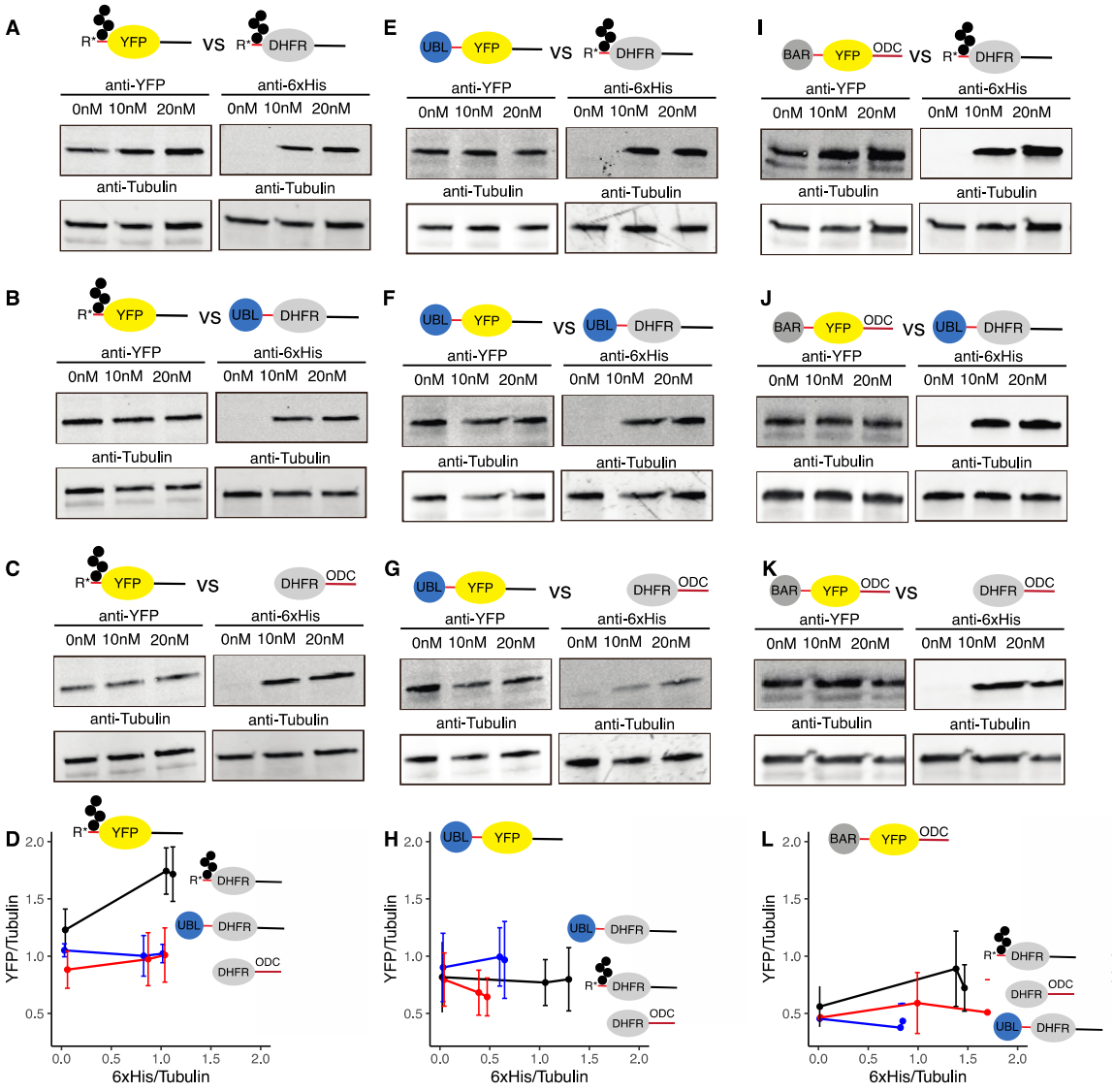

Figure 2.1.2: Steady state levels by western blot of N-end rule, UBL, and ODC substrates in the presence of competitors.

(A) Immunoblotting of ReKK*-YFP-NS construct and of estradiol-inducible ReKK-DHFR-Su9-His competitor in the presence of 0nM, 10nM, and 20nM concentrations of estradiol in the wildtype BY4741 yeast background.

(B) Immunoblotting of ReKK*-YFP-NS construct and of estradiol-inducible UBL-DHFR-Su9-His competitor in the presence of 0nM, 10nM, and 20nM concentrations of estradiol in the wildtype BY4741 yeast background.

(C) Immunoblotting of ReKK*-YFP-NS construct and of estradiol-inducible DHFR-ODC-His competitor in the presence of 0nM, 10nM, and 20nM concentrations of estradiol in the wildtype BY4741 yeast background.
(D) Plots of normalized YFP/Tubulin signal for ReKK*-YFP-NS construct from A-C as a function of normalized 6xHis/Tubulin signal for each of the competitors.
(E) Immunoblotting of UBL-YFP-NS construct and of estradiol-inducible ReKK-DHFR-Su9-His competitor in the presence of 0nM, 10nM, and 20nM concentrations of estradiol in the wildtype BY4741 yeast background.
(F) Immunoblotting of UBL-YFP-NS construct and of estradiol-inducible UBL-DHFR-Su9-His competitor in the presence of 0nM, 10nM, and 20nM concentrations of estradiol in the wildtype BY4741 yeast background.
(G) Immunoblotting of UBL-YFP-NS construct and of estradiol-inducible DHFR-ODC-His competitor in the presence of 0nM, 10nM, and 20nM concentrations of estradiol in the wildtype BY4741 yeast background.
(H) Plots of normalized YFP/Tubulin signal for UBL-YFP-NS construct from E-G as a function of normalized 6xHis/Tubulin signal for each of the competitors.
(I) Immunoblotting of Barstar-YFP-ODC construct and of estradiol-inducible ReKK-DHFR-Su9-His competitor in the presence of 0nM, 10nM, and 20nM concentrations of estradiol in the wildtype BY4741 yeast background.
(J) Immunoblotting of Barstar-YFP-ODC construct and of estradiol-inducible UBL-DHFR-Su9-His competitor in the presence of 0nM, 10nM, and 20nM concentrations of estradiol in the wildtype BY4741 yeast background.
(K) Immunoblotting of Barstar-YFP-ODC construct and of estradiol-inducible DHFR-ODC-His competitor in the presence of 0nM, 10nM, and 20nM concentrations of estradiol in the wildtype BY4741 yeast background.
(L) Plots of normalized YFP/Tubulin signal for Barstar-YFP-ODC construct from I-K as a function of normalized 6xHis/Tubulin signal for each of the competitors.

Data information: In (A-C, E-G, I-K), experiments were performed in triplicate, one representative immunoblot shown. In (D, H, and L) data represent the average of the replicates from three experiments. Standard error shown.

The plasmids used are shown in Table 2.1. The strains used are BLS 933, BLS 934, BLS 935, BLS 930, BLS 931, BLS 932, BLS 936, BLS 937, and BLS 938 and are shown in Table 2.2.

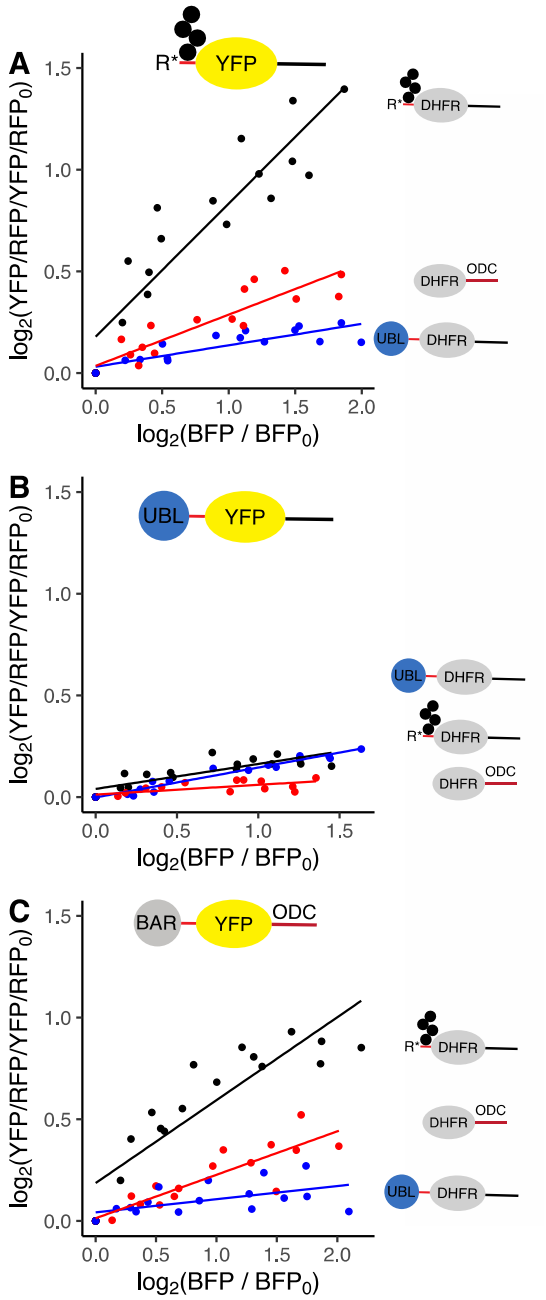

Figure 2.1.1: Steady state levels by flow cytometry of N-end rule, UBL, and ODC substrates in the presence of competitors.

(A) Plots of log2 transformed normalized YFP/RFP fluorescence for ReKK*-YFP-NS in the presence of ReKK-DHFR-Su9 (black), DHFR-ODC (red), or UBL-DHFR-Su9 (blue) competitors as a function of log2 transformed normalized BFP

fluorescence, which is expressed 1-to-1 on the same inducible promoter separated by a P2A ribosomal skipping site from the competitor. BFP fluorescence, therefore is a proxy for expression of the competitor.

(B) Plots of log2 transformed normalized YFP/RFP fluorescence for UBL-YFP-NS in the presence of ReKK-DHFR-Su9 (black), DHFR-ODC (red), or UBL-DHFR-Su9 (blue) competitors as a function of log2 transformed normalized BFP fluorescence, which is expressed 1-to-1 on the same inducible promoter separated by a P2A ribosomal skipping site from the competitor. BFP fluorescence, therefore is a proxy for expression of the competitor.

(C) Plots of log2 transformed normalized YFP/RFP fluorescence for Barstar-YFP-ODC in the presence of ReKK-DHFR-Su9 (black), DHFR-ODC (red), or UBL-DHFR-Su9 (blue) competitors as a function of log2 transformed normalized BFP fluorescence, which is expressed 1-to-1 on the same inducible promoter separated by a P2A ribosomal skipping site from the competitor. BFP fluorescence, therefore is a proxy for expression of the competitor.

Data information: In (A-C), experiments were performed in triplicate, data represent the combination of replicates from three experiments. The line is a linear regression fit to the data.

The plasmids used are shown in Table 2.1. The strains used are BLS 877, BLS 920, BLS 917, BLS 927, BLS 928, BLS 929, BLS 881, BLS 922, BLS 919 and are shown in Table 2.2.

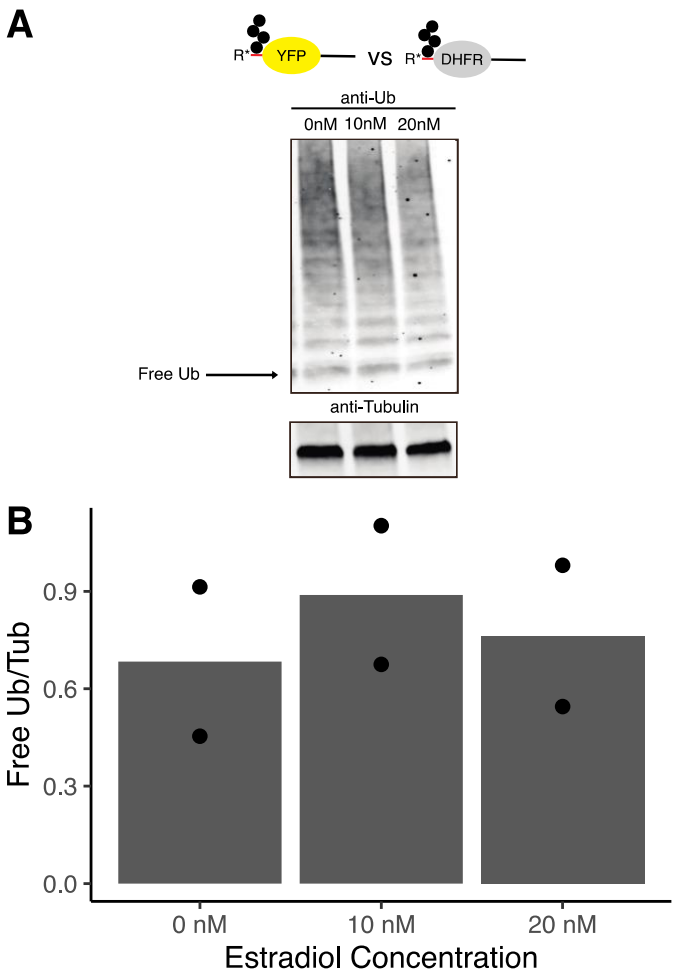

Figure 2.1.5: Free ubiquitin by western blot in strain expressing N-end rule substrate and in the presence of N-end rule competitor.

(A) Immunoblotting of ubiquitin in a strain expressing ReKK*-YFP-NS construct and the estradiol-inducible ReKK-DHFR-Su9 in the presence of 0nM, 10nM, and 20nM concentrations of estradiol in the wildtype BY4741 yeast background.
(B) Plot of normalized Free Ubiquitin/Tubulin signal from A against estradiol concentration. The bars are averages of 2 independent experiments. The points are the individual experiments.

The plasmid used is shown in Table 2.1. The strain used is BLS 933 and is shown in Table 2.2.

To the contrary, induction of UBL and ODC competitors do not slow the degradation of the N-end rule substrate (Figure 2.1B and C). At most, induction of these competitors lead to a 2-fold change in the initial rate. (Figure 2.1D). This effect is, again, consistent in the steady-level of the sensor before the cycloheximide chase. Western blotting showed no accumulation of YFP with an increase in UBL and ODC competitors (Figure 2.1.2A-D). This is also consistent by flow cytometry (Figure 2.1.1A).

Surprisingly, when we monitored the degradation of the UBL substrate in the presence of competitors, we found that a 4-fold increase in expression of any of the three competitors causes a very small decrease in initial rate, not even 2-fold (Figure 2.1E, F, G, and H). This effect is consistent in the steady-level of the sensor before the cycloheximide chase. Western blotting showed no accumulation of YFP with an increase in any of the three competitors (Figure 2.1.2E-H). This is also consistent by flow cytometry (Figure 2.1.1B).

Finally, we tested how the ubiquitin independent sensor, ODC, responds to the introduction of competitors. We found that all three competitors lead to a 2-4 fold decrease in the initial rate after a 4-fold increase in expression of the competitors (Figure 2.1 I, J, K, and L). This effect is consistent in the steady-level of the sensor before the cycloheximide chase. Western blotting showed not much accumulation of YFP with an increase in any of the three competitors (Figure 2.1.2I-L). This is also consistent by flow cytometry (Figure 2.1.1C).

Can the proteasome degrade more than one substrate at a time?

We next aimed to describe the competition dynamics observed in Figure 2.1 with a kinetic model. For this, we built kinetic models in KinTek explorer [90–92] to fit the data. The model is described in Figure 2.2A and in more detail in Table 2.3. The first step

in the model is synthesis of the YFP substrate by its gene, followed by binding of the substrate to the proteasome, represented by P, followed by degradation and release of the proteasome. Then we introduced the competitor into the model, where the first step is synthesis of the competitor. Then, degradation of the competitor with first a binding step and then degradation step. There is also the possibility of the competitor first binding the proteasome, followed by binding of the substrate, then simultaneous degradation. Another possibility is the reverse of this, where the substrate first binds the proteasome followed by the competitor. These possibilities were also included in the model.

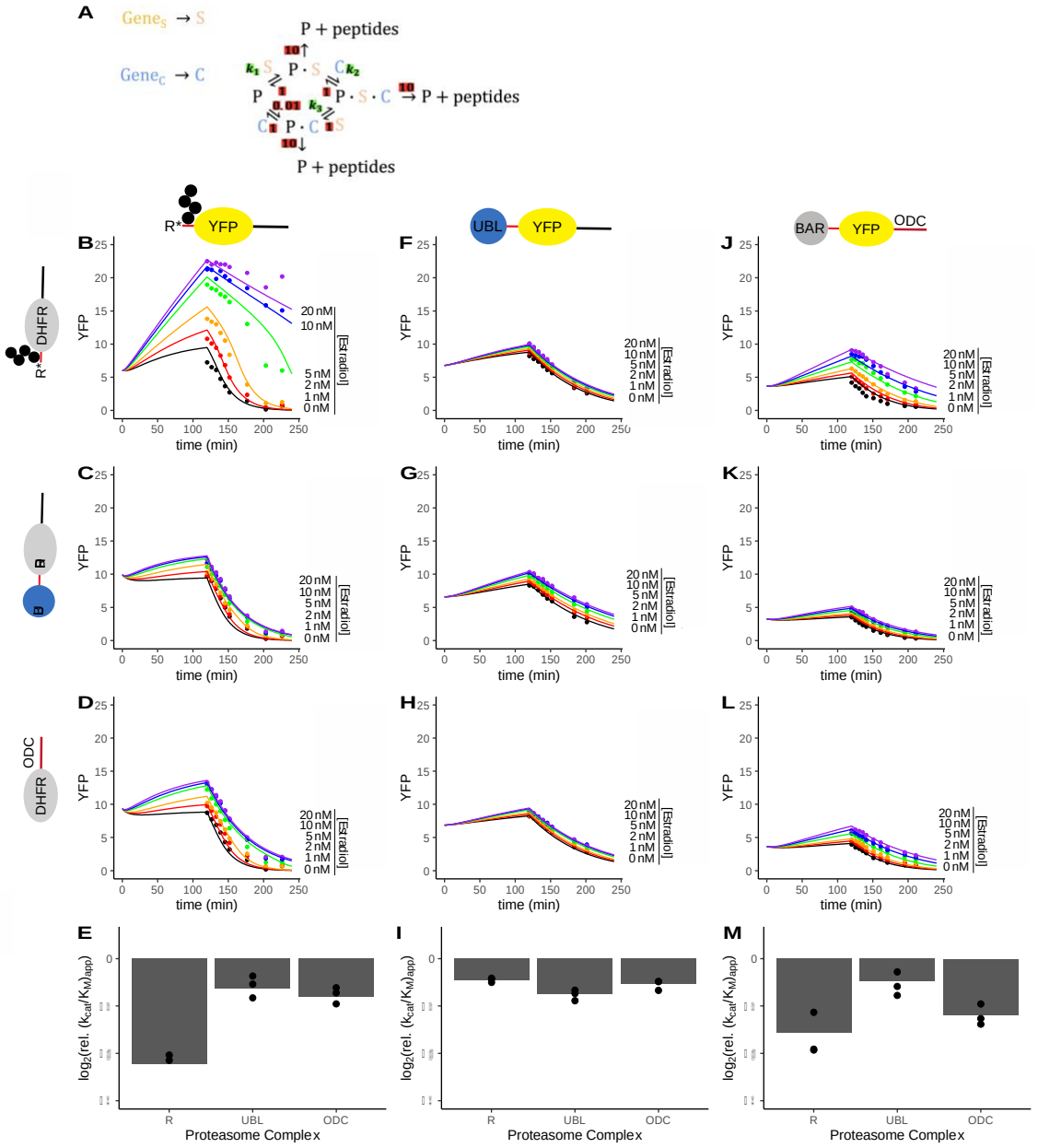

Figure 2.2: Kinetic model of competition dynamics at the proteasome for N-end rule, UBL, and ODC substrates.

(A) The reaction scheme for the kinetic model used to fit the competition data in Figure 1 with KinTek Explorer. All but the constrained parameters (green: k1, k2, and k3) were locked to nominal values (red). The kinetic model is described in Appendix Table 2.3.

(B) Time courses of raw YFP fluorescence illustrating in vivo degradation of ReKK*-YFP-NS construct in the presence of estradiol-inducible ReKK-DHFR-Su9 competitor in the presence of 0nM (black), 1nM (red), 2nM (orange), 5nM (green), 10nM (blue), 20nM (purple) concentrations of estradiol. Lines represent the best fit of the data to the kinetic model defined in A. The first 120 minutes simulate expression of the competitor before cycloheximide addition.

(C) Time courses of raw YFP fluorescence illustrating in vivo degradation of ReKK*-YFP-NS construct in the presence of estradiol-inducible UBL-DHFR-Su9 competitor in the presence of 0nM (black), 1nM (red), 2nM (orange), 5nM (green), 10nM (blue), 20nM (purple) concentrations of estradiol. Lines represent the best fit of the data to the kinetic model defined in A. The first 120 minutes simulate expression of the competitor before cycloheximide addition.

(D) Time courses of raw YFP fluorescence illustrating in vivo degradation of ReKK*-YFP-NS construct in the presence of estradiol-inducible DHFR-ODC competitor in the presence of 0nM (black), 1nM (red), 2nM (orange), 5nM (green), 10nM (blue), 20nM (purple) concentrations of estradiol. Lines represent the best fit of the data to the kinetic model defined in A. The first 120 minutes simulate expression of the competitor before cycloheximide addition.

(E) Plots of log2 transformed relative kcat/KM values for degradation of ReKK*-YFP-NS construct on proteasome bound to the indicated competitor and free proteasome.

(F) Time courses of raw YFP fluorescence illustrating in vivo degradation of UBL-YFP-NS construct in the presence of estradiol-inducible ReKK-DHFR-Su9 competitor in the presence of 0nM (black), 1nM (red), 2nM (orange), 5nM (green), 10nM (blue), 20nM (purple) concentrations of estradiol. Lines represent the best fit of the data to the kinetic model defined in A. The first 120 minutes simulate expression of the competitor before cycloheximide addition.

(G) Time courses of raw YFP fluorescence illustrating in vivo degradation of UBL-YFP-NS construct in the presence of estradiol-inducible UBL-DHFR-Su9 competitor in the presence of 0nM (black), 1nM (red), 2nM (orange), 5nM (green), 10nM (blue), 20nM (purple) concentrations of estradiol. Lines represent the best fit of the data to the kinetic model defined in A. The first 120 minutes simulate expression of the competitor before cycloheximide addition.

(H) Time courses of raw YFP fluorescence illustrating in vivo degradation of UBL-YFP-NS construct in the presence of estradiol-inducible DHFR-ODC competitor in the presence of 0nM (black), 1nM (red), 2nM (orange), 5nM (green), 10nM (blue), 20nM (purple) concentrations of estradiol. Lines represent the best fit of the data to the kinetic model defined in A. The first 120 minutes simulate expression of the competitor before cycloheximide addition.

(I) Plots of log2 transformed relative kcat/KM values for degradation of UBL-YFP-NS construct on proteasome bound to the indicated competitor and free proteasome.

(J) Time courses of raw YFP fluorescence illustrating in vivo degradation of Barstar-YFP-ODC construct in the presence of estradiol-inducible ReKK-DHFR-Su9 competitor in the presence of 0nM (black), 1nM (red), 2nM (orange), 5nM (green), 10nM (blue), 20nM (purple) concentrations of estradiol. Lines represent the best fit of the data to the kinetic model defined in A. The first 120 minutes simulate expression of the competitor before cycloheximide addition.

(K) Time courses of raw YFP fluorescence illustrating in vivo degradation of Barstar-YFP-ODC construct in the presence of estradiol-inducible UBL-DHFR-Su9 competitor in the presence of 0nM (black), 1nM (red), 2nM (orange), 5nM (green), 10nM (blue), 20nM (purple) concentrations of estradiol. Lines represent the best fit of the data to the kinetic model defined in A. The first 120 minutes simulate expression of the competitor before cycloheximide addition.

(L) Time courses of raw YFP fluorescence illustrating in vivo degradation of Barstar-YFP-ODC construct in the presence of estradiol-inducible DHFR-ODC competitor in the presence of 0nM (black), 1nM (red), 2nM (orange), 5nM (green), 10nM (blue), 20nM (purple) concentrations of estradiol. Lines represent the best fit of the data to the kinetic model defined in A. The first 120 minutes simulate expression of the competitor before cycloheximide addition.

(M) Plots of log2 transformed relative kcat/KM values for degradation of Barstar-YFP-ODC construct on proteasome bound to the indicated competitor and free proteasome.

Data information: In (B-D, F-H, and J-L), experiments were performed in triplicate, one representative kinetic experiment shown. The data are from the experiments in Figure 2.1. In (E, I, and M) data represent the combination of replicates from the three experiments. The points represent individual competition experiments. The bars are averages of the three independent experiments. Relative kcat/KM was calculated by dividing the kcat/KM for free proteasome (10/(1+10/k1)) by the kcat/KM for competitor-bound proteasome (10/(1+10/k3)).

Reaction Setup		
Reaction	**k^+**	**k^-**
Substrate + Proteasome → Substrate:Proteasome	k1	1
Substrate:Proteasome → Proteasome + Peptides	10	0
Competitor + Proteasome → Competitor:Proteasome	0.01	1
Competitor:Proteasome → Proteasome + Peptides	10	0

Substrate:Proteasome + Competitor → Substrate:Competitor:Proteasome	k2	1
Competitor:Proteasome + Substrate → Substrate:Competitor:Proteasome	k3	1
Substrate:Competitor:Proteasome → Proteasome + Peptides	10	0
Gene-Substrate → Substrate + Gene-Substrate	1	0
Gene-Competitor → Competitor + Gene-Competitor	1	0
Experiment Simulation Setup-t1-120minutes		
Species	**Concentration (a.u.)**	
Substrate	Starting YFP signal	
Proteasome	25	
Competitor	0	
Gene Substrate	10	
Gene Competitor	BFP signal	
Experiment Simulation Setup-t2-120minutes		
Species	**Concentration (a.u.)**	
Substrate	0	
Proteasome	0	
Competitor	0	
Gene Substrate	[%0]	
Gene Competitor	[%0]	

Table 2.3: Kinetic model to compare kinetic efficiency of free proteasome vs. competitor bound proteasome.

Using this model, we fit the data using a computer simulation in KinTek Explorer [90–92] to determine the apparent rates of each of the reactions in Figure 2.2A. The first 120 minutes of the simulation simulate the expression of the competitor after the addition of estradiol. Then, cycloheximide is added to shut off expression, and this is simulated by turning off expression of the substrates and competitors. The model fit quite well to the data, as shown in Figure 2.2 B-D, F-H, and J-L. We locked all but the binding rate to nominal values because the other parameters were not well constrained when fitting the data.

After this, we calculated the apparent kcat/Km, the catalytic efficiency, and performed a constraint analysis, where we allowed the catalytic efficiency to float, and measured Chi2minimum/Chi2 as a function of that floating catalytic efficiency. These plots are shown in Figure 2.1.3 for each of the different competition experiments. The binding rates were well-constrained for all fits.

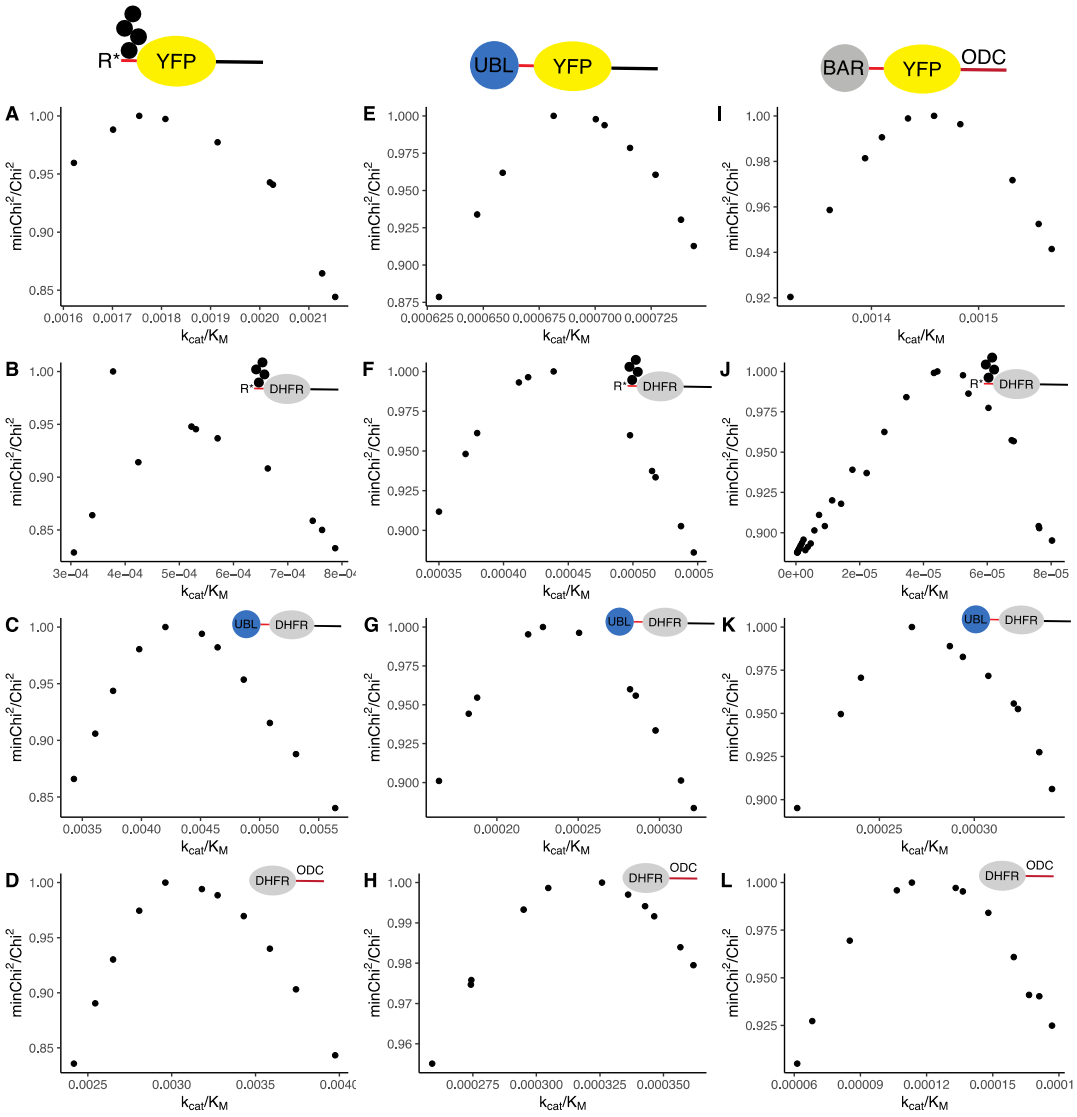

Figure 2.1.3: Constraint analysis of the kinetic model fits to the competition data for the determined catalytic efficiency.

(A-L) 1D confidence contours for individual fits to the kinetic model, showing the normalized Chi2 as a function of the variable parameter, demonstrating that each of the fits provide upper and lower limits for the variable parameters.

The fold-change in catalytic efficiency of free proteasome to competitor-bound proteasome indicates the likelihood that a substrate could be degraded in parallel with a competitor on the same proteasome. A larger fold-change indicates that the proteasome is less capable of degrading those two proteins at a time, while a smaller fold-change indicates a great likelihood that the proteasome could degrade both proteins simultaneously.

For the N-End rule substrate, there is a roughly 32-fold decrease in catalytic efficiency when the proteasome is bound to the N-End rule competitor, while there is a very small, at most 2-fold change in catalytic efficiency when the other two competitors are bound to the proteasome (Figure 2.2E), suggesting that the N-end rule substrate degradation is unaffected by binding of the UBL and ODC competitors, but not with the N-end rule competitor.

Then, we looked at the change in catalytic efficiency for the UBL sensor, and found a modest, roughly 4-fold decrease for proteasome bound to a UBL competitor, and a slightly smaller change for the other two competitors (Figure 2.2I). This suggests that the UBL substrate degradation is unaffected by binding of any of the three competitors on the proteasome.

Finally, we looked at the ODC substrate, and found a 4 to 8-fold decrease in catalytic efficiency for proteasome bound to the N-End rule and ODC competitors, with a very small decrease for UBL (Figure 2.2M). This suggests that the ODC substrate degradation may be modestly affect by binding of any of the three competitors, but not to a huge extent.

We found that N-end rule substrate degradation is affected by binding of the proteasome to N-end rule competitors, but not by binding to UBL or ODC competitors.

Furthermore, UBL and ODC substrates may not be affected by binding of any of the three competitors.

UBL substrates can bind to multiple receptors, making them more robust substrates less sensitive to competitors

Next, we asked why UBL does not compete much, even with itself? The previous kinetic model revealed that UBL substrate degradation may not be affected by binding of any of the three competitors, while ubiquitinated substrates may be affected by proteasome binding to a ubiquitinated competitor. Martinez-Fonts et al show that UBL substrates degrade well on proteasomes possessing Rpn1, Rpn10, or Rpn13, suggesting it can bind all three receptors. Whereas, ubiquitinated substrates only bind Rpn10 [27].

Applying these findings, we modeled the degradation of substrates in the presence of competitors, with one receptor (Figure 2.3A) or with UBL able to bind any of the three receptors consistent with Martinez-Fonts et al (Figure 2.3B) to determine if this observation may be able to explain our data. The kinetic models are described in greater detail in Table 2.4.

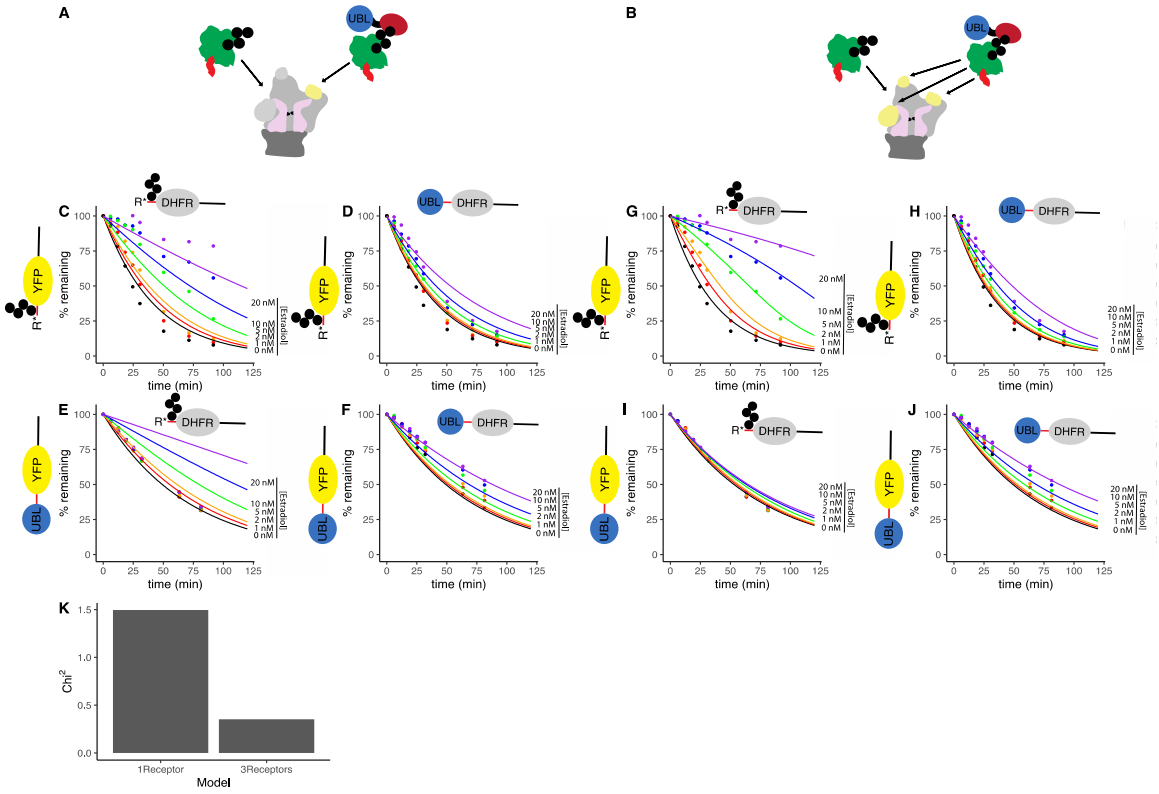

Figure 2.3: Kinetics models of N-End and UBL substrate binding to one or three receptors.

(A) Illustration of 1 receptor model used to fit the data from Figure 2.1 in KinTek Explorer, whereby UBL and N-End substrates compete for binding at the same receptor.

(B) Illustration of 3 receptor model used to fit the data from Figure 2.1 in KinTek Explorer, whereby UBL competes for binding at three receptors, while N-End substrates compete for binding at one receptor.

(C) Normalized time courses of YFP fluorescence illustrating in vivo degradation of ReKK*-YFP-NS construct in the presence of estradiol-inducible ReKK-DHFR-Su9 competitor in the presence of 0nM (black), 1nM (red), 2nM (orange), 5nM (green), 10nM (blue), 20nM (purple) concentrations of estradiol. Lines represent the best fit of the data to the 1 receptor model described in A.

(D) Normalized time courses of YFP fluorescence illustrating in vivo degradation of ReKK*-YFP-NS construct in the presence of estradiol-inducible UBL-DHFR-Su9 competitor in the presence of 0nM (black), 1nM (red), 2nM (orange), 5nM (green), 10nM (blue), 20nM (purple) concentrations of estradiol. Lines represent the best fit of the data to the 1 receptor model described in A.

(E) Normalized time courses of YFP fluorescence illustrating in vivo degradation of UBL-YFP-NS construct in the presence of estradiol-inducible ReKK-DHFR-Su9 competitor in the presence of 0nM (black), 1nM (red), 2nM (orange), 5nM (green), 10nM (blue), 20nM (purple) concentrations of estradiol. Lines represent the best fit of the data to the 1 receptor model described in A.

(F) Normalized time courses of YFP fluorescence illustrating in vivo degradation of UBL-YFP-NS construct in the presence of estradiol-inducible UBL-DHFR-Su9 competitor in the presence of 0nM (black), 1nM (red), 2nM (orange), 5nM (green), 10nM (blue), 20nM (purple) concentrations of estradiol. Lines represent the best fit of the data to the 1 receptor model described in A.

(G) Normalized time courses of YFP fluorescence illustrating in vivo degradation of ReKK*-YFP-NS construct in the presence of estradiol-inducible ReKK-DHFR-Su9 competitor in the presence of 0nM (black), 1nM (red), 2nM (orange), 5nM (green), 10nM (blue), 20nM (purple) concentrations of estradiol. Lines represent the best fit of the data to the 3 receptor model described in B.

(H) Normalized time courses of YFP fluorescence illustrating in vivo degradation of ReKK*-YFP-NS construct in the presence of estradiol-inducible UBL-DHFR-Su9 competitor in the presence of 0nM (black), 1nM (red), 2nM (orange), 5nM (green), 10nM (blue), 20nM (purple) concentrations of estradiol. Lines represent the best fit of the data to the 3 receptor model described in B.

(I) Normalized time courses of YFP fluorescence illustrating in vivo degradation of UBL-YFP-NS construct in the presence of estradiol-inducible ReKK-DHFR-Su9 competitor in the presence of 0nM (black), 1nM (red), 2nM (orange), 5nM (green), 10nM (blue), 20nM (purple) concentrations of estradiol. Lines represent the best fit of the data to the 3 receptor model described in B.

(J) Normalized time courses of YFP fluorescence illustrating in vivo degradation of UBL-YFP-NS construct in the presence of estradiol-inducible UBL-DHFR-Su9 competitor in the presence of 0nM (black), 1nM (red), 2nM (orange), 5nM (green), 10nM (blue), 20nM (purple) concentrations of estradiol. Lines represent the best fit of the data to the 3 receptor model described in B.

(K) Quantified Chi2 for the 1 receptor model (A) and 3 receptor model (B) global fits to the data, demonstrating that the 3 receptor model fits the data better than the 1 receptor model.

Data information: In (C-J), experiments were performed in triplicate, one representative kinetic experiment shown and kinetic fit shown. The data are from the experiments in Figure 2.1. The models used for fitting the data is described in Appendix Table 2.4. For the three receptor model, N-end rule substrates/competitors were only allowed to bind receptor1, while UBL substrates/competitors were allowed to bind receptor1, receptor2, or receptor3.

One Receptor Model Reaction Setup		
Reaction	**k^+**	**k^-**
Receptor1 + Substrate → Receptor1:Substrate	k1	1
Receptor1:Substrate → Receptor1 + Peptides	10	0
Receptor1 + Competitor → Receptor1:Competitor	k2	1
Receptor1:Competitor → Receptor1 + Peptides	10	0
One Receptor Model Experiment Simulation Setup-120minutes		
Species	**Concentration (a.u.)**	
Substrate	1	
Proteasome (Receptor1)	0.1	
Competitor	0,10,20,50,100,200	

Three Receptor Model Reaction Setup		
Reaction	**k^+**	**k^-**
Receptor1 + Substrate → Receptor1:Substrate	k1	1
Receptor1:Substrate → Receptor1 + Peptides	10	0
Receptor2 + Substrate → Receptor2:Substrate	k1	1
Receptor2:Substrate → Receptor2 + Peptides	10	0
Receptor3 + Substrate → Receptor3:Substrate	k1	1
Receptor3:Substrate → Receptor3 + Peptides	10	0
Receptor1 + Competitor → Receptor1:Competitor	k2	1

Receptor1:Competitor → Receptor1 + Peptides	10	0
Receptor2 + Competitor → Receptor2:Competitor	k2	1
Receptor2:Competitor → Receptor2 + Peptides	10	0
Receptor3 + Competitor → Receptor3:Competitor	k2	1
Receptor3:Competitor → Receptor3 + Peptides	10	0
Three Receptor Model Experiment Simulation Setup-120minutes		
Species	**Concentration (a.u.)**	
Substrate	1	
Proteasome (Receptor1)	0.1	
Competitor	0,10,20,50,100,200	

Table 2.4: Kinetic model to compare one receptor vs. three receptor availability.

The kinetic model with only one available receptor binding site deviates substantially from the experimental data (Figure 2.3C-F). We found that a kinetic model having three available receptors for UBL, which is consistent with [27], fit our data far better than a kinetic model where R and UBL compete for only one binding site. Some data suggest that UBL domains can activate proteasome activity [69]. This suggests that UBLs may have increased binding capacity in addition to proteasome activity activation.

Together, these findings suggest two explanations for why our UBL substrate competes less with itself: (1) UBL can bind multiple receptors, thus leading to increased binding capacity on the proteasome, and (2) UBL binding activates the proteasomes, which may compensate, to some extent, for the inhibitive effect of competition.

UBL substrates are not sensitive to an accumulation of ubiquitinated proteins caused by MG-132 treatment

Our main observation is that the ubiquitin pathway competes with ubiquitin competitors, but UBL and ODC do not. Since we tested this with a synthetic ubiquitin competitor, we wanted to test if this applies to endogenously ubiquitinated competitors.

We used MG-132 to inhibit the proteasome in vivo for all three of our sensors. We observed slowed degradation for all three sensors in the presence of MG-132 (Figure 2.4A-C). And proteasome inhibition also leads to an accumulation of ubiquitinated proteins. We blotted for ubiquitin after MG-132 treatment and observed an increase in the accumulation of ubiquitinated species (Figure 2.4J-O).

When we washed out MG-132 and allowed the cells to recover for one hour, then all substrates were degraded back to no-treatment level, demonstrating that the treatment was reversible (Figure 2.4G-I). And the accumulation of ubiquitinated proteins returned to pre-treatment levels, demonstrating that this accumulation was also reversible (Figure 2.4J-O).

However, if we wash out MG-132 and measure degradation immediately, the UBL and ODC sensors are degraded to no treatment levels (Figure 2.4E and F), while the N-End rule sensor is still inhibited (Figure 2.4D). This may be because the N-End rule sensor is competing for degradation with the accumulated ubiquitin species (Figure 2.4J and M), while the UBL and ODC sensors do not compete with the accumulated ubiquitin species (Figure 2.4K and N, L and O) and can recover much more quickly.

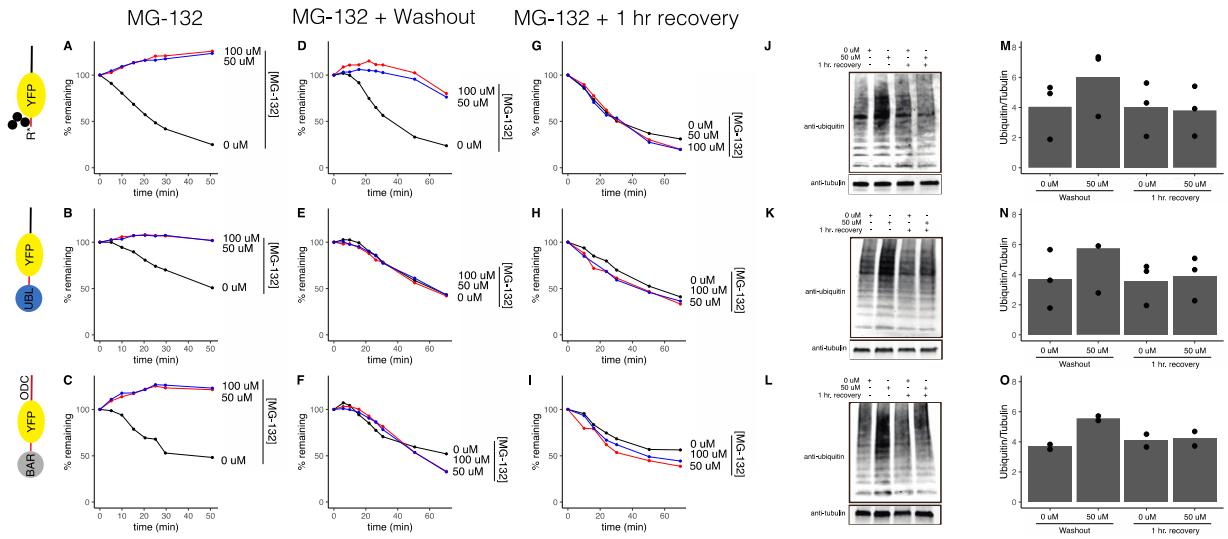

Figure 2.4: N-End substrate competes with accumulation of endogenous ubiquitinated species, while UBL and ODC substrates do not.

(A-C) Normalized time courses of YFP fluorescence illustrating in vivo degradation of ReKK*-YFP-NS, UBL-YFP-NS, and Barstar-YFP-ODC constructs in the presence of 0uM (black), 50uM (red), or 100uM (blue) concentrations of MG-132.
(D-F) Normalized time courses of YFP fluorescence illustrating in vivo degradation of ReKK*-YFP-NS, UBL-YFP-NS, and Barstar-YFP-ODC constructs immediately after 1 hour treatment with 0uM (black), 50uM (red), or 100uM (blue) concentrations of MG-132, followed by a wash-out of MG-132.
(G-I) Normalized time courses of YFP fluorescence illustrating in vivo degradation of ReKK*-YFP-NS, UBL-YFP-NS, and Barstar-YFP-ODC constructs with 1 hour recovery after a 1 hour treatment with 0uM (black), 50uM (red), or 100uM (blue) concentrations of MG-132, followed by a wash-out of MG-132.
(J-L) Immunoblotting of ubiquitin in the strains expressing ReKK*-YFP-NS, UBL-YFP-NS, and Barstar-YFP-ODC constructs immediately, or after 1 hour recovery from treatment with 0uM, or 50uM concentrations of MG-132.

(M-O) Plot of normalized Ubiquitin/Tubulin signal from J-L against MG-132 concentration with and without 1 hour recovery.

Data information: In (A-C, D-F, and G-I), experiments were performed in triplicate, one representative kinetic experiment shown. In (J-L) experiments were performed in triplicate, one representative immunoblot shown. In (M-OL) data represent the average of the replicates from three experiments. The points are individual experiments.

The strains used are BLS 949, BLS 948, and BLS 946 and are shown in Table 2.2.

Ubiquitinated substrates are sensitive to misfolding stress conditions, while UBL and ODC substrates are not

Because we observed that the N-end rule substrate competes with the accumulation of endogenous ubiquitin species, but the UBL substrate does not, we wanted to determine how these three pathways are affected by proteotoxic stress in the cell, since a typical response to protein misfolding is degradation by the proteasome [4–6].

To induce protein misfolding, we introduced the drug canavanine, an amino acid analog of arginine. Canavanine gets incorporated into newly synthesized polypeptides leading to protein misfolding and cellular stress [93].

The addition of 3 μg/mL of canavanine leads to a 4-fold decrease in the initial rate for degradation of the N-end rule substrate (Figure 2.5A and D). Canavanine has no effect on degradation for the UBL and ODC substrates, even at the 3 μg/mL concentration (Figure 2.5B-D). This is likely because the N-End rule substrate is competing for degradation with the accumulation of misfolded proteins which clog up the ubiquitin pathway, but not the UBL and ODC pathways.

UBL and ubiquitinated substrates are involved in separate pathways to the proteasome, with UBL substrates seemingly having more capacity due to multi-receptor binding.

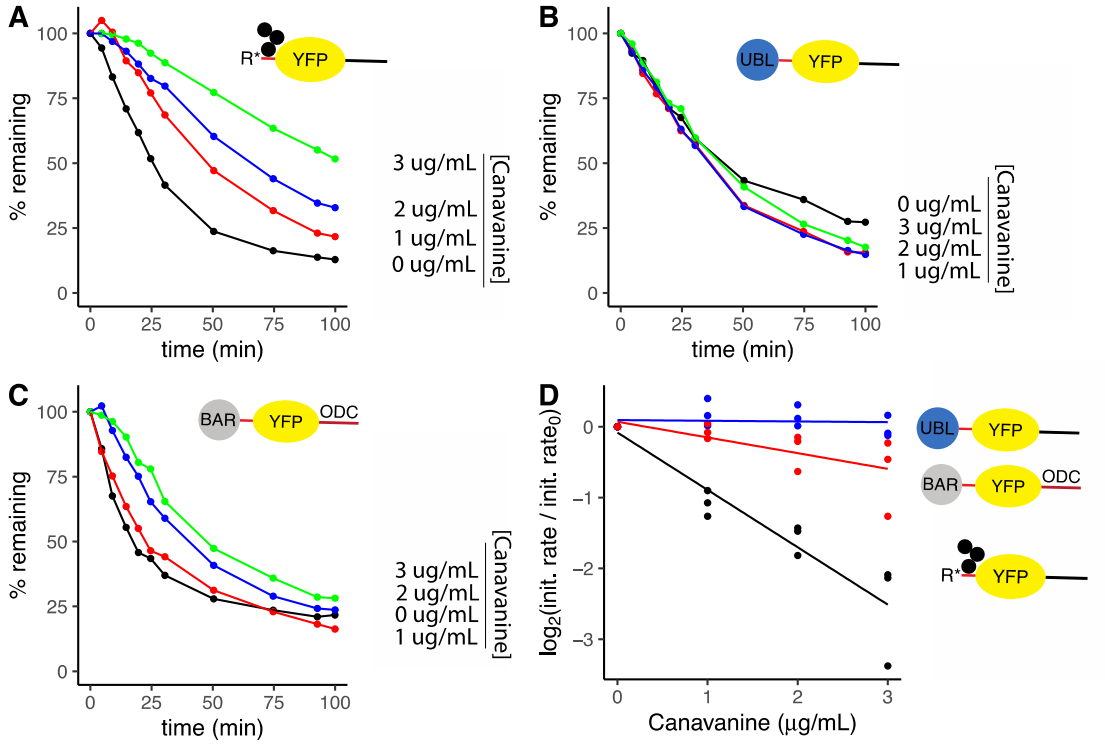

Figure 2.5: Sensitivity of N-End, UBL, and ODC substrates to protein misfolding stress caused by canavanine.

(A) Normalized time courses of YFP fluorescence illustrating *in vivo* degradation of ReKK*-YFP-NS construct in the presence of 0 µg/mL (black), 1 µg/mL (red), 2 µg/mL (blue), and 3 µg/mL (green) concentrations of canavanine.

(B) Normalized time courses of YFP fluorescence illustrating *in vivo* degradation of UBL-YFP-NS construct in the presence of 0 µg/mL (black), 1 µg/mL (red), 2 µg/mL (blue), and 3 µg/mL (green) concentrations of canavanine.

(C)

(D) Normalized time courses of YFP fluorescence illustrating *in vivo* degradation of Barstar-YFP-ODC construct in the presence of 0 µg/mL (black), 1 µg/mL (red), 2 µg/mL (blue), and 3 µg/mL (green) concentrations of canavanine.

(E) Plots of $\log_2$ transformed normalized initial rates of degradation of the three constructs from A-C as a function of canavanine concentration.

Data information: In (A-C), experiments were performed in triplicate, one representative kinetic experiment shown. In D data represent the combination of replicates from three experiments. The lines are linear regression fits to the data.

The strains used are BLS 872, BLS 926, and BLS 868 and are shown in Table 2.2.

Ubiquitinated substrates compete at the level of proteasome capacity

The ubiquitin proteasome system is a part of a feedback loop, whereby increased loads on the proteasome leads to increased expression. Rpn4, a transcription factor for proteasome subunits, can be ubiquitinated by the E3 ligase, Ubr2, leading to its degradation. When the load on the proteasome is increased, Rpn4 is not degraded, leading to its accumulation and increase in expression of proteasome [79].

We wanted to determine how proteasome expression levels may affect the competition dynamics of our N-end rule substrate against an N-end rule competitor. We compared the competition dynamics in WT vs. a ubr2Δ mutant, where proteasome expression is increased due to the stabilization of Rpn4.

The ubr2Δ mutant lead to faster degradation of the N-end rule substrate (Figure 2.6A-B), even in the presence of the N-end rule competitor (Figure 2.6A-C). These data are consistent by western blotting as well (Figure 2.1.4).

We wanted to make sure our observations of competition in WT vs. the ubr2Δ mutant were consistent with a kinetic model where the ubr2Δ mutant has increased proteasome expression. We built two kinetic models like ones in Figure 3. More details about the model used here are in Table 2.5. The first model had the same amount of proteasome in WT vs. ubr2Δ mutant (1x Proteasome Model). As shown in Figure 2.6D-E, the fit was not good. However, when we switched the model to account for double the proteasome in the ubr2Δ mutant compared to WT (2x Proteasome Model), the fit was improved (Figure 2.6F-G). This observation is confirmed when quantifying and comparing the Chi2 for each model. As shown in Figure 2.6H, the Chi2 is larger in the 1x Proteasome Model compared to the 2x Proteasome Model, suggesting that the 1x Proteasome Model deviates more from the experimental data than the 2x Proteasome Model.

Taken together, these data suggest that an increase in proteasome expression may increase the degradation of the N-end rule substrate. However, as the load on the proteasome is ramped up by an increase in expression of the N-end rule competitor, the degradation rates return to WT levels.

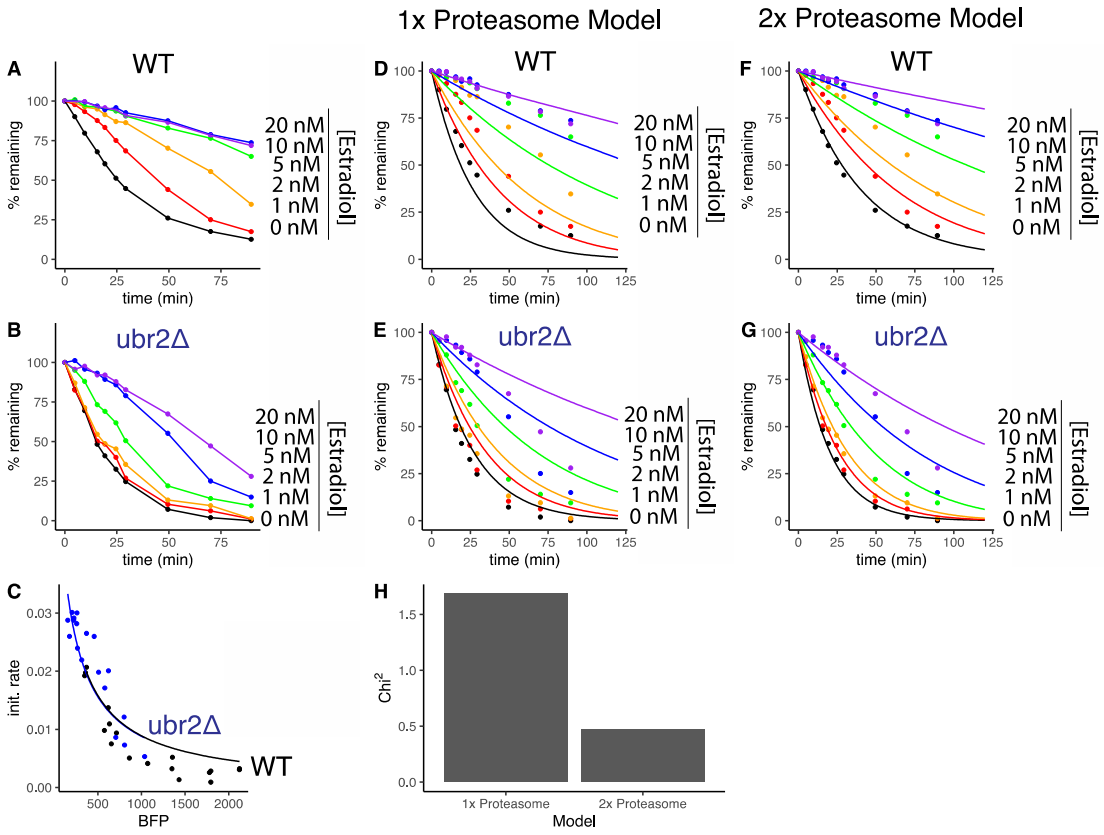

Figure 2.6: Competition between N-End substrate and N-End competitor for binding to the proteasome, with increasing proteasome expression.

(A) Normalized time courses of YFP fluorescence illustrating in vivo degradation of ReKK*-YFP-NS construct in the presence of estradiol-inducible ReKK-DHFR-Su9 competitor in the presence of 0nM (black), 1nM (red), 2nM (orange), 5nM (green), 10nM (blue), 20nM (purple) concentrations of estradiol in the wildtype BY4741 yeast background.

(B) Normalized time courses of YFP fluorescence illustrating in vivo degradation of ReKK*-YFP-NS construct in the presence of estradiol-inducible ReKK-DHFR-

Su9 competitor in the presence of 0nM (black), 1nM (red), 2nM (orange), 5nM (green), 10nM (blue), 20nM (purple) concentrations of estradiol in the ubr2Δ yeast background.

(C) Plots of initial rates of degradation for ReKK*-YFP-NS from A-B in wildtype (black) and ubr2Δ (blue) backgrounds as a function of BFP fluorescence, which is expressed 1-to-1 on the same inducible promoter separated by a P2A ribosomal skipping site from the competitor. BFP fluorescence, therefore is a proxy for expression of the competitor.

(D) Normalized time courses of YFP fluorescence illustrating in vivo degradation of ReKK*-YFP-NS construct in the presence of estradiol-inducible ReKK-DHFR-Su9 competitor in the presence of 0nM (black), 1nM (red), 2nM (orange), 5nM (green), 10nM (blue), 20nM (purple) concentrations of estradiol in the wildtype BY4741 yeast background. Lines represent the best fit of the data to a kinetic model whereby proteasome levels are equal in WT and ubr2Δ (1x Proteasome Model).

(E) Normalized time courses of YFP fluorescence illustrating in vivo degradation of ReKK*-YFP-NS construct in the presence of estradiol-inducible ReKK-DHFR-Su9 competitor in the presence of 0nM (black), 1nM (red), 2nM (orange), 5nM (green), 10nM (blue), 20nM (purple) concentrations of estradiol in the ubr2Δ yeast background. Lines represent the best fit of the data to a kinetic model whereby proteasome levels are equal in WT and ubr2Δ (1x Proteasome Model).

(F) Normalized time courses of YFP fluorescence illustrating in vivo degradation of ReKK*-YFP-NS construct in the presence of estradiol-inducible ReKK-DHFR-Su9 competitor in the presence of 0nM (black), 1nM (red), 2nM (orange), 5nM (green), 10nM (blue), 20nM (purple) concentrations of estradiol in the wildtype BY4741 yeast background. Lines represent the best fit of the data to a kinetic model whereby proteasome levels are 2-fold higher ubr2Δ than in WT (2x Proteasome Model).

(G) Normalized time courses of YFP fluorescence illustrating in vivo degradation of ReKK*-YFP-NS construct in the presence of estradiol-inducible ReKK-DHFR-Su9 competitor in the presence of 0nM (black), 1nM (red), 2nM (orange), 5nM (green), 10nM (blue), 20nM (purple) concentrations of estradiol in the ubr2Δ yeast background. Lines represent the best fit of the data to a kinetic model whereby proteasome levels are 2-fold higher ubr2Δ than in WT (2x Proteasome Model).

(H) Quantified Chi2 for the best global fits of the data to the 1x Proteasome Model and the 2x Proteasome Model, demonstrating that the 2x Proteasome model fits the data better than the 1x Proteasome Model.

Data information: In (A-B, and D-G), experiments were performed in triplicate, one representative kinetic experiment shown. In C data represent the combination of replicates from three experiments. The points represent individual competition

experiments. The lines are fits to the 2x kinetic model. The kinetic models used in D-H are described in Table 2.5.

The plasmids used are shown in Table 2.1. The strains used are BLS 933 and BLS 1001 and are shown in Table 2.2.

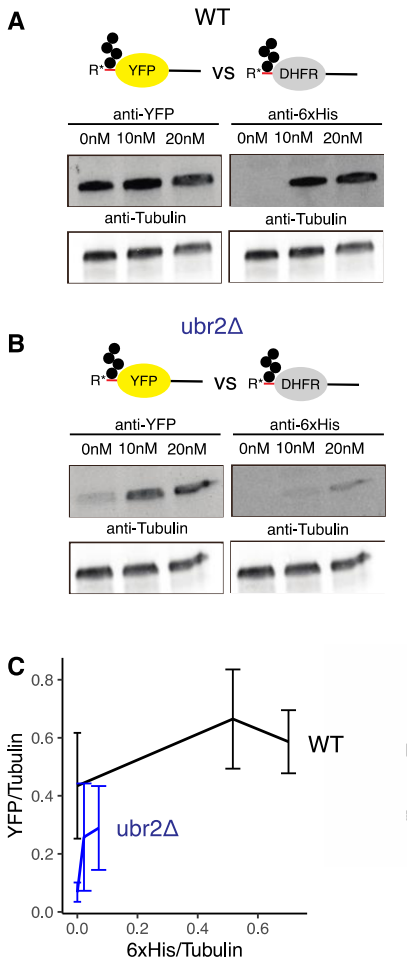

Figure 2.1.4: Steady state levels by western blot of N-end rule substrate in the presence of N-end rule competitor in WT and ubr2Δ backgrounds.

(A) Immunoblotting of ReKK*-YFP-NS construct and of estradiol-inducible ReKK-DHFR-Su9-His competitor in the presence of 0nM, 10nM, and 20nM concentrations of estradiol in the wildtype BY4741 yeast background.

(B) Immunoblotting of ReKK*-YFP-NS construct and of estradiol-inducible ReKK-DHFR-Su9-His competitor in the presence of 0nM, 10nM, and 20nM concentrations of estradiol in the ubr2Δ yeast background.

(C) Plots of normalized YFP/Tubulin signal for ReKK*-YFP-NS construct from A and B as a function of normalized ReKK-DHFR-Su9-His/Tubulin signal in the WT (black) and ubr2Δ (blue) backgrounds. The points are averages of 2 independent experiments. The errors are standard error.

The plasmids used are shown in Table 2.1. The strains used are BLS 933 and BLS 1001 and are shown in Table 2.2.

One Receptor Model Reaction Setup		
Reaction	**k^+**	**k^-**
Proteasome + Substrate → Proteasome:Substrate	k1	1
Proteasome:Substrate → Proteasome + Peptides	10	0
Proteasome + Competitor → Proteasome:Competitor	k2	1
Proteasome:Competitor → Proteasome + Peptides	10	0
One Receptor Model Experiment Simulation Setup-120minutes		
Species	**Concentration (a.u.)**	
Substrate	1	
Proteasome	0.1 for WT and ubr2Δ strains in 1x model or 0.1 for WT and 0.2 for ubr2Δ in 2x model	
Competitor	0,100,200,500,1000,2000	

Table 2.5: Kinetic model to compare WT vs. ubr2Δ competition dynamics in R*eKK-YFP-NS vs. ReKK-DHFR-Su9

DISCUSSION

The proteasome targets substrates for degradation by at least three distinct pathways: ubiquitinated proteins bind directly to ubiquitin receptors on the proteasome, ubiquitinated proteins bind to UBL-UBA shuttle factors that deliver them to the proteasome, or ubiquitin-independent degradation. We designed model substrates with different proteasome targeting signals, along with a parallel set of dark competitors to explore the pathways they take to the proteasome. Ubiquitinated substrates were modelled with an N-end rule degron. UBL substrates were modelled with a Rad23 UBL fusion. Ubiquitin independent degradation was modelled with a C-terminal ODC fusion.

The N-end rule substrate competed with the N-end rule competitor, but surprisingly did not compete with the UBL and ODC competitors. In Martinez-Fonts et al, different degradation targeting signals require different proteasome receptors for degradation. Ubiquitinated substrates require Rpn10, while UBL substrates can be degraded on any of the three receptors, Rpn10, Rpn13, and Rpn1 [27]. So, it's possible that the explanation for this is that substrates compete at the level of receptor binding, and not tail insertion.

This was surprising, however, because the proteasome possesses only one entry channel for degradation to initiate, and we predicted that this would be a rate limiting step in competition between substrates. Single molecule FRET-based biochemistry assays have tracked the kinetics of ubiquitin binding to receptors, and tail insertion into the pore. Ubiquitin binding is thought to be significantly faster [94] than tail insertion. It takes 1.6 seconds for the tail to insert, followed by a rapid conformational switch that takes 0.4 seconds. The ubiquitin chain is then removed within about 5 seconds, and the mechanical unfolding, translocation, and cleavage of the substrate takes an additional 11 seconds. Therefore, the data overwhelmingly suggest that the majority of

substrate processing time is spent on deubiquitination and unfolding/translocation. Furthermore, some in vitro competition assays have suggested that ubiquitin-chain interactions with receptors are short lived, and that substrates with better initiation regions competed more than substrates with poor initiation regions [10]. We, therefore, initially hypothesized that substrates would compete at the level of tail insertion.

However, our data support a model where receptor binding is most limiting, and their tails may be inserted simultaneously. This can be supported by the evidence of some substrates initiating degradation at an internal initiation region, which must form a loop with a width of at least two polypeptide chains when entering the channel, suggesting that more than one polypeptide chain may fit in the entry channel [95]. Also, some proteasomes are doubly capped, meaning they may be able to degrade polypeptides in both directions simultaneously [96].

With this model, then, the ubiquitinated substrate competes with itself because it competes for binding at the same receptor on the proteasome, while a UBL competitor can bind a different receptor. This is further supported when we switched the substrate to UBL, where we saw much less competition with any of the three competitors. This makes sense because UBL can bind any of the three receptors, and so the competitors are not directly competing for binding at the same receptor.

We directly tested competition at the level of tail insertion with the ODC substrate, which is thought to directly engage the entry channel to initiate degradation. We observed a modest level of competition with any of the three competitors, consistent with a basal level of competition at engagement into the channel. This modest level of competition is consistent with our model that the channel can engage more than one polypeptide at a time.

Our data suggest substrates that bind to the same receptor binding site on the proteasome compete, while substrates that bind to different receptor binding sites do not affect the degradation of others. We built a kinetic model to quantify how well a proteasome bound to any given competitor may degrade any given substrate. To do this, we determined the relative kcat/KMapp from free proteasome to proteasome bound to a competitor, and found that the kcat/KMapp decreased significantly for the ubiquitinated substrate when the proteasome was bound to a ubiquitinated competitor. However, the kcat/KMapp for the ubiquitinated competitor did not change significantly for the ubiquitinated substrate when the proteasome was bound to a UBL or ODC competitor. The kcat/KMapp for the UBL substrate did not change much when the proteasome was bound to any of the three competitors, either. These findings are consistent with the idea that competitor binding to the proteasome does not interfere with degradation of a substrate, just so it is targeted through a different pathway.

We were surprised to find that substrates are unaffected by competitor delivered through different pathways, and even that the UBL substrate is unaffected by a UBL competitor. Biochemical assays have revealed that the Rad23 UBL can bind and target substrates through Rpn10, Rpn13, or Rpn1, while ubiquitinated substrates can only target through Rpn10 [27]. We modelled this to determine if this interpretation was enough to explain the data. We compared the fit of our data to a kinetic model whereby UBL can bind any of the three receptors against a model whereby UBL substrates compete for the same receptor binding. We quantified the goodness of fit to each model to determine which our data are more consistent with. The kinetic model with only one available receptor binding site deviates substantially from the experimental data (Figure 2.3C-F), while the kinetic model having three available receptors for UBL was consistent with our experimental data.

Furthermore, ubiquitinated substrate degradation was dependent on the level of proteasome. The degradation of the ubiquitinated substrate was faster in a ubr2Δ mutant than in WT, even in the presence of ubiquitinated competitor. However, as the amount of the ubiquitinated competitor was increased further, the degradation returned to WT levels. This suggests that the Ubr2/Rpn4 feedback loop is sufficient to improve degradation of the N-end rule substrate, even in the presence of competitor to a point until the proteasome is so overloaded, likely because it leads to an increased proteasome load. Similarly, having multiple receptors on the proteasome could mean that more than one substrate can be degraded at a time if a receptor is accessible to the substrate, thus leading to increased binding capacity on the proteasome.

We also showed that our UBL and ODC substrates are not sensitive to an accumulation of ubiquitinated proteins caused by MG-132 treatment, or an accumulation of misfolded proteins caused by canavanine treatment, while our ubiquitinated substrate was sensitive to both. This is likely because ubiquitinated proteins are limited to binding at Rpn10, while UBL can bind any of the three receptors [27], and ODC does not need to interact with a receptor. These data demonstrate that UBL substrates are not sensitive to cellular stress that leads to an increase in proteasome load.

Rad23 and other UBL-UBA proteins could serve to open more accessibility to the proteasome by providing binding of ubiquitin chains to more than just Rpn10, thus decreasing competition of priority substrate degradation under stress.

For example, Sic1, a Cdk1-Clb complex inhibitor, prevents premature cell cycle progression from G1 to S phase. Degradation of Sic1 by the proteasome relieves inhibition of Cdk1-Clb complexes and allows progression to S phase [97]. Sic1 degradation has been demonstrated to be mediated by direct binding to Rpn10, or by binding to Rad23 [98]. UBL-UBA shuttle factors, such as Rad23 and Dsk2, may serve as

a backup route to the proteasome for high-priority substrates, such as Sic1, during stress. For instance, ubiquitinated proteins accumulate on proteasomes in yeast strains that lack Cdc48 function [99,100]. Additionally, it has been demonstrated that Rad23 and Dsk2 further increase the amount of ubiquitinated substrate occupancy on the proteasome in strains that lack Cdc48 function [99]. Furthermore, deleting RAD23 and DSK2 in a cdc48 mutant strain results in a progressively worse growth defect [101], which suggests that Rad23 and Dsk2 may be involved in alleviating the growth defects of cdc48 mutants, maybe because they serve to deliver high-priority substrates to the proteasome when the load is high.

We found that the nature of proteasome binding tags creates a dominant hierarchy where ubiquitin-like domains compete out ubiquitinated substrates and that substrates targeted by UBLs are largely unaffected by cellular stress. This provides a surprising explanation for the functionality of UBL-UBA shuttling factors in cells: they may serve to deliver high-priority substrates for degradation under cellular stress or increased proteasome load.

MATERIALS AND METHODS

Yeast Proteasome Substrates Design

Yeast YFP substrate variants were built off a central YFP (sYFP2) domain and constructed with either an N-end rule degron, an N-terminal UBL domain derived from the first 80 amino acids of S. cerevisiae Rad23, or a C-terminal degron derived from the last 52 amino acids of ornithine decarboxylase (ODC) [9]. The ODC substrate also contained an N-terminal barstar domain to improve expression of the substrate. N-end rule substrates consisted of a ubiquitin domain followed by a destabilizing Arg residue followed by a 19 amino acid linker derived from E. coli lacI, which contains two Lys

residues (ReKK*). However, amino acids 4-13 were replaced with a serine-rich linker derived from herpes virus 1 ICP4 to prevent the N-terminal degron from being a disordered region that could initiate degradation. The N-end rule and UBL substrates also contained the C-terminal disordered initiation region, NS, derived from influenza A virus non-structural protein 1 (NS1) and is described in [9].

To correct for cell-to-cell variation in transcriptional, translational, or cell size variation, RFP dsRed-Express2 was expressed upstream of YFP separated by a P2A ribosomal skipping site. The ratio of YFP over RFP for individual cells was a measure of the steady state concentration of YFP variants.

Substrates were integrated into the ORF of HO1 in S. cerevisiae strain BY4741 and expressed from a constitutive TPI1 promoter. Correct integration was confirmed by selection with nourseothricin and sanger sequencing.

Yeast Proteasome Competitors Design

The competitor variants were built off a central E. Coli DHFR domain with similar degrons to the substrates. N-end rule competitors consisted of a ubiquitin domain followed by a destabilizing Arg residue followed by a 19 amino acid linker derived from E. coli lacI, which contains two Lys residues (ReKK). The UBL competitor consisted of an N-terminal UBL domain derived from the first 80 amino acids of S. cerevisiae Rad23. Both the UBL and N-end rule competitors contained the C-terminal disordered initiation region, Su9, which is 51 amino acids from subunit 9 of the Fo component of the Neurospora crassa ATP synthase and has been previously characterized as an efficient initiation region [9]. The ODC competitor consisted of a C-terminal fusion of a degron derived from the last 52 amino acids of ornithine decarboxylase (ODC) [9].

To detect levels of expression of the dark competitors, tagBFP was expressed upstream of DHFR separated by a P2A ribosomal skipping site. The level of tagBFP was indicative of total expression levels of the competitor.

Competitors were expressed from a 2-micron plasmid (pYES2) with a URA3 selection marker and the estradiol-inducible promoter Z4EV as previously described [89]. The plasmids were transformed into the S. cerevisiae strain BY4741 with the substrates.

Plasmids used in this study are shown in Table 2.1. The yeast strains constructed and used in this study are shown in Table 2.2.

Flow Cytometry

Cells were grown in synthetic complete (SC) medium at 25oC to mid-log phase after 7-8 doublings and harvested for direct fluorescent measurement of RFP and YFP channels by an LSR Fortessa (BD biosciences) flow cytometer. Time courses of YFP fluorescence were measured to determine in vivo degradation rates by inhibition of protein synthesis through the addition of 125 µM cycloheximide and YFP fluorescence measurements were taken for 120 minute time courses.

Competition assays were performed by first adding varying concentrations of estradiol to the yeast cultures for 2 hours. MG-132 assays were performed by first adding varying concentrations of MG-132 to cultures for 1 hour, and then either directly harvesting, or centrifuging and replacing the media with fresh SC to wash out the MG-132, and harvested directly, or allowed to recover again for 1 hour before harvesting. Canavanine assays were performed by adding varying concentrations of canavanine for 2 hours before harvesting.

Degradation rates were calculated. Background (average fluorescence of lowest signal fluorescence in an experiment) was subtracted and fluorescence plotted as a

function of time. Normalized fluorescence was calculated as a percentage from time 0. The decay curves were fitted to the equation describing a single exponential decay ($y = Ae^{-kt} + C$) using the software Prism (version 7). Initial degradation rate was determined by multiplying the amplitude of degradation (% fluorescence) by the rate constant (min^{-1}). If a single exponential fit was not appropriate, the first 30 minutes of the curve was fit to a linear function, and the slope was used as the initial rate for degradation.

The data were analyzed by FlowJo (FlowJo version 10.2). Cells were gated first along the FSC-A vs. SSC-A axes to eliminate dead cells. They were then gated against SSC-H vs. SSC-W and FSC-H vs. FSC-W axes to eliminate doublets. Finally, cells were gated to only include RFP-positive cells. Data was collected for at least 10,000 cells and we report the median of those at least 10,000 cells per data point.

Western Blots

Cells were grown in synthetic complete (SC) medium at 25oC to mid-log phase after 7-8 doublings and harvested. Competition assays and MG-132 assays were treated the same as in the flow cytometry experiments before harvesting.

Cells were harvested by centrifugation at 8,000xg for 30 seconds at 4oC. The pellet was resuspended in 1 mL cold water and harvested by centrifugation at 8,000xg for 30 seconds at 4oC. Cells were treated with 2.0 M LiOAc and then 0.4 M NaOH for 5 minutes each on ice. Cells were suspended in 100 μL of lysis buffer (0.1M NaOH, 0.05M EDTA, 2% SDS, 2% b-mercaptoethanol with protease and phosphatase inhibitor). The lysates were incubated at 90oC for 10 mins, and then neutralized by adding 2.5 μL of 4M acetic acid and vortexed for 30 seconds. Lysates were again incubated at 90oC for 10 mins and cleared by centrifugation at 16,000xg for 10 mins.

Protein extracts were analyzed by western blotting by first running 50-100 μg of total protein extract on 4-20% Mini-PROTEAN TGX gels (BioRad catalog no. 4561094) at 120V. Protein content was then transferred from the gel to a nitrocellulose membrane with the Trans-Blot Turbo RTA Transfer System (BioRad catalog no. 1704158) . YFP fusion proteins were detected with a mouse monoclonal anti-enhanced GFP antibody (1:3000, Clontech, catalog no. 632569) and an IRDye 800CW goat anti-mouse secondary antibody (1:15000, LI-COR, catalog no. 926-32210). DHFR competitors were labeled with a C-terminal his tag and detected with a mouse monoclonal anti-histidine antibody (1:3000, Millipore Sigma, catolog no.05-949) and an IRDye 800CW goat anti-mouse secondary antibody (1:15000, LI-COR, catalog no. 926-32210). Ubiquitin was detected with a rabbit polyclonal anti-ubiquitin antibody (1:1000, Abcam, catolog no. 19247) and an IRDye 680RD goat anti-rabbit secondary antibody (1:15000, LI-COR, catalog no. 926-68071). Tubulin was detected with a rabbit monoclonal anti-tubulin antibody (1:3000, Abcam, catolog no. 184970) and an IRDye 680RD goat anti-rabbit secondary antibody (1:15000, LI-COR, catalog no. 926-68071).

Protein amounts were estimated by direct infrared fluorescence imaging (Odyssey LI-COR Biosciences).

Kinetic Modelling

Data were fit to defined kinetic models by numerical integration of rate equations in the model, as described in [90–92]. The enzyme and substrate concentrations were estimated and set to reasonable and consistent values. The exact enzyme and substrate concentrations could not be defined because these experiments were performed in vivo. However, because we only compare relative kinetic parameters, the exact concentrations are not necessary if they remain internally consistent.

The fits in Figure 2.2 simulate expression of the competitor for the 2 hours prior to data collection, and then shut off expression of the competitor and substrates when cycloheximide is added and measurements are taken. Constraint analysis was performed whereby the goodness of fit is assessed while varying any given rate in the model. Rates that were not well constrained by the data were locked to nominal values, because the data cannot define all individual parameters, but defines well the ratio of parameters. Relative kcat/KM was calculated by dividing the kcat/KM for free proteasome (10/(1+10/k1)) by the kcat/KM for competitor-bound proteasome (10/(1+10/k2)). The values for k1 and k2 are defined in Figure 2.2A.

The model used for fitting the data in Figure 2.2 is described in Table 2.3. The models used for fitting the data in Figure 2.3 are in Table 2.4. For the three receptor model, N-end rule substrates/competitors were only allowed to bind receptor1, while UBL substrates/competitors were allowed to bind receptor1, receptor2, or receptor3. The models used for fitting the data in Figure 2.6 are in Table 2.5.

Contributions

BLS, KT, GC, and AR designed and conducted experiments and interpreted data, BLS, KT, and CY constructed unique reagents for the study, and AM conceived the study, designed experiments, and interpreted data. BLS, and AM wrote the manuscript.

Chapter 3: Proteasomal degradation requires specific spacing between ubiquitin tag and degradation initiation

INTRODUCTION

The Ubiquitin Proteasome System (UPS) is the major pathway of regulated protein degradation in eukaryotes. It clears damaged and misfolded proteins from cells, digests foreign proteins as part of the adaptive immune response, and controls the concentration of regulatory proteins involved in diverse cellular processes [102]. The 26S proteasome is the proteolytic machine at the center of the UPS. Proteins are primarily targeted to the proteasome by the covalent attachment of one or more ubiquitin molecules to lysine residues within target proteins by the sequential action of E1, E2, and E3 enzymes. The process forms polyubiquitin chains in which the ubiquitin moieties are linked through isopeptide bonds between the C-terminus of one ubiquitin and one of the seven Lys residues or the N-terminal Met residue of another ubiquitin [7,23,103]. Once a ubiquitinated protein is recognized by the proteasome, degradation initiates at a stretch of disordered amino acids within the substrate [1,4,15,26,42,83,104–108].

The proteasome is composed of a cylindrical 20S Core Particle (CP) and a 19S Regulatory Particle (RP) that caps either or both ends of the CP [83]. Access to the proteolytic chamber in the CP is controlled by the RP, which recognizes substrates and transfers them to the CP for degradation. Substrates travel from the RP to the CP via the substrate translocation channel, a passage that, because it is narrow, allows entry of unfolded polypeptides but excludes folded domains. This channel within the RP and is formed by a heterohexameric ring of ATPases of the AAA+ family, known as Rpt1-Rpt6. At least three subunits of the RP recognize ubiquitin: Rpn10, Rpn13, and Rpn1 [56–

58,109]. The degradation rates of ubiquitinated substrates typically show the strongest dependence on Rpn10, which is situated closest to the entrance of the substrate translocation channel. Rpn13 is located at the top of the RP, somewhat further from the entrance channel than Rpn10 [56,58,110], while Rpn1 is located on the opposite side of the entrance channel relative to Rpn10.

Rpn10, Rpn13, and Rpn1 can also bind UBL domains of UBL-UBA proteins [56–59]. UBL UBA proteins contain an N-terminal UBL domain connected by a flexible linker to one or more copies of a Ubiquitin-Associating (UBA) domain, which binds ubiquitin. Hence, UBL UBA proteins are thought to act as extrinsic substrate receptors by binding polyubiquitin through their UBA domain(s) and the proteasome through their UBL domain [26,60,68,106–108,111–115]. Some UBL-UBA proteins are required for the degradation of select natural proteins, though the mechanism of action remains unclear [98].

Recognition by ubiquitin receptors is not sufficient for substrate degradation. The proteasome must also physically engage the target protein at a segment of unstructured amino acids to initiate degradation [42,116]. This initiation region inserts into the substrate translocation channel and is engaged by hydrophobic pore loops (pore-1 loops) of the ATPase ring. The initiation region must be of the appropriate length and composition for effective degradation [8,9,15,95,117,118]. Initiation regions at the C-terminus of a protein must be some 30 residues in length for efficient degradation, but internally located initiation regions must be much longer [15,42,95,104,116,117].

The proteasome must be able to precisely distinguish between its substrates and other ubiquitinated proteins in the cell to avoid promiscuous degradation. Intriguingly, ubiquitination and the presence of an initiation region do not always lead to rapid or efficient degradation [27]. How then does the proteasome select its substrates? Perhaps

the arrangement of ubiquitin modification sites and the initiation region within some substrates prevents their simultaneous recognition by ubiquitin and initiation region receptors of the proteasome, preventing effective degradation [117]. The initiation region binding site is situated within the substrate translocation channel, while the three ubiquitin receptors of the RP are located at distinct distances and directions away from the channel [83,102]. It stands to reason that an initiation region must at least be long enough to bridge the distance between the entrance to the translocation channel and the pore loops for effective engagement.

Here we determine how the position of the initiation region relative to a ubiquitin tag affects substrate selection by the proteasome by measuring the degradation of defined model substrates in which an initiation region is placed varying distances from the ubiquitin chain on the substrate. Our data suggest that the receptor that mediates substrate binding determines whether the proteasome can initiate degradation, presumably due to its distance from the pore loops within the substrate translocation channel. These observations provide new insight into the mechanism of substrate selection by the proteasome.

RESULTS

Ubiquitin chain length and initiation

We first sought to determine how initiation region length affects the degradation of substrates possessing the canonical degradation-targeting signal (Ub4K48) [61]. To this end, we built substrates based on a central fluorescent protein domain (derived from GFP) with an N-terminal in-frame ubiquitin domain and a C-terminal initiation region (Fig 3.1a). We attached defined K48-linked ubiquitin chains to the N-terminal ubiquitin domain in purified base protein and measured fluorescence over time in the presence of

purified proteasome, as described previously (see methods) [27]. Here we refer to the initiation region as a tail because of its location at the C-terminus of the fluorescent model protein. Tails were either 18 or 38 amino acids in length (Table 3.3). RP and CP were affinity purified from Saccharomyces cerevisiae with high salt washes to remove co-purifying proteasome-interacting proteins [57]. The proteasome was reconstituted by mixing CP and RP in a 1:2 molar ratio.

Tail Name	**Base Substrate**	**Amino Acid Sequence**	**Tail Length (amino acids)**
18	GFP	PRLRYQPLLRSGRISPAE	18 aa
38	GFP	PRLRYQPLLRISQNCEAAILRASQTRLNTISGRIS PAE	38 aa
96	GFP	PRLRYQPLLRISQNCEAAILRASQTRLNTIGAYG STVPRSQSFEQDSRQRTQSWTALRVGAIPAATS SVAYLNWHNGQIDNEPQLDMNRQRISPAE	96 aa
Su9	YFP	RMASTRVLASRLASQMAASAKVARPAVRVAQ VSKRTIQTGSPLQTRAYSS	49 aa
SP25	YFP	RSPESMREEYRKEGSPESMREEYRKEGSPESMR EEYRKEGSPESMREEYRKEGSPESMREEYRKE	65 aa
19	YFP	PRGLRYQPLLRSGRISPAE	19 aa

Table 3.3: Amino acid sequences of initiation regions (i.e., tails) used in this study.

In presence of excess proteasome, thus under single turnover conditions, substrate with the longer tail was degraded rapidly, whereas that with a short tail remained stable (Fig 3.1b,c), as observed previously [42,104,116,117]. Assuming that the initiation region is too short to reach the pore loops in the substrate translocation channel, it is possible

that increasing the length of the ubiquitin chain would change how the substrate binds Ub/UBL receptors, perhaps positioning the short tail for productive engagement by the proteasome. However, increasing the length of the ubiquitin chain from five to nine ubiquitin moieties did not enhance degradation of the short-tail substrate (Fig 3.1d,e). Interestingly, the longer ubiquitin chain reduced degradation of the longer-tail substrate, a pattern observed in previous steady-state experiments [27]. Thus, extending the ubiquitin chain does not compensate for a short initiation region.

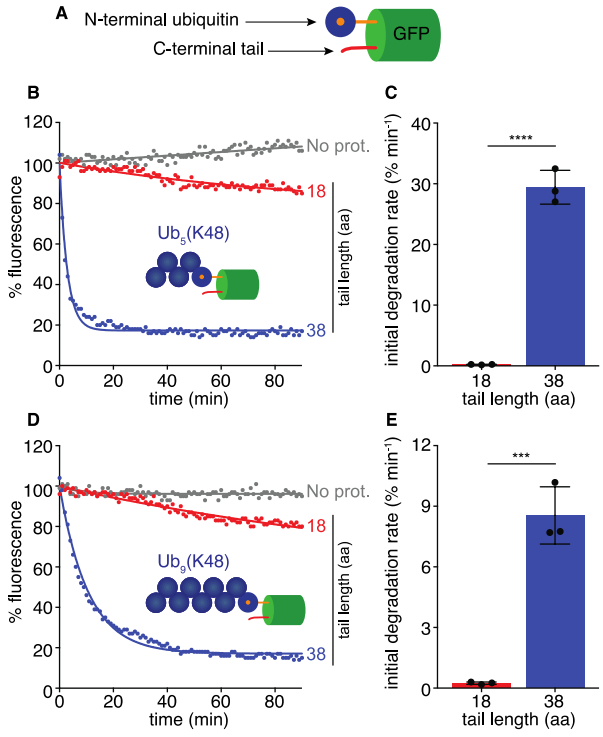

Figure 3.1: Ubiquitin chain length cannot compensate for initiation region length.

(M) Schematic of in vitro ubiquitinated model substrates. Substrates consist of an N-terminal in-frame ubiquitin domain (dark blue with orange center) that serves as the attachment point for ubiquitin chains of precise length, followed by a GFP domain (green), and a C-terminal initiation region referred to as a tail (red).

(N) In vitro degradation kinetics of Ub5(K48)-tagged GFP substrates with 18 (red) or 38 (blue) amino acid (aa) length tails under single turnover conditions (5 nM substrate,

25 nM wildtype proteasome) plotting substrate fluorescence as a percentage of the initial fluorescence as a function of time in minutes. No proteasome (no prot) control included.

(O) Initial degradation rates of substrates with the indicated tail from B calculated by fitting kinetics to single exponential decay.

(P) In vitro degradation kinetics of Ub9(K48)-tagged GFP substrates with 18 (red) or 38 (blue) amino acid (aa) length tails under single turnover conditions (5 nM substrate, 25 nM wildtype proteasome) plotting substrate fluorescence as a percentage of the initial fluorescence as a function of time in minutes.

(Q) Initial degradation rates of substrates with the indicated tail from D calculated by fitting kinetics to single exponential decay.

Data information: In (B,D), experiments were performed in triplicate, one representative kinetic experiment shown. In (C, E) data represent the mean from three experiments and error bars represent the standard deviations (SD). **** $P < 0.0001$ and *** $P < 0.001$ (two-tailed unpaired t test).
Proteasome types are described in Table 3.1.

Strain Name	**Genotype**	**Proteasome Label**
YYS40 *	*MAT α RPN11-FLAG::HIS3*	RP (wildtype)
YYS37 *	*MAT α PRE1-FLAG::HIS3*	CP
SY1962a	*MAT α RPN11-FLAG::HIS3 rpn1-AKAA-ARR::HGR rpn13-PRU::NATmx*	Rpn10
SY1961a	*MAT α RPN11-FLAG::HIS3 rpn1-AKAA-ARR::HGR rpn10-UIM::KANmx*	Rpn13
SY1572b	*MAT α RPN11-FLAG::HIS3 rpn10-UIM::KANmx rpn13-PRU::NATmx*	Rpn1
SY1960a	*MAT α RPN11-FLAG::HIS3 rpn1-AKAA-ARR::HGR rpn10-UIM::KANmx rpn13-PRU::NATmx UBP6-pADH1-Ub::URAmx*	QM (quadruple mutant)
BLS635	*MAT a RPN11-FLAG::HIS3 rpn1-AKAA-ARR:: rpn13::KANmx4*	Rpn10 (Rpn13Δ)

Table 3.1: Proteasome mutant yeast strains used in this study.

Moving the initiation region away from the ubiquitin chain

We then asked whether moving the tail further from the ubiquitin chain by altering the base substrate itself would increase degradation. We inserted stable α-helices of varying length between GFP and the tail to move the tail further from the ubiquitin chain (Fig 3.2a).

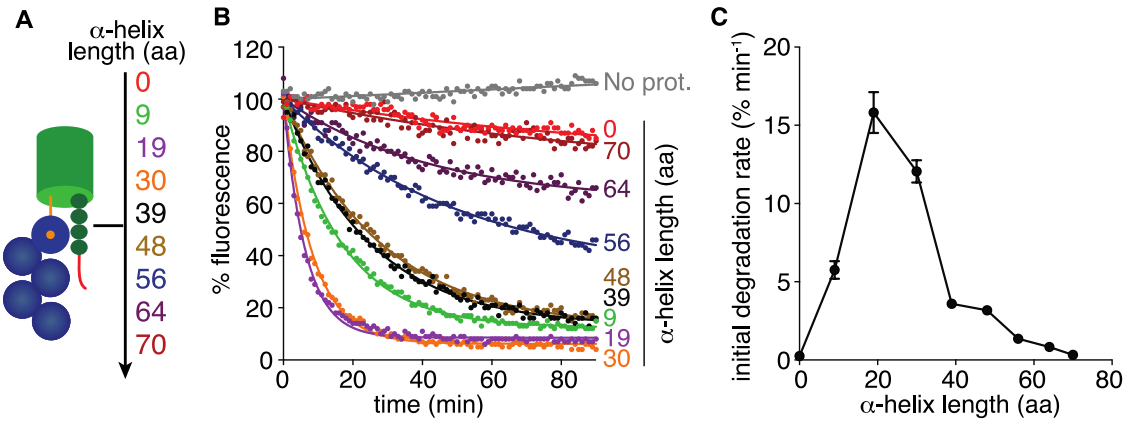

Figure 3.2: The initiation region must be placed at a distance from a ubiquitin chain to trigger efficient degradation.

(A) Schematic of *in vitro* ubiquitinated model spacing substrates. Substrates contain an N-terminal Ub_5(K48) tag (dark blue circles), a C-terminal 15 tail (red), and varying amino acid (aa) lengths of α-helices inserted between the GFP and tail (dark green circles). The amino acid lengths of the α-helices used are shown as numbers.

(B) *In vitro* degradation kinetics of spacing substrates from A under single turnover conditions (5 nM substrate, 25 nM wildtype (WT) proteasome) plotting substrate fluorescence as a percentage of the initial fluorescence as a function of time in minutes. The amino acid (aa) length of the α-helix is shown to the right of the corresponding curve.

(C) Initial degradation rates of substrates from B calculated by fitting kinetics to single exponential decay or linear equation. Graph plots the rate as a function of amino acid length of the α-helix.

Data information: In (B), experiments were performed in triplicate, one representative kinetic experiment shown. In (C) data are plotted as a mean calculated from at least three experiments +/- the SD.

These α-helices, referred to here as linkers, were derived from mouse myosin VI and were found to be stable even in isolation in the absence of stabilizing tertiary interactions [9,119]. Degradation of the substrates increased sharply with the addition of a linker of only 9 residues. Extension of the linker to 19 residues accelerated degradation further to its peak rate, after which lengthening the linker further to 30 residues or more suppressed degradation again. The linkers were not functioning as initiation regions since removing the tail inhibited degradation substantially (Fig 3.1.1a), presumably because the amino acid sequences of the linkers are charged and compositionally biased (Table 3.4), which prevents proteasomal recognition [9]. These results suggest that efficient degradation of a ubiquitinated substrate requires placing the initiation region at the right distance from the ubiquitin chain; as placing the ubiquitin chain too close or too far relative the initiation region strongly suppresses degradation.

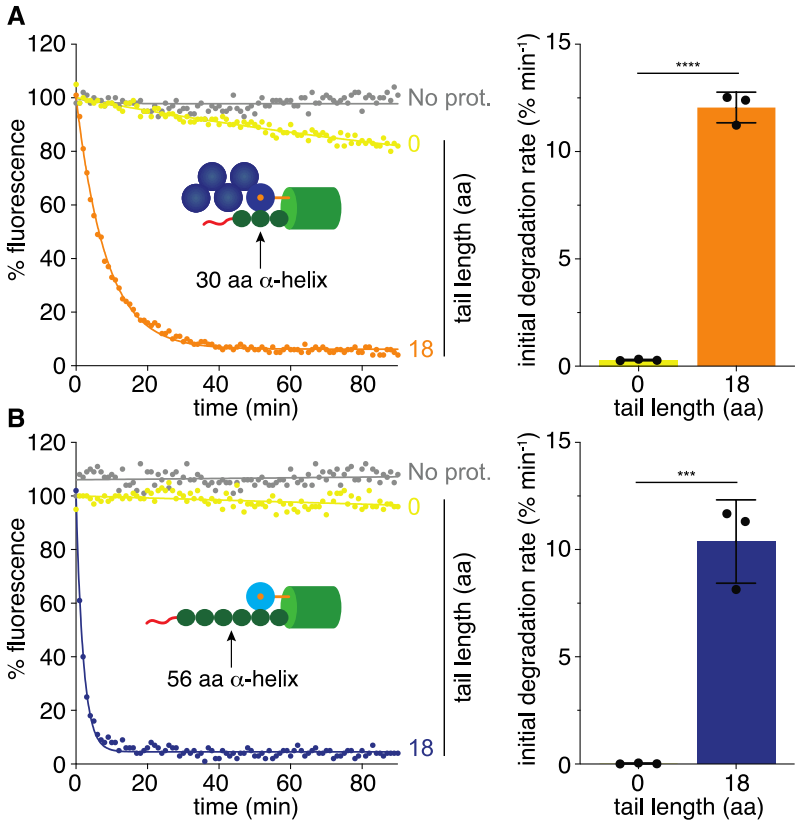

Figure 3.1.1: The α-helices do not function as effective initiation regions

(A) (Left) *In vitro* degradation kinetics of Ub_5(K48)-tagged GFP substrate with the 30 amino acid (aa) long α-helix linker and either a 15 (orange) or 0 aa length tail (yellow) under single turnover conditions (5 nM substrate, 25 nM wildtype (WT) proteasome). Substrate fluorescence is plotted as a percentage of the initial fluorescence as a function of time in minutes. No proteasome (no prot) control included. (Right) Initial degradation rates of substrates with the indicated tail calculated by fitting kinetics to single exponential decay.

(B) (Left) *In vitro* degradation kinetics of UBL-tagged GFP substrate with the 56 amino acid (aa) long α-helix linker and either a 15 tail (blue) or 0 aa length tail (yellow) under single turnover conditions (5 nM substrate, 25 nM WT proteasome). Substrate fluorescence is plotted as a percentage of the initial fluorescence as a function of time in minutes. (Right) Initial degradation rates of substrates with the indicated tail calculated by fitting kinetics to single exponential decay.

Data information: In (A,B), experiments were performed in triplicate, one representative kinetic experiment shown. In (A,B) rate data represent the means from three experiments and error bars represent the standard deviations (SD). **** $P < 0.0001$ and *** $P < 0.001$ (two-tailed unpaired t test).

Helix Identification	Amino Acid Sequence
α9	EEEERRRQQ
α19	EEEERRRQQEEEAERLRRI
α30	EEEERRRQQEEEAERLRRIQEEMERERRRR
α39	EEEERRRQQEEEAERLRRIQEEMERERRRREEDEERRRR
α48	EEEERRRQQEEEAERLRRIQEEMERERRRREEDEERRRREEEERRMRL
α56	EEEERRRQQEEEAERLRRIQEEMERERRRREEDEERRRREEEERRMRL EMEARRRQ
α64	EEEERRRQQEEEAERLRRIQEEMERERRRREEDEERRRREEEERRMRL EMEARRRQEEEERRRR
α70	EEEERRRQQEEEAERLRRIQEEMERERRRREEDEERRRREEEERRMRL EMEARRRQEEEERRRREDDERR

Table 3.4: Amino acid sequences of α-helices used in this study.

Degradation of model substrates mediated by specific proteasomal ubiquitin receptors

The three ubiquitin receptors of the RP are located at different distances and directions from the entrance to the substrate translocation channel, which houses the pore-1 loops responsible for engaging initiation regions (see discussion) [16,120–123]. Rpn10 is adjacent and closest to the translocation channel (65-95 Å from pore-1 loops), Rpn1 is located on the opposite side of the RP from Rpn10 (~100 Å from pore-1 loops), but at its outer surface furthest from the translocation channel, and Rpn13 is at the top of the RP at a somewhat shorter distance from the translocation channel than Rpn1 (~107 Å from pore-1 loops). Thus, the optimal linker length between ubiquitination site and

initiation region could be characteristic of the particular ubiquitin receptor, on the assumption that concurrent binding of the ubiquitin chain by the receptor and of the initiation region by the pore-1 loops is required for degradation. To test this model, we engineered proteasomes in which only a single identified receptor was functional, thereby limiting substrate binding to one receptor. Each receptor was mutated so as to specifically abolish ubiquitin binding, using well-characterized substitution mutants: Rpn10 in its UIM element (rpn10-UIM) [68]; Rpn13 in its PRU domain (rpn13-PRU) [56,58]; and Rpn1 in its T1 and T2 sites (rpn1-ARR-AKAA) [57]. Here we refer to proteasomes by the single receptor that retains Ub/UBL binding (Table 3.1). Proteasomes in which ubiquitin binding to all three receptors is attenuated are called Quadruple Mutant (QM).

Rpn10 and wildtype proteasomes degraded ubiquitinated substrates equally well (Compare Fig 3.3a and Fig 3.2b) suggesting that K48-linked ubiquitin chains targeted the substrates to degradation principally through Rpn10, consistent with previous findings [27]. Degradation was strongly reduced on Rpn13 proteasome (Fig 3.3b), Rpn1 proteasome (Fig 3.3c), and QM proteasome (Fig 3.3d), though not completely abolished. The narrow width of the peak in degradation rates (Fig 3.3a) relative to linker length seen for degradation mediated by Rpn10 suggests that the spacing requirements are surprisingly well defined, considering that the UIM is thought to be flexibly connected to the proteasome. In the absence of Rpn10 Ub/UBL binding, the residual degradation appears less dependent on the linker length and spacing, perhaps because the residual degradation is mediated by multiple receptors with differing linker length optimal [124–126].

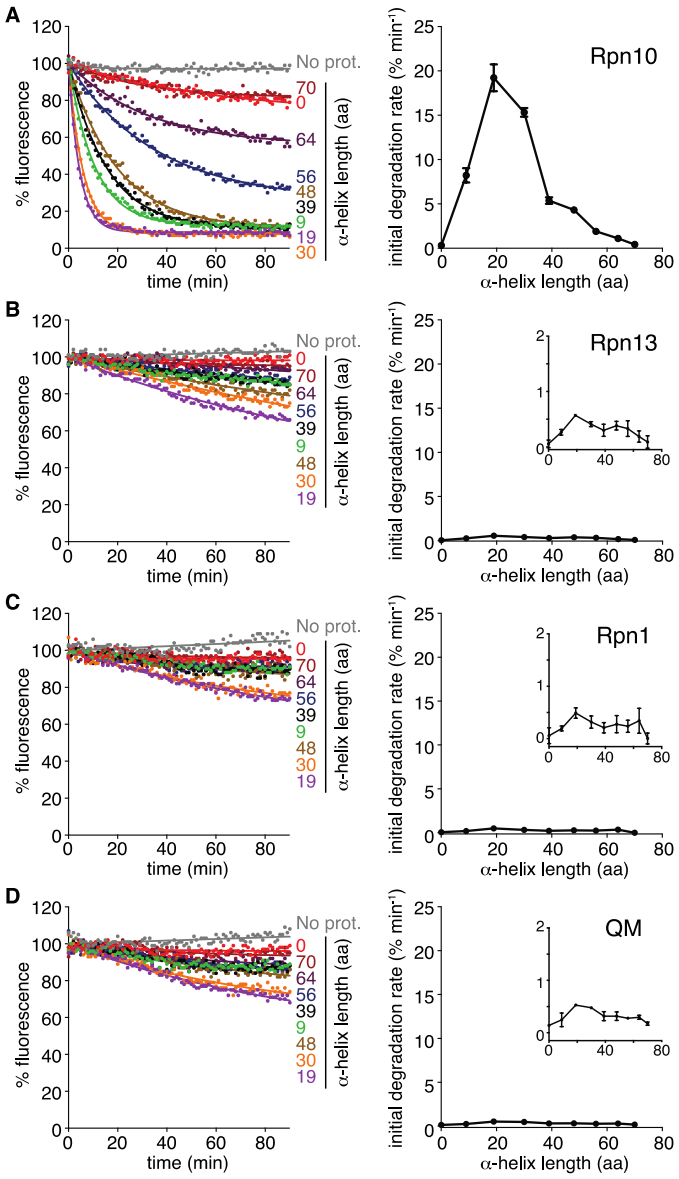

Figure 3.3: Optimal spacer lengths of proteasomal ubiquitin receptors

(A-D) (Left) *In vitro* degradation kinetics of ubiquitinated model spacing substrates under single turnover conditions (5 nM substrate, 25 nM proteasome) by the indicated proteasome receptor mutant (Rpn10, Rpn13, Rpn1, QM). Graphs plot substrate fluorescence as a percentage of the initial fluorescence as a function of time in minutes. The amino acid (aa) length of the α-helix is shown to the right of the corresponding curve. (Right) Initial degradation rates of ubiquitinated spacing substrates from the left

calculated by fitting kinetics to single exponential decay or linear equation. Graphs plot the rate as a function of amino acid length of the α-helix.
Data information: In (A-D, left), experiments were performed in triplicate, one representative kinetic experiment shown. In (A-D), rate data are plotted as a mean calculated from at least three experiments +/- the SD.
Proteasome types are described in Table 3.1.

Degradation of model substrates with an UBL tag

UBL-UBA proteins are thought to function as extrinsic substrate receptors, and there are three in yeast (Rad23, Dsk2, Ddi1) [56–60,68,111–114]. They can bind all three ubiquitin receptors of the proteasome through their UBL domain and bind ubiquitin chains through their UBA domains. To investigate degradation of substrates targeted to the proteasome via UBL-UBA proteins while bypassing the complexities of protein complex formation, we fused the UBL domain from yeast Rad23 directly to the N-terminus of GFP, and appended tails of 18 or 96 amino acids in length to the C-terminus (Fig 3.4a) (Table 3.3). As observed for substrate with ubiquitin chains, UBL substrate with the short tail resisted degradation whereas substrate with the longer tail was degraded readily (Fig 3.4b,c). We again moved the short tail away from the UBL tag by inserting linkers of increasing length after the GFP domain. At first, degradation accelerated slowly with linker length, but then increased sharply, peaking with a 56 residue linker, before decreasing again (Fig 3.4e,f). The linkers themselves did not allow the proteasome to engage the substrates as shown by control experiments in which removing the tail inhibited degradation (Fig 3.1.1b).

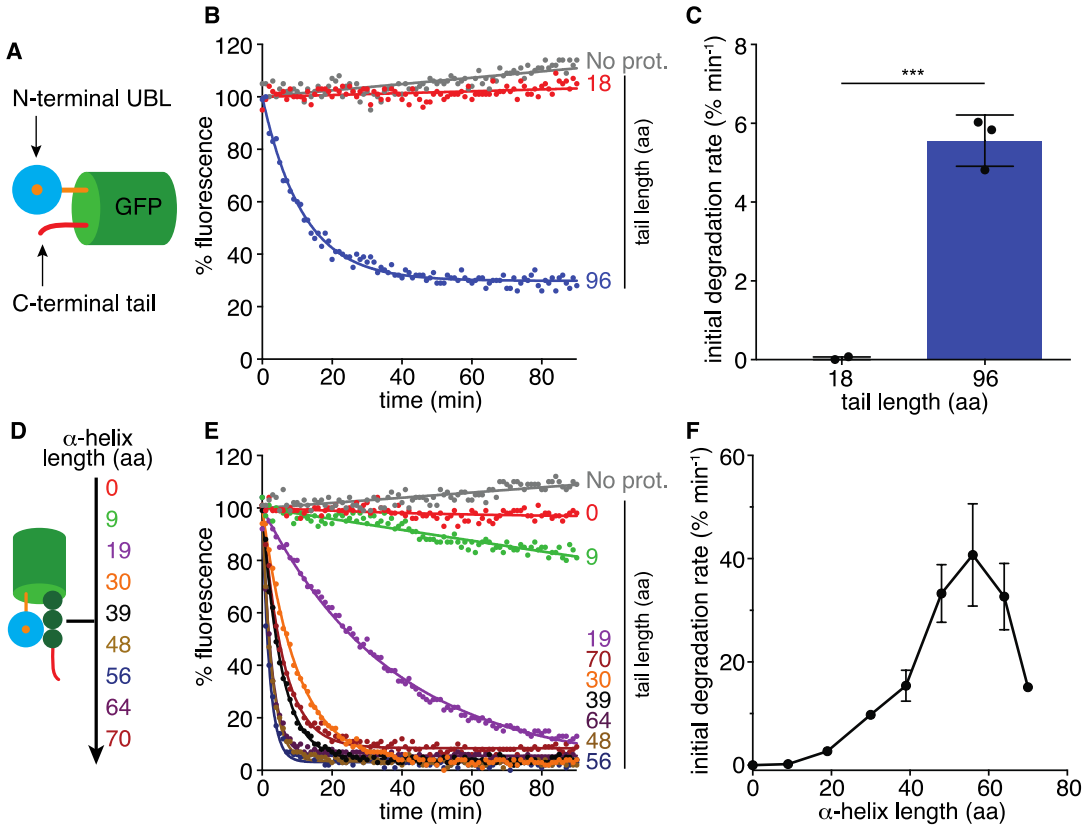

Figure 3.4: Optimal spacer length of UBL-tagged substrates is much longer than that of ubiquitin-tagged substrates

(A) Schematic of *in vitro* UBL model substrates. Substrates consist of the UBL domain of *S. cerevisiae* Rad23 (cyan with orange center) at the N-terminus, followed by a GFP domain (green), and a tail (red) at the C-terminus.

(B) *In vitro* degradation kinetics of UBL-tagged GFP substrates with 18 (red) or 96 (blue) amino acid (aa) length tails under single turnover conditions (5 nM substrate, 25 nM wildtype (WT) proteasome) plotting substrate fluorescence as a percentage of the initial fluorescence as a function of time in minutes.

(C) Initial degradation rates of substrates with the indicated tail from B calculated by fitting kinetics to single exponential decay.

(D) Schematic of *in vitro* UBL model spacing substrates. Substrates contain an N-terminal UBL tag (cyan circle), a C-terminal 18 tail (red), and varying amino acid (aa) lengths of α-helices inserted between the GFP and tail (dark green circles). The amino acid lengths of the α-helices used are shown as numbers.

(E) *In vitro* degradation kinetics of spacing substrates from E under single turnover conditions (5 nM substrate, 25 nM WT proteasome) plotting substrate fluorescence as a percentage of the initial fluorescence as a function of time in minutes. The amino acid length of the α-helix is shown to the right of the corresponding curve.
(F) Initial degradation rates of substrates from E calculated by fitting kinetics to single exponential decay. Graph plots the rate as a function of amino acid length of the α-helix.
Data information: In (B,E), experiments were performed in triplicate, representative kinetic experiment shown. In (C), data represent the means calculated from three experiments. Error bars represent the standard deviations (SD). *** $P < 0.001$ (two-tailed unpaired t test). In (F), data are plotted as a mean calculated from at least three experiments +/- the SD.

Degradation of UBL substrates required greater distance between the two parts of the degradation signal than the ubiquitin substrates. It also proceeded largely through different Ub/UBL receptors. Substrates with the UBL domain were degraded equally well on Rpn13 and wildtype proteasome (compare Fig 3.4e,f and Fig 3.5b), as expected [27], and degradation was strongly reduced on Rpn10 (Fig 3.5a) and QM (Fig 3.5d) proteasomes. The slow degradation by Rpn10 proteasome (Fig 3.5a) appeared to be mostly through residual binding to the mutated Rpn13, because deleting the Rpn13 subunit entirely in the Rpn10 proteasome (i.e., Rpn10 (Rpn13Δ)) reduced degradation further (Fig 3.1.2). The remaining degradation by Rpn10 (Rpn13Δ) proteasome was likely due to the UBL domain binding the proteasome elsewhere because replacing the UBL domain with a protein of similar size but unrelated in sequence (Barstar) stabilized the substrate completely, even when all Ub/UBL binding sites were functional in wildtype proteasome (Fig 3.1.3). In comparison, Rpn1 proteasome degraded the UBL substrates almost as well as Rpn13 proteasome (Fig 3.5c), suggesting that Rpn1 can also serve as a UBL receptor for degradation. Degradation through Rpn13 and Rpn1 changed with separation between UBL domain and tail in similar ways, likely because the two receptors are located at similar distances from the pore-1 loops.

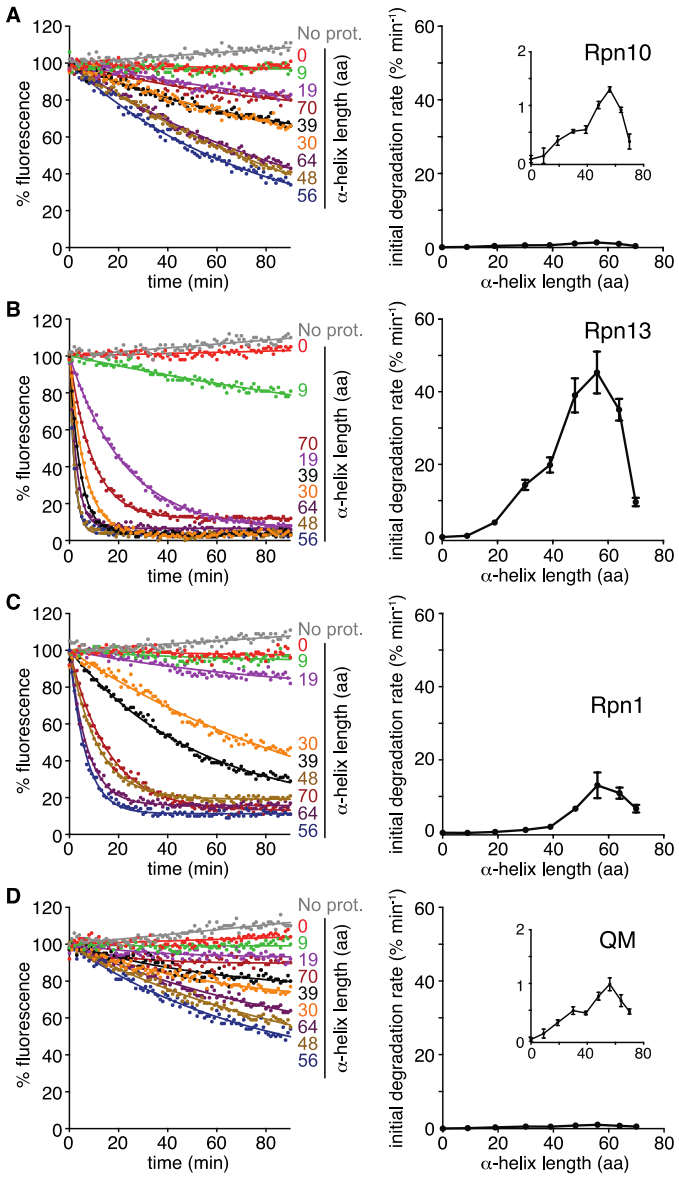

Figure 3.5: Degradation of UBL-tagged spacing substrates by proteasome receptor mutants reveals a preference for Rpn13

(A-D) (Left) *In vitro* degradation kinetics of UBL spacing substrates under single turnover conditions (5 nM substrate, 25 nM proteasome) by the indicated proteasome receptor mutant (Rpn10, Rpn13, Rpn1, QM). Graphs plot substrate fluorescence as a percentage of the initial fluorescence as a function of time in minutes. The amino acid (aa) length of the α-helix is shown to the right of the corresponding curve. (Right) Initial degradation rates of UBL spacing substrates calculated by fitting degradation kinetics to

single exponential decay or linear equation. Graphs plot the rate as a function of amino acid length of the α-helix.
Data information: In (A-D, left), experiments were performed in triplicate, one representative kinetic experiment shown. In (A-D, right), rate data are plotted as a mean calculated from at least three experiments +/- the SD.
Proteasome types are described in Table 3.1.

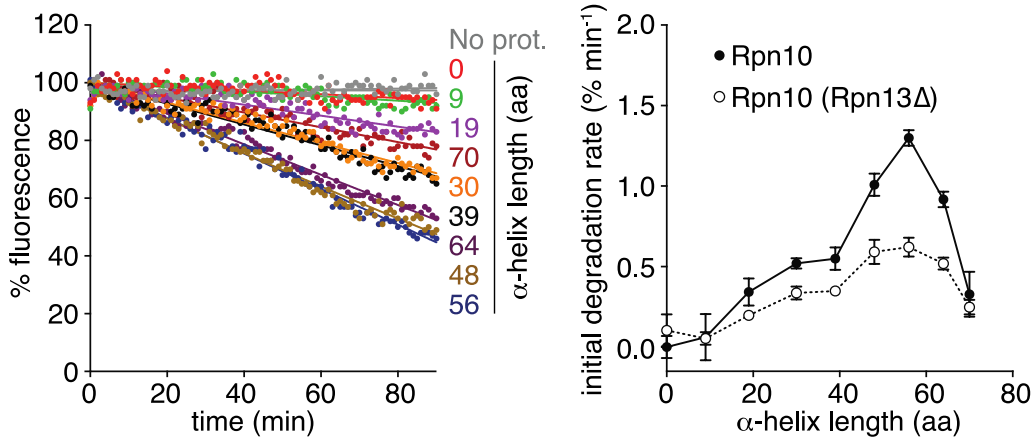

Figure 3.1.2: Degradation of UBL-tagged spacing substrates on Rpn10 only proteasome is due to residual binding to mutated Rpn13

(Left) *In vitro* degradation kinetics of UBL spacing substrates under single turnover conditions (5 nM substrate, 25 nM proteasome) by Rpn10(*Rpn13*Δ) proteasome. Graph plots substrate fluorescence as a percentage of the initial fluorescence as a function of time in minutes. The amino acid (aa) length of the α-helix is shown to the right of the corresponding curve. (Right) Initial degradation rates of UBL spacing substrates by the indicated proteasome were calculated by fitting kinetics to single exponential decay or linear equation. Graph plots the rate as a function of aa length of the α-helix.
Data information: experiments were performed in triplicate, one representative kinetic experiment shown. Rate data are plotted as a mean calculated from at least three experiments +/- the SD.
Proteasome types are described in Table 3.1.

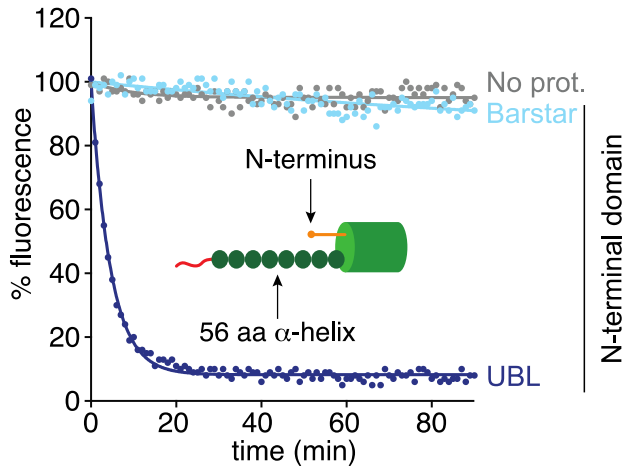

Figure 3.1.3: Degradation of UBL-tagged substrate is due to UBL binding the proteasome

In vitro degradation kinetics of model GFP substrates with the 56 amino acid (aa) length α-helix, 18 tail, and the indicated N-terminal domain under single turnover conditions (5 nM substrate, 25 nM wildtype (WT) proteasome). Graph plots substrate fluorescence as a percentage of the initial fluorescence as a function of time in minutes. The N-terminal domain is shown to the right of the corresponding curve.
Data information: experiment was performed in triplicate, one representative kinetic experiment shown.

Degradation of model substrates in yeast

We asked next whether the distance between the proteasome-binding tags and the initiation region also controlled degradation in cells. We expressed model substrates analogous to those used in the in vitro experiments, alongside a stable red fluorescent reference protein and followed degradation by monitoring the fluorescence signals originating from the substrate and reference protein in single yeast cells by flow cytometry. We measured degradation rates by stopping protein synthesis with cycloheximide and monitored steady state accumulation by calculating the ratio of substrate fluorescence to reference protein fluorescence, as done previously [9,118]. The

yeast model substrates contained YFP instead of GFP and the UBL substrates were otherwise identical (Fig 3.6c). The ubiquitinated substrates differed further as ubiquitination was induced by an N-end degron attached to the N-terminus [87,127] and so ubiquitin chains were attached on Lys residues in a 14-residue N-terminal tail attached to the YFP domain (Fig 3.6a). Nevertheless, degradation proceeded from the C-terminal tail as replacing a tail that is well recognized by the proteasome (Su9) with a tail that is poorly recognized (SP25) inhibited degradation (Fig. 3.1.4a) [9]. Degradation of the ubiquitinated substrate depended on UBR1, which encodes the N-end rule E3, and neither ubiquitin nor UBL substrate relied on the autophagy machinery (Fig 3.1.4b).

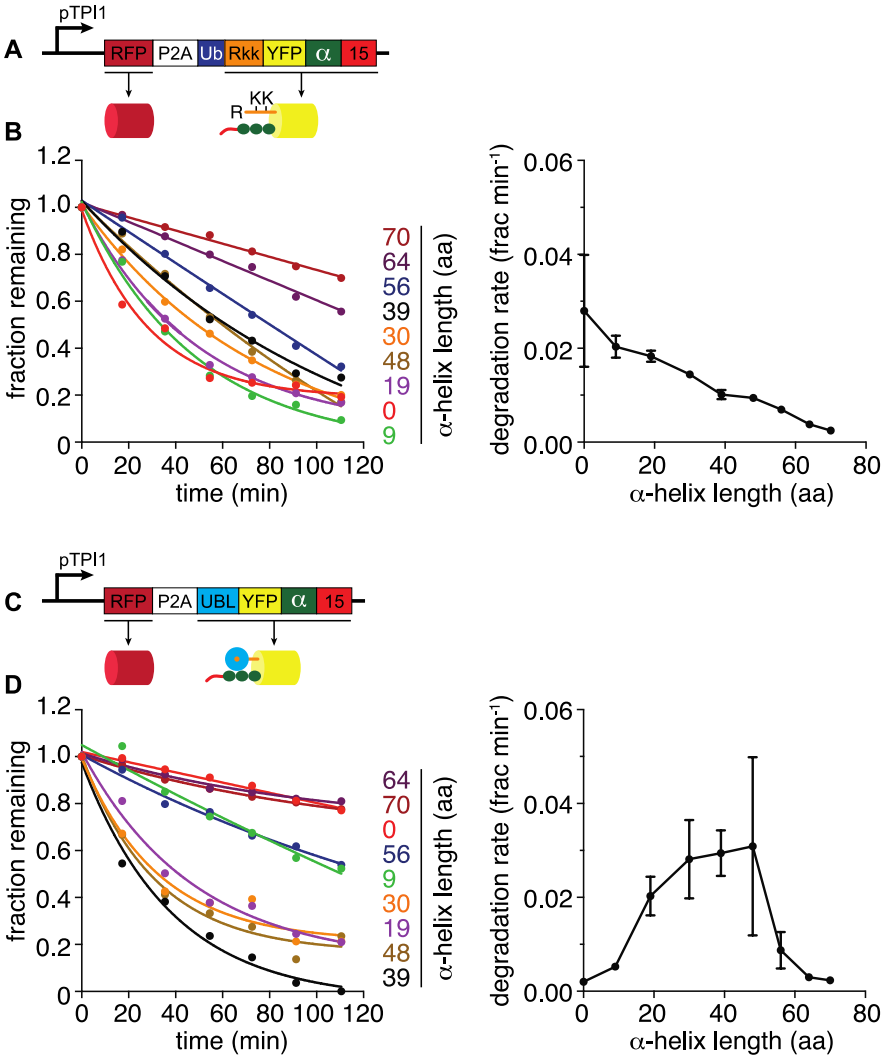

Figure 3.6: Observation of spacing differences in vivo

(A,C) Substrate design of fluorescence-based degradation assay in *S. cerevisiae*. DsRedExpress2 (RFP), followed by a ribosome skipping sequence (P2A), and model YFP substrate are expressed from a single promoter (pTPI1) to ensure equal production of the RFP reference protein and the YFP model substrates.
(A) Ubiquitinated model substrates consist of an N-terminal in-frame ubiquitin domain (dark blue), followed by a modified N-end rule degron Rkk (orange), YFP (yellow), and a C-terminal tail (red). Upon expression in yeast, the ubiquitin domain is cleaved by ubiquitin hydrolases, exposing the modified N-end rule degron Rkk. Ubiquitin ligases recognize the degron and then ubiquitinate the lysine residues within the Rkk, which targets the substrate to the proteasome.

(C) UBL model substrates consist of the UBL domain of *S. cerevisiae* Rad23 (cyan with orange center) at the N-terminus, followed YFP, and a C-terminal tail (red).
(B,D) Yeast cells were treated with 125 µM cycloheximide to inhibit protein synthesis and YFP fluorescence was measured roughly every 20 minutes for approximately 120 minutes.
(B) (Left) *In vivo* degradation kinetics of ubiquitinated YFP spacing substrates. Fluorescence plotted as a fraction of the initial fluorescence as a function of time and fitted to a single exponential decay or linear equation to calculate degradation rates. The amino acid (aa) length of the α-helix is shown to the right of the corresponding curve. (Right) Initial degradation rates of ubiquitinated YFP spacing substrates calculated by fitting degradation kinetics to single exponential decay or linear equation. Graph plots the rate as a function of amino acid length of the α-helix
(D) (Left) *In vivo* degradation kinetics of UBL YFP spacing substrates. (Right) Initial degradation rates of UBL YFP spacing substrates calculated by fitting degradation kinetics to single exponential decay or linear equation. Graph plots the rate as a function of amino acid length of the α-helix
Data information: In (B,D), experiments were performed in triplicate, one representative kinetic experiment shown. Degradation rate data are plotted as a mean calculated from at least three experiments +/- the SD
Yeast strains are described in Table 3.5.

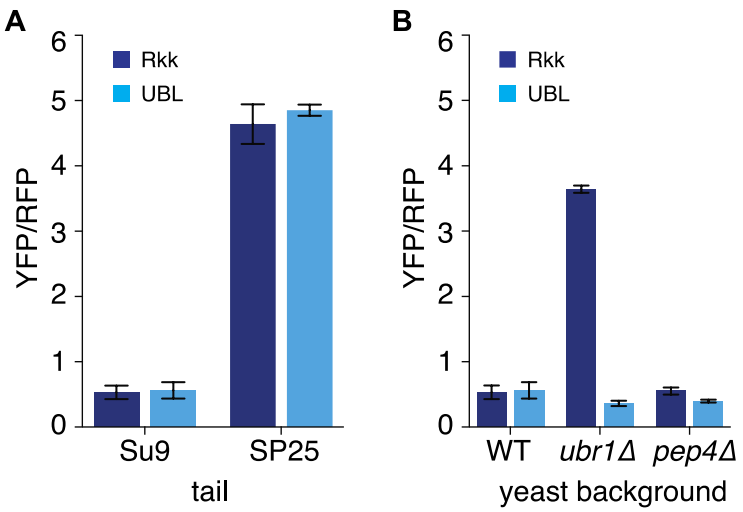

Figure 3.1.4: Model YFP proteins are proteasome substrates and degraded in a ubiquitin-dependent and autophagy-independent manner

(A) Corrected medians of cellular YFP fluorescence (median YFP/RFP values) representing steady-state degradation of yeast cultures expressing YFP substrates

targeted to the proteasome through an N-end degron (Rkk, dark blue) or UBL domain (cyan) with Su9 or SP25 tail. Proteasome substrates were expressed in the genetic background *by4741* (WT, wild type)

(B) Corrected medians of cellular YFP fluorescence (median YFP/RFP values) representing steady-state degradation of yeast cultures expressing YFP substrates targeted to the proteasome through an N-end degron (Rkk, dark blue) or UBL domain (cyan) with Su9 tail. Proteasome substrates were expressed in the genetic background *by4741* with no additional mutations (WT, wild type), the open reading frame of UBR1 deleted (*ubr1*Δ) to abolish ubiquitination by the N-end rule pathway, or the open reading frame of PEP4 deleted (*pep4*Δ) to reduce proteolytic activity involved in autophagy.

Data information: experiments were performed in triplicate. YFP/RFP ratios are plotted as a mean calculated from at least three experiments +/- the SD.
Yeast strains are described in Table 3.5.

Strain Name	**Genotype**
JBK 001	MATa ho::natMX6_pTPI1_DsRed_P2A_Ub-Rkk_N10SRR-Cd20-sYFP-19-His6_tADH his3Δ1 leu2Δ0 met15Δ0 ura3Δ0
JBK 002	MATa ho::natMX6_pTPI1_DsRed_P2A_Ub-Rkk_N10SRR-Cd20-sYFP-ahelix09-19-His6_tADH his3Δ1 leu2Δ0 met15Δ0 ura3Δ0
JBK 005	MATa ho::natMX6_pTPI1_DsRed_P2A_Ub-Rkk_N10SRR-Cd20-sYFP-ahelix19-19-His6_tADH his3Δ1 leu2Δ0 met15Δ0 ura3Δ0
JBK 006	MATa ho::natMX6_pTPI1_DsRed_P2A_Ub-Rkk_N10SRR-Cd20-sYFP-ahelix30-19-His6_tADH his3Δ1 leu2Δ0 met15Δ0 ura3Δ0
JBK 003	MATa ho::natMX6_pTPI1_DsRed_P2A_Ub-Rkk_N10SRR-Cd20-sYFP-ahelix39-19-His6_tADH his3Δ1 leu2Δ0 met15Δ0 ura3Δ0
JBK 004	MATa ho::natMX6_pTPI1_DsRed_P2A_Ub-Rkk_N10SRR-Cd20-sYFP-ahelix48-19-His6_tADH his3Δ1 leu2Δ0 met15Δ0 ura3Δ0
JBK 007	MATa ho::natMX6_pTPI1_DsRed_P2A_Ub-Rkk_N10SRR-Cd20-sYFP-ahelix56-19-His6_tADH his3Δ1 leu2Δ0 met15Δ0 ura3Δ0
JBK 008	MATa ho::natMX6_pTPI1_DsRed_P2A_Ub-Rkk_N10SRR-Cd20-sYFP-ahelix64-19-His6_tADH his3Δ1 leu2Δ0 met15Δ0 ura3Δ0
JBK 009	MATa ho::natMX6_pTPI1_DsRed_P2A_Ub-Rkk_N10SRR-Cd20-sYFP-ahelix70-19-His6_tADH his3Δ1 leu2Δ0 met15Δ0 ura3Δ0
JBK 010	MATa ho::natMX6_pTPI1_DsRed_P2A_Rad23-sYFP-19-His6_tADH his3Δ1 leu2Δ0 met15Δ0 ura3Δ0
JBK 011	MATa ho::natMX6_pTPI1_DsRed_P2A_Rad23-sYFP-ahelix09-19-His6_tADH his3Δ1 leu2Δ0 met15Δ0 ura3Δ0
JBK 012	MATa ho::natMX6_pTPI1_DsRed_P2A_Rad23-sYFP-ahelix19-19-His6_tADH his3Δ1 leu2Δ0 met15Δ0 ura3Δ0
JBK 013	MATa ho::natMX6_pTPI1_DsRed_P2A_Rad23-sYFP-ahelix30-19-His6_tADH

	his3Δ1 leu2Δ0 met15Δ0 ura3Δ0
JBK 014	MATa ho::natMX6_pTPI1_DsRed_P2A_Rad23-sYFP-ahelix39-19-His6_tADH his3Δ1 leu2Δ0 met15Δ0 ura3Δ0
JBK 015	MATa ho::natMX6_pTPI1_DsRed_P2A_Rad23-sYFP-ahelix48-19-His6_tADH his3Δ1 leu2Δ0 met15Δ0 ura3Δ0
JBK 016	MATa ho::natMX6_pTPI1_DsRed_P2A_Rad23-sYFP-ahelix56-19-His6_tADH his3Δ1 leu2Δ0 met15Δ0 ura3Δ0
JBK 017	MATa ho::natMX6_pTPI1_DsRed_P2A_Rad23-sYFP-ahelix64-19-His6_tADH his3Δ1 leu2Δ0 met15Δ0 ura3Δ0
JBK 018	MATa ho::natMX6_pTPI1_DsRed_P2A_Rad23-sYFP-ahelix70-19-His6_tADH his3Δ1 leu2Δ0 met15Δ0 ura3Δ0
BLS 623	MATa [pBLS005] his3Δ1 leu2Δ0 met15Δ0 ura3Δ0
BLS 742	MATa [pBLS005] pep4::kanMX4 his3Δ1 leu2Δ0 met15Δ0 ura3Δ0
BLS 746	MATa [pBLS005] ubr1::kanMX4 his3Δ1 leu2Δ0 met15Δ0 ura3Δ0
BLS 613	MATa [pBLS137] his3Δ1 leu2Δ0 met15Δ0 ura3Δ0
BLS 744	MATa [pBLS137] pep4::kanMX4 his3Δ1 leu2Δ0 met15Δ0 ura3Δ0
BLS 748	MATa [pBLS137] ubr1::kanMX4 his3Δ1 leu2Δ0 met15Δ0 ura3Δ0
BLS 611	MATa [pBLS138] his3Δ1 leu2Δ0 met15Δ0 ura3Δ0
BLS 617-1	MATa [pBLS047] his3Δ1 leu2Δ0 met15Δ0 ura3Δ0

Table 3.5: Yeast strains used in this study. All strains made for this study

In yeast, degradation was most effective when the tail and ubiquitination site were placed next to each other, and degradation was faster for substrate without an additional linker inserted after the YFP domain, and gradually decreased as linker length increased (Fig 3.6b). In vitro degradation was most efficient with a linker of 19 residues inserted after the fluorescent protein (Fig 3.2c) but note that the N-end degron used in the yeast substrates inserts eleven unstructured residues before the fluorescent domain, which may function similarly to the short linkers used in the in vitro model substrates by positioning the tail a bit further from the ubiquitination site. The geometry of the ubiquitin chain in the two substrates also differs in the attachment point itself, where the chain is attached to a Lys residue in a folded domain in vitro and to Lys residue in an unstructured region in yeast.

Substrates targeted to the proteasome with a UBL domain were poorly degraded without a linker (Fig 3.6d) and degradation rates steadily improved as linker length increased until it plateaued, and then sharply decreased as linkers were lengthened past 56 residues. Substrates with very long linkers were degraded as poorly as substrate lacking any linker. Thus, degradation of UBL substrates in cells again followed the same pattern as in vitro. Degradation in yeast was somewhat more tolerant to separation and proceeded similarly well with linkers between 19 and 56 residues in length, roughly translated to 28.5 and 84 Å in length, respectively.

DISCUSSION

Controlling protein concentration through the precisely targeted degradation via the UPS is central to the regulation of many processes such as cell cycle progression, DNA repair, signaling cascades, and others. The proteasome must be able to degrade almost any protein but do so in a highly selective manner. Proteasomal degradation requires localization of the target protein to the proteasome, typically through a ubiquitin chain conjugated to the target protein, as well as a disordered region within the target protein of appropriate length and amino acid composition [2,7,15,69]. However, ubiquitination is also involved in regulating nonproteolytic processes [128], and intrinsically disordered regions are found throughout the entire proteome. Therefore, if ubiquitination and the existence of a disordered region were the only requirements for proteasomal degradation, most cellular proteins could be subject to proteasomal degradation at any given time. Instead, proteins can escape degradation, even with ubiquitin modifications and disordered regions, suggesting the degradation-targeting code is more nuanced than currently defined [27,117]. Here, we investigated a steric requirement for the degradation signal in proteasomal degradation.

We find that the position of the ubiquitin modification in a protein relative to the initiation region modulates its degradation in vitro and in yeast. The reason is likely found in the structure of the proteasome itself and the location of the ubiquitin binding receptors on the proteasome relative to the ATPase ring, where disordered initiation regions are inserted and physically engaged by the pore-1 loops. Previous biochemical studies show initiation regions must be of a certain minimal length to target for degradation [8,9,42,116–118,129]. For instance, C-terminal initiation regions must be approximately 30 residues in length for effective degradation [15,42,116,117]. We find here that shorter initiation regions can trigger degradation if they are placed the required distance from a proteasome-binding tag. Thus, substrate degradation can be controlled by the spatial arrangement of the proteasome-binding tag and the initiation region on a protein.

Ancillary cellular factors such as UBL-UBA proteins and Cdc48 are believed to function in the UPS [130–132]. UBL-UBA proteins are thought to shuttle substrates to the proteasome by binding ubiquitin chains and the proteasome through their UBA domain(s) and UBL domain, respectively [26,68,106–108,113–115,132,133]. The UBL and UBA domain(s) are connected through long flexible linkers, which likely allow the domains, and any bound proteins, to explore many orientations relative to each other, contrasting the relative spatial rigidity of the Ub/UBL receptors and pore-1 loop positions on the proteasome [8,134]. Thus, UBL-UBA proteins could loosen the strict initiation region and ubiquitin chain spacing requirements observed in vitro by positioning of substrates so that disordered regions are close to the entrance to the substrate channel and the pore-1 loops. Cdc48, a homohexameric AAA+ ATPase, is thought to work upstream of the proteasome by unfolding proteins prior to delivery to the proteasome [135,136]. Thus, in effect Cdc48 could lengthen the initiation region in substrates, allowing it to

reach the pore-1 loops regardless of the placement of the ubiquitin chain in the folded state of the substrate protein.

Degradation of the fluorescent model substrates with different linkers followed similar patterns in vitro and in yeast (Figs 3.2, 3.4, and 3.6). The ubiquitin-dependent substrates both showed fastest degradation when the ubiquitin chain was close to the initiation region, whereas UBL substrates were degraded best when the initiation region was placed further from the UBL domain. The degradation profiles did differ in the details, most notably for the ubiquitinated substrates in which the constructs differed in the attachment sites of the ubiquitin chains. In addition, the peaks in degradation rates were noticeably broader in yeast than in vitro. Nevertheless, the fact that degradation of the substrates investigated here follows similar patterns in vitro and in yeast suggests that they interact directly with the proteasome, bypassing the accessory factors discussed above. We suspect that UBL-UBA proteins and Cdc48 did not recognize the model substrates because of some property of the ubiquitin chains such as their length [137], linkage, or branching pattern [28,64], or because they were not localized to the same subcellular location [138]. The mechanism by which such extrinsic cellular factors contribute to degradation of some natural proteins requires further investigation.

The Ub/UBL binding sites of Rpn13 and Rpn1 are approximately 107 Å and 100 Å away from the pore loops, which must engage the initiation region for degradation to proceed. The Ub/UBL binding site of Rpn10 has not been resolved, but the last resolved residue of the proteasome docked VWA domain of Rpn10 is 95 Å away from the pore-1 loops. The Ub/UBL binding domain is connected to the VWA domain by a flexible 20 amino acid long linker [110], which may allow the Ub/UBL binding domain to approach the pore-1 loops and decrease the separation by some 30 Å. Substrates targeted to the proteasome by K48 linked ubiquitin chains are recognized primarily through Rpn10 and

are degraded most rapidly when the ubiquitin chain is close to the initiation region. Substrates targeted to the proteasome by UBL domains are primarily recognized by Rpn13 and degraded most rapidly when the UBL domain is placed further from the initiation region compared to substrates with K48 linked ubiquitin chains. Thus, substrates targeted to the proteasome by ubiquitin chains and UBL domains require very different arrangements of proteasome-binding tag and initiation region for rapid degradation, probably because their Ub/UBL receptors on the proteasome are positioned at different distances form the pore-1 loops (Fig. 3.7).

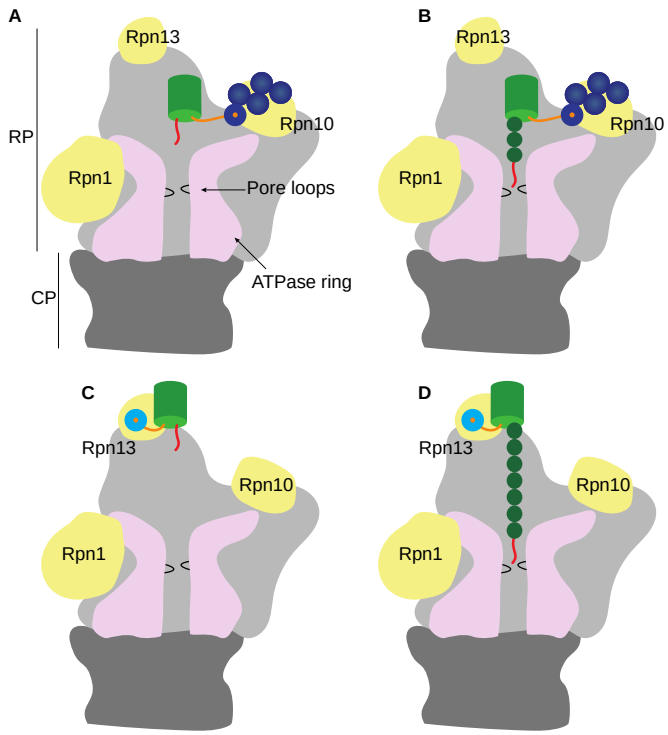

Figure 3.7: Model illustrating how position of initiation region relative to a proteasome-binding tag modulates engagement by the proteasome

(A-D) Cartoon of the proteasome highlighting the three known ubiquitin receptors (yellow) and the pore loops within the translocation channel formed by the ATPase ring

(pink) of the RP. Substrates with variously arranged proteasome-binding tag and initiation region (red) superimposed on proteasome. Ubiquitin chains shown in dark blue and UBL domain shown in cyan.

(A) The initiation region of a ubiquitinated substrate is unable to reach the pore loops when bound to Rpn10.

(B) Degradation of substrate from A can be achieved when the initiation region is placed a short distance from the ubiquitin chain and by proxy Rpn10.

(C) The initiation region of a substrate targeted to the proteasome through a UBL domain is unable to reach the pore loops when bound to Rpn13.

(D) Degradation of substrate from C can be achieved when the initiation region is placed a far distance from the UBL domain and by proxy Rpn13.

The previously underappreciated importance of steric requirements in proteasome-mediated degradation has the potential to improve design of therapeutics that utilize the proteasome. Inducible degradation of endogenous cellular proteins has potential to address otherwise undruggable targets, offering new therapeutic applications [139–141]. PROTACs (PROteolysis-TArgeting Chimeras) are small heterobifunctional molecules that induce the degradation of a protein of interest (POI) through the UPS by combining an E3 ubiquitin ligase binding part and a POI binding part in the same molecule connected by a short linker [142,143]. Ubiquitination is induced when a PROTAC brings together the E3 ligase and the POI, leading to the POI's ubiquitination and degradation by the proteasome. Although there are more than 600 E3 ligases in humans, only a handful of E3 ligases have been successfully leveraged by PROTACs to induce protein degradation. In some cases, PROTACs fail to induce degradation even when they are found to bind to both E3 and POI [39,144]. For example, a PROTAC recruiting the E3 ligase VHL was unable to induce the degradation of nonreceptor tyrosine kinases c-Abl and Arg despite formation of a stable ternary complex in cell extracts [144]. It is possible that the PROTACs formed complexes between E3s and POIs but either failed to successfully ubiquitinate the target, or that ubiquitination was

successful but led to the placement of the ubiquitin chain in a position that did not allow the proteasome to engage a disordered region in the POI when bound to a ubiquitin receptor on the proteasome. Therefore, keeping this limitation in mind could improve the design of PROTACs and expand the landscape of PROTAC-based therapies.

Taken together, our data demonstrate that the proteasome can effectively degrade substrates with short initiation regions if they are positioned a certain distance from a ubiquitin chain. Moreover, this distance depends on which ubiquitin receptor mediates substrate recognition, likely due to the distance of the ubiquitin receptor to the pore loops which engage the initiation region. Our findings suggest that the ubiquitin chain and disordered region of substrates must be spatially compatible with the architecture of the proteasome to permit their productive engagement and degradation, and may explain why some proteins with a ubiquitin chain and initiation region are not successfully degraded by the proteasome. Understanding the mechanistic constraints that apply to the degradation-targeting signal and its relationship to the architecture of the proteasome sheds light on how the proteasome achieves highly precise substrate selection to maintain cellular functioning. At the same time, two targeting mechanisms with different structural requirements acting in tandem may provide a more robust proteasome function in the face of a highly heterogenous pool of substrates.

MATERIALS AND METHODS

Molecular Biology

In Vitro Substrate Proteins

Ub-GFP-tail and UBL-GFP-tail fusion constructs were described previously [27]. Ubiquitin containing constructs, from N- to C-terminus, consist of the coding sequence

for S. cerevisiae ubiquitin (Ub) with a G76V mutation, a GSGGSG linker, A. victoria circular permutant of superfolder GFP (CP8), a G linker, the first 15 or 35 amino acids from S. cerevisiae cytochrome b2 with lysine residues replaced by arginine, and a 6xHis tag. Ubiquitin-like domain (UBL) containing constructs were made by replacing the Ub coding region of the Ub-GFP-tail constructs with the first 80 amino acids of S. cerevisiae Rad23. UBL constructs, from N- to C-terminus, consist of UBL derived from Rad23, a GSGGSG linker, A. victoria circular permutant of superfolder GFP (CP8), a G linker, the first 15 or 95 amino acids from S. cerevisiae cytochrome b2 with lysine residues replaced by arginine, and a 6xHis tag. Ub-GFP-α-helix-tail and UBL-GFP-α-helix-tail fusion constructs were made by inserting a TS linker, an ER/K α-helix motif of specified amino acid length, followed by a GALM linker between the GFP domain and the tail in the Ub-GFP-tail and UBL-GFP-tail constructs, respectively. Ub-GFP-α-helix(30) was made by removing the tail from Ub-GFP-α-helix(30)-15 and leaving the C-terminal 6xHis tag. UBL-GFP-α-helix(56) was made by removing the tail and 6xHis tag from UBL-GFP-α-helix(56)-15 and moving the 6xHis tag to the N-terminus. Barstar-GFP-α-helix(56)-15 was made by replacing the UBL domain of UBL-GFP-α-helix(56)-15 with the coding region from E. coli Barstar protein. All α-helix constructs lacked the C-terminal E244 in GFP to reduce electrostatic interactions between GFP and the Glutamic acid/Glu/E rich α-helix motif. The α-helices were derived from Mus musculus myosin VI [119]. Amino acid sequences of tails and α-helices used in this study are indicated in Table 3.3 and Table 3.4, respectively. Plasmids used in this study are shown in Table 3.2.

Plasmid ID Number	**Protein**	**Vector**	**Function/Use/purpose**

pCD#018	Ub-CP8-35-His6	pET-3a	Proteasome substrate
pCD#023	Ub-CP8-15-His6	pET-3a	Proteasome substrate
pCD#024	Ub-CP8-α9-15-His6	pET-3a	Proteasome substrate
pCD#025	Ub-CP8-α19-15-His6	pET-3a	Proteasome substrate
pCD#041	Ub-CP8-α30-15-His6	pET-3a	Proteasome substrate
pCD#049	Ub-CP8-α39-15-His6	pET-3a	Proteasome substrate
pCD#051	Ub-CP8-α48-15-His6	pET-3a	Proteasome substrate
pCD#053	Ub-CP8-α56-15-His6	pET-3a	Proteasome substrate
pCD#055	Ub-CP8-α64-15-His6	pET-3a	Proteasome substrate
pCD#026	Ub-CP8-α70-15-His6	pET-3a	Proteasome substrate
pCD#073	Ub-CP8-α30-His6	pET-3a	Proteasome substrate
pCD#071	UBL(80)-CP8-35-His6	pET-3a	Proteasome substrate
pCD#077	UBL(80)-CP8-15-His6	pET-3a	Proteasome substrate
pCD#078	UBL(80)-CP8-α9-15-His6	pET-3a	Proteasome substrate
pCD#079	UBL(80)-CP8-α19-15-His6	pET-3a	Proteasome substrate
pCD#080	UBL(80)-CP8-α30-15-His6	pET-3a	Proteasome substrate
pCD#081	UBL(80)-CP8-α39-15-His6	pET-3a	Proteasome substrate
pCD#082	UBL(80)-CP8-α48-15-His6	pET-3a	Proteasome substrate
pCD#083	UBL(80)-CP8-α56-15-His6	pET-3a	Proteasome substrate
pCD#084	UBL(80)-CP8-α64-15-His6	pET-3a	Proteasome substrate
pCD#085	UBL(80)-CP8-α70-15-His6	pET-3a	Proteasome substrate
pCD#112	His6-UBL(80)-CP8-α56	pET-3a	Proteasome substrate
pCD#037	Ube1	pET28	Ubiquitin chain synthesis

pCD#013	E2-25K	pGEX-6P-1	Ubiquitin chain synthesis
pCD#004	Ubiquitin (wildtype)	pET-3a	Ubiquitin chain synthesis
pCD#030	His6-HRV3C-Ub(K48R)	pET-3a	Ubiquitin chain synthesis
pCD#017	His6-HRV3C Protease	pETDuet	His-tag cleavage
pCD#016	GST-HRV3C Protease	pGEX-4T-1	GST-tag cleavage
pBLS005	pTPI1_4A_DsRed_P2A_Ub-Rkk_N10SRR-CΔ20-sYFP-Su9_tADH	YCplac33	*In vivo* proteasome substrate plasmid
pBLS137	pTPI1_4A_DsRed_P2A_UBL(80)-sYFP-Su9_tADH	YCplac33	*In vivo* proteasome substrate plasmid
pBLS138	pTPI1_4A_DsRed_P2A_UBL(80)-sYFP-SP25_tADH	YCplac33	*In vivo* proteasome substrate plasmid
pBLS047	pTPI1_4A_DsRed_P2A_Ub-Rkk_N10SRR-CΔ20-sYFP-SP25_tADH	YCplac33	*In vivo* proteasome substrate plasmid

Table 3.2: Plasmids used in this study

Protein Expression and Purification

In Vitro Substrate Proteins

His-tagged GFP containing protein variants were purified as previously described [27], with modifications. Substrate constructs were purified via immobilized metal affinity chromatography through a C-terminal 6xHis-tag by gravity purification. Proteins were expressed in E. coli Rosetta (DE3)pLysS (Novagen) cells from pET3a-derived

plasmids. A starter culture was inoculated in 25 mL of 2xYT media with 100 ug/mL ampicillin and 34 ug/mL chloramphenicol and grown to OD600 of ~ 0.5 at 37℃ then stored at 4℃ overnight. The starter culture was diluted 1:100 and grown in 2 L of 2xYT media with 100 ug/mL ampicillin and 34 ug/mL chloramphenicol to OD600 of ~ 0.5 at 37℃. Culture was then cooled to 16℃ and induced with 0.4 mM dioxane-free isopropyl B-D-1-thiogalactopyranoside (IPTG) (Calbiochem) overnight at 16℃. Cells were harvested by centrifugation at 5,000xg for 10 min, resuspended in ~30 mL of NPI-10 (10 mM imidazole, 50 mM phosphate buffer pH 8, 300 mM NaCl), and stored at -80C. For purification, cold NPI-10 buffer was added up to 50 mL. Cells were supplemented with 1X Protease Inhibitor Cocktail Set V EDTA-Free (Calbiochem), 10 mM MgCl2, and DNase I (MP Biomedical) and thawed in a room temperature water bath. Cells were then lysed between 10,000 and 15,000 psi in a high-pressure homogenizer (EmulsiFlex-C3 homogenizer, Avestin) for 10 minutes at 4℃. Lysate was cleared by centrifugation at 38,400xg for 20 min at 4℃. Clarified lysate was then filtered through a 0.45 µm syringe filter and mixed with 2 mL of washed TALON® Metal Affinity Resin beads (Takara). The mixture was allowed to bind under nutation at 4℃ for 1 hr. The mixture was poured into a PD-10 column and allowed to settle by gravity. The column was washed once with 5 CV (column volume) of NPI-10 and once with 10 CV of NPI-35 (35 mM imidazole, 50 mM phosphate buffer pH 8, 300 mM NaCl). Protein was eluted three times with 1 CV of NPI-250 (250 mM imidazole, 50 mM phosphate buffer pH 8, 300 mM NaCl). The eluate was concentrated between 1 and 1.5 mL and buffer exchanged in an Amicon Ultra Centrifugation filter with a 10 kDa cutoff into 50 mM TrisHCl of pH at least 1 unit above pI of the protein, 50 mM NaCl, and 0.5 mM DTT. Protein concentration was determined by Pierce Assay. Glycerol was added to 5%, protein aliquoted, flash frozen using liquid nitrogen, and stored at -80℃. Purity was assessed by SDS-PAGE analysis. Proteins with

95 amino acid length initiation regions were purified as described above expect with the addition of 1 mM PMSF to thawed cells.

Ubiquitin and Ubiquitin Variants

His6-HRV3C-Ub(K48R) was purified as described previously [27] by immobilized metal affinity chromatography through an N-terminal 6xHis-tag using a HisTrap FF Crude 5 mL column (GE) on an FPLC system (AKTAPurifier). Protein was expressed and lysed as described above for substrate constructs. Lysate was cleared by centrifugation at 38,400xg for 20 min at 4℃ two times. Clarified lysate was then filtered through a 0.45 µm syringe filter and applied to a 5 mL HisTrap FF Crude column on an FPLC system at a rate of 3 mL/min. The column was washed with 5 CV of NPI-10, washed with 10 CV of NPI-20 (20 mM imidazole, 50 mM phosphate buffer pH 8, 300 mM NaCl), and protein eluted with 10 CV of NPI-250 in 2 mL fractions. Fractions containing protein were pooled, concentrated between 1 and 2 mL, and buffer exchanged in an Amicon Ultra Centrifugation filter with a 3 kDa cutoff into 50 mM TrisHCl pH 7.6 and 50 mM NaCl. Protein concentration was determined by Pierce Assay. The protein was aliquoted, flash frozen using liquid nitrogen, and stored at -80℃. Purity was assessed by SDS-PAGE analysis.

Ubiquitin (S. cerevisiae) was purified using published methods [145] by cation exchange chromatography using a Resource S 6 mL column (GE) on an FPLC system (AKTAPurifier). Ubiquitin was expressed as described above except that the 2 L culture was induced with 0.4 mM dioxane-free isopropyl B-D-1-thiogalactopyranoside (IPTG) (Calbiochem) for four hrs at 37℃. Cells were harvested by centrifugation at 5,000xg for 10 min, resuspended in ~30 mL of 50 mM TrisHCl pH 7.6 and stored at -80℃. For purification, cold 50 mM TrisHCl pH 7.6 was added up to 50 mL. Cells were

supplemented with 1X Protease Inhibitor Cocktail Set V EDTA-Free (Calbiochem), 10 mM MgCl2, and DNase I (MP Biomedical) and thawed in a room temperature water bath. Cells were then lysed between 10,000 and 15,000 psi in a high-pressure homogenizer (EmulsiFlex-C3 homogenizer, Avestin) for 10 minutes. Lysate was cleared by centrifugation at 38,400xg for 20 min at 4℃. Perchloric acid was added to clarified lysate (0.5% (v/v)) and precipitated proteins removed by centrifugation at 38,400xg for 20 min at 4℃. Supernatant was dialyzed against 2 L of 50 mM ammonium acetate pH 4.5 at 4℃ for four hours in SnakeSkin® dialysis tubing with a 3.5 kDa cutoff (ThermoScientific). Dialysis was repeated in 2 L of fresh buffer overnight at 4℃. The dialysate was filtered through a 0.45 µm syringe filter then applied to a Resource S 6 mL column (GE). Column was washed with 5 CV of 50 mM ammonium acetate pH 4.5 and ubiquitin eluted by applying a linear gradient of 0 to 500 mM NaCl in 50 mM ammonium acetate pH 4.5 over 20 CV in 2 mL fractions. Fractions containing ubiquitin were pooled, concentrated between 1 and 2 mL, and buffer exchanged in an Amicon Ultra Centrifugation filter with a 3 kDa cutoff into 50 mM TrisHCl pH 7.6 and 50 mM NaCl. Concentration was determined by Pierce Assay, protein aliquoted, flash frozen using liquid nitrogen, and stored at -80℃. Purity was assessed by SDS-PAGE analysis.

Ubiquitination enzymes

Ube1 (Mus musculus) was purified as described previously [146] by immobilized metal affinity chromatography through an N-terminal 6xHis-tag by gravity purification with some modifications described. Ube1 was expressed in E. coli Rosetta (DE3)pLysS (Novagen) cells from a pET28-derived plasmid. A starter culture was inoculated in 50 mL of LB media with 25 ug/mL kanamycin and 34 ug/mL chloramphenicol and grown to OD600 of ~ 0.6 at 37℃ then stored at 4℃ overnight. The starter culture was diluted

1:200 and grown in 1 L of LB media with 25 ug/mL kanamycin and 34 ug/mL chloramphenicol to OD600 of ~ 0.6 at 37℃. Culture was then cooled to 16℃ and induced with 0.5 mM dioxane-free isopropyl B-D-1-thiogalactopyranoside (IPTG) (Calbiochem) overnight at 16℃. Cells were harvested by centrifugation at 5,000xg for 10 min, resuspended in ~30 mL of NPI-10 and stored at -80℃. For purification, cold NPI-10 was added to 50 mL. Cells were supplemented with 0.1% TritonX-100, 1 mM DTT, 1X Protease Inhibitor Cocktail Set V EDTA-Free (Calbiochem), 10 mM MgCl2, and DNase I (MP Biomedical) and thawed in a room temperature water bath. Cells were then lysed between 10,000 and 15,000 psi in a high-pressure homogenizer (EmulsiFlex-C3 homogenizer, Avestin) for 10 minutes at 4℃. Lysate was cleared by centrifugation at 38,400xg for 20 min at 4℃. Clarified lysate was then filtered through a 0.45 µm syringe filter and mixed with 1.5 mL of washed Ni-NTA Agarose beads (Qiagen). The mixture was allowed to bind under nutation at 4℃ for 2 hr. The mixture was poured into a PD-10 column and allowed to settle by gravity. The column was washed three times with 10 CV of NPI-10, once with 10 CV of NPI-20, and eluted three times with 1 CV of NPI-250. The eluate was concentrated to ~1.0 mL and buffer exchanged in an Amicon Ultra Centrifugation filter with a 30 kDa cutoff into 10 mM TrisHCl pH 8, 1 mM EDTA, and 1 mM DTT. Protein concentration was determined by Pierce Assay and assumed 40% pure as described in published protocols (Carvalho et al, 2012). Protein was aliquoted, flash frozen using liquid nitrogen, and stored at -80℃.

E2-25K (Homo sapiens) was purified by affinity chromatography as a GST-fusion protein by gravity purification and GST-tag removed by GST-HRV3C protease as described by the published protocol (Cannon et al, 2015) with some modifications. E2-25K was expressed in E. coli Rosetta (DE3)pLysS (Novagen) cells from a pGEX-6P-1-derived plasmid. A starter culture was inoculated in 25 mL of 2xYT media with 100

ug/mL ampicillin and 34 ug/mL chloramphenicol and grown to OD600 of ~ 0.6 at 37℃ then stored at 4℃ overnight. The starter culture was diluted 1:100 and grown in 2 L of 2xYT media with 100 ug/mL ampicillin and 34 ug/mL chloramphenicol to OD600 of ~ 0.6 at 37℃. Culture was then cooled to 16℃ and induced with 0.4 mM dioxane-free isopropyl B-D-1-thiogalactopyranoside (IPTG) (Calbiochem) overnight at 16℃. Cells were harvested by centrifugation at 5,000xg for 10 min, resuspended in ~30 mL of 1X PBS and stored at -80℃. For purification, cold 1X PBS was added to 50 mL. Cells were supplemented with 1% TritonX-100, 1 mM DTT, 1X Protease Inhibitor Cocktail Set V EDTA-Free (Calbiochem), 10 mM MgCl2, and DNase I (MP Biomedical) and thawed in a room temperature water bath. Cells were then lysed between 10,000 and 15,000 psi in a high-pressure homogenizer (EmulsiFlex-C3 homogenizer, Avestin) for 10 minutes at 4℃. Lysate was cleared by centrifugation at 38,400xg for 20 min at 4℃. Clarified lysate was then filtered through a 0.45 µm syringe filter and mixed with 2.5 mL of washed Glutathione Sepharose 4B beads (GE). The mixture was allowed to bind under nutation at 4℃ for 2 hr. The mixture was poured into a PD-10 column and allowed to settle by gravity. The column was washed three times with 10 CV of 1X PBS supplemented with 1 mM DTT then washed once with 10 CV of GST HRV3C cleavage buffer (150 mM NaCl, 50 mM TrisHCl pH 7.4, 1 mM EDTA, 1 mM DTT). The column was filled with GST HRV3C cleavage buffer and incubated with GST-HRV3C Protease overnight at 4℃. E2-25K was eluted twice with 3 CV of GST HRV3C cleavage buffer. Eluate was concentrated between 1 and 1.8 mL and buffer exchanged in an Amicon Ultra Centrifugation filter with a 10 kDa cutoff into 50 mM TrisHCl pH 7.6, 50 mM NaCl, and 0.5 mM DTT. Protein concentration was determined by Pierce Assay. Glycerol was added to 5%, protein aliquoted, flash frozen using liquid nitrogen, and stored at -80℃. Purity was assessed by SDS-PAGE analysis.

Affinity Tag Protease

His6-HRV3C Protease was purified by immobilized metal affinity chromatography through an N-terminal 6xHis-tag by gravity purification. Protein was purified as described above for His-tagged substrate constructs.

Ubiquitin Chain Synthesis

Ub4(K48) and Ub8(K48) ubiquitin chains were generated using enzymes that are part of the natural synthesis machinery and purified following the published protocols [27,147] as described below. Chains were synthesized from a mixture of wildtype ubiquitin and an N-terminally 6xHis-tagged ubiquitin in which lysine residue 48 was mutated to arginine so chain synthesis terminated with the His-tagged ubiquitin molecule. Polyubiquitin chains of different lengths were then isolated in three steps: an initial enrichment using the N-terminal 6xHis-tag (elution with His6-HRV3C protease) was followed by purification on a cation exchange column (Resource S) using a linear salt gradient and finally size exclusion chromatography (Superdex 75).

K48-linked ubiquitin chains were generated using H. sapiens ubiquitin-conjugating enzyme E2 25K together with the M. musculus ubiquitin activating enzyme (E1) Ube1 acting on a mixture of wildtype S. cerevisiae ubiquitin and a mutant of S. cerevisiae ubiquitin carrying the mutation K48R and an N-terminal 6xHis-tag attached through a linker containing a HRV3C protease cleavage site (His-HRV3C-Ub(K48R)). Chains of four ubiquitin moieties in length were synthesized by incubating 7.5 mg mL−1 wildtype ubiquitin and 7.5 mg mL−1 His HRV3C-Ub(K48R), in one-fifth volume of PBDM8 buffer (250 mM Tris-HCl pH 8.0, 25 mM MgCl2, 50 mM creatine phosphate, 3 units mL−1 inorganic pyrophosphatase, 3 units mL−1 creatine phosphokinase), 2.5 mM ATP, and 0.5 mM DTT, with 30 μM E2-25K, and 0.4 μM E1 at 37℃ overnight. The

reactions were quenched with 5 mM DTT and aggregates were removed by centrifugation at 15,000 x g for 5 min at 4℃. The supernatants were then diluted with an equal volume of NPI-10, 1 mL of washed Ni-NTA beads (Qiagen catalog no. 30210) were added for each 50 mg of total ubiquitin in the reaction, and the mixtures were allowed to bind under nutation at 4 °C for 1 h. The mixture was then poured into an empty PD-10 column and allowed to settle by gravity. The column was washed twice with 10 CV of NPI-10, followed by 10 CV of HRV3C cleavage buffer (50 mM Tris HCl pH 7.4, 150 mM NaCl, 1 mM DTT). His6-HRV3C protease in HRV3C cleavage buffer was then added to the column, the column capped and nutated overnight at 4 ˚C. Finally, the chains were eluted with 1 CV HRV3C cleavage buffer. For the next purification step by cation exchange chromatography, the eluate was acidified by the addition of 0.03 volumes of 2 N acetic acid to a pH of 4 and loaded on to 6 mL Resource S (GE catalog no. 17-1180-01) in a Tricorn column equilibrated with 50 mM ammonium acetate pH 4.5. The column was washed with 2 CV of 50 mM ammonium acetate pH 4.5 and the chains were eluted in the same buffer with a NaCl gradient as follows: 1 CV of 0 to 200 mM NaCl, 25 CV of 200 to 450 mM NaCl, and 1 CV of 450 to 1000 mM NaCl in 50 mM ammonium acetate pH 4.5, taking 2 mL fractions. The peak containing the chains of the desired length was concentrated to 0.5 mL using an Amicon Ultra Centrifugation filter with a 3 kDa molecular weight cutoff. The chains were purified further on a Superdex Hi-Load 75-pg (GE catalog no. 28-9893-33) column at a rate of 0.25 mL min−1 in ubiquitin size exclusion buffer (150 mM NaCl, 50 mM Tris-HCl pH 7.6, 0.5 mM EDTA), collecting 2 mL fractions. Fractions containing chains of the desired length were concentrated and exchanged into 50 mM Tris-HCl pH 7.6 using an Amicon Ultra Centrifugation filter with a 3 kDa molecular weight cutoff. Chain concentration was

determined by Pierce Assay. Protein was aliquoted, flash frozen using liquid nitrogen, and stored at -80℃. Purity was assessed by SDS-PAGE analysis.

Ubiquitinated Substrate Synthesis

Ubiquitinated substrates were generated following the published protocol [27]. Polyubiquitin chains were attached to the ubiquitin domain in the target protein using the same enzymes used to create the polyubiquitin chains. After incubation with enzymes and free ubiquitin chains, the reaction was quenched with 5 mM DTT and aggregates were removed by centrifugation at 15,000 x g for 5 min at 4 °C. Base protein was separated from unreacted ubiquitin chains and enzymes by nickel affinity chromatography using the C-terminal His-tag on the base protein. The reaction was mixed with 1.5 mL of washed Ni-NTA Agarose beads (Qiagen). The mixture was allowed to bind under nutation at 4℃ for 1 hr. The mixture was poured into a PD-10 column and allowed to settle by gravity. The column was washed once with 5 CV of NPI-10 and once with 10 CV of NPI-20. Protein was eluted three times with 1 CV of NPI-250. Finally, modified and unmodified base protein were separated by size exclusion chromatography. The eluate from the nickel column was concentrated to 0.5 mL using an Amicon Ultra Centrifugation filter with a 30 kDa molecular weight cutoff and applied to a Superdex Hi-Load 200-pg (GE catalog no. 28-9893-35) column at a flow rate of 0.25 mL min−1 in ubiquitin size exclusion buffer supplemented with 1 mM DTT, collecting 2 mL fractions. Fractions containing ubiquitinated substrate were pooled, concentrated, and buffer exchanged into 50 mM Tris-HCl pH 7.6 and 0.5 mM DTT using an Amicon Ultra Centrifugation filter with a 30 kDa molecular weight cutoff. Protein concentration was determined by Pierce Assay. Glycerol was added to 5%, protein aliquoted, flash frozen using liquid nitrogen, and stored at -80℃. Purity was assessed by SDS-PAGE analysis.

Proteasome Purification

Proteasome was purified from S. cerevisiae following published protocols [148] with modifications described below. The Core Particle (CP) and Regulatory Particle (RP) of the proteasome were purified separately using 3xFLAG tags fused to Pre1 and Rpn11, respectively. The CP was purified from YYS37 and the regulatory particles were purified from strains indicated in Table 3.1. Strains created for this study were constructed using standard methods described [57] and are isogenic SUB61 (MAT α lys2-801 leu2-3,2-112 ura3-52 his3-Δ200 trp1-1(am) [149].

Starter yeast cultures were inoculated into 5 mL of YPD with 2% glucose and grown for 24 hrs at 30℃. Culture was diluted 1:100 into 2 L of YPD with 2% glucose and grown to OD600 ~ 2 at 30℃. Cells were centrifuged at 5,000xg for 10 min, washed with cold water, and centrifuged again at 5,000xg for 10 min. Cells were then washed in 1X Buffer A (50 mM TrisHCl pH 7.6, 5% glycerol), centrifuged at 5,000xg for 10 min, and stored at -80℃. For purification, cells were resuspended in ARS Wash Buffer (50 mM TrisHCl pH 7.6, 5% glycerol, 1 mM ATP, 10 mM MgCl2, 1 mM DTT, 20 mM creatine phosphate, 0.02 mg/mL creatine phosphokinase). Cells were lysed between 25,000 and 30,000 psi in a high-pressure homogenizer (EmulsiFlex-C3 homogenizer, Avestin) for 10 minutes at 4℃. Lysates were clarified by centrifuging at 30,000xg for 30 min at 4℃. Clarified lysate was filtered with a 0.45 µm filter syringe then supplemented with 5 mM ATP, 10 mM creatine phosphate, and 0.01 mg/mL creatine phosphokinase. Supplemented lysate was then mixed with 1 mL of pre-washed anti-FLAG M2 agarose beads (Sigma) and allowed to bind under nutation at 4℃ for 2 hrs. The mixture was then collected in a PD-10 column and allowed to settle by gravity. The column was washed twice with 15 CV of ATP Wash Buffer (50 mM TrisHCl pH 7.6, 5% glycerol, 2 mM ATP, 5 mM MgCl2, 1 mM DTT) then once with ATP500 buffer (50 mM TrisHCl pH

7.6, 5% glycerol, 2 mM ATP, 5 mM MgCl2, 1 mM DTT, 500 mM NaCl). The column was filled with ATP500 buffer, capped, and nutated for 1 hr at 4℃. Mixture was allowed to settle by gravity, washed twice with 15 CV of ATP500 buffer, washed twice with 15 CV of ATP Wash Buffer, and excess buffer was removed by centrifuging at 500xg for 5 sec. Column was incubated with 0.75 mL of Elution Buffer (0.15 mg/mL 3xFLAG peptide in ATP Wash Buffer) for 20 min at room temperature and proteasome eluted by centrifuging at 500xg for 5 sec. A second elution was performed using 0.5 mL Elution Buffer, and the two elutions were pooled. Concentration was determined by Pierce Assay. The concentration of the Elution Buffer was subtracted from the concentration of the pooled eluates to determine the proteasome concentration. Eluate was aliquoted, flash frozen in liquid nitrogen, and stored at -80℃. Proteasome composition and purity was assessed by SDS-PAGE analysis.

Kinetic Plate Reader Degradation Assays

Single turnover degradation assays were performed as previously described [27] with modifications. In short, 25 nM reconstituted proteasome was presented to 5 nM purified substrates in the presence of an ATP Regeneration System (ARS) at 30℃ in 384-well plates (flat bottom, low flange, non-binding, black, Corning).

Proteasomes were first reconstituted in a 1:2 ratio at twice that of the final concentration by incubating 50 nM CP and 100 nM RP in presence of 2X ARS (2 mM ATP, 20 mM creatine phosphate, 0.2 mg/mL creatine phosphokinase), 1X Degradation Buffer (50 mM TrisHCl pH 7.6, 5 mM MgCl2, 1% glycerol), and 8 mM DTT at 30℃ for 30 min. Substrates were diluted to twice that of the final concentration (i.e., 10 nM) using protein buffer (4 mg/mL BSA, 1X Degradation Buffer, 100 mM NaCl). Reactions were initiated by mixing 20 µL of proteasome mixture with 20 µL of substrate mixture. Thus,

final reactions contained 25 nM proteasome and 5 nM substrate in 1X ARS (1 mM ATP, 10 mM creatine phosphate, 0.1 mg/mL creatine phosphokinase), 4 mM DTT, 1X Degradation Buffer, 2 mg/mL BSA, and 50 mM NaCl.

Substrate fluorescence (488 nm excitation, 520 nm emission) was measured every 60 seconds for 90 minutes in a plate reader (Infinite M1000 PRO, Tecan). Background (average fluorescence of well containing everything except substrate) was subtracted from proteasome containing reactions and fluorescence plotted as a function of time. Likewise, background (average fluorescence of well containing everything except substrate and proteasome) was subtracted from reactions lacking proteasome and fluorescence plotted as a function of time. The decay curves were fitted to the equation describing a single exponential decay ($y = Ae^{-kt} + C$) using the software Prism (version 7). Initial degradation rate was determined by multiplying the amplitude of degradation (% fluorescence) by the rate constant (min-1).

Yeast Model Substrate Design and Expression

Yeast YFP substrate variants were built off a central YFP (sYFP2) domain and constructed with either an N-end rule degron, or an N-terminal UBL domain derived from the first 80 amino acids of S. cerevisiae Rad23. N-end rule substrates consisted of a ubiquitin domain followed by a destabilizing Arg residue followed by a 19 amino acid linker derived from E. coli lacI, which contains two Lys residues (Rekk). However, amino acids 4-13 were replaced with a serine-rich linker derived from herpes virus 1 ICP4 to prevent the N-terminal degron from being a disordered region that could initiate degradation. To correct for cell-to-cell variation in transcriptional, translational, or cell size variation, RFP dsRed-Express2 was expressed upstream of YFP separated by a P2A

ribosomal skipping site. The ratio of YFP over RFP for individual cells was a measure of the steady state concentration of YFP variants.

The N-end rule degron and UBL yeast substrates with Su9 and SP25 tails were individually expressed from CEN plasmids using a constitutive TPI1 promoter. The Su9 tail represents 51 amino acids from subunit 9 of the Fo component of the Neurospora crassa ATP synthase and has been previously characterized as an efficient initiation region [9]. The SP25 tail consists of 5 repeats of peptide region 2 in influenza A virus M2 protein used to produce antisera and has been previously characterized to be a poor initiation region [9]. Plasmids were then transformed into WT, ubr1Δ, and pep4Δ yeast strains. Plasmids used in this study are shown in Appendix Table S2. The deletion strains were obtained from the yeast gene deletion collection [150].

Ubiquitinated and UBL substrates were depleted when attaching a tail that is recognized by the proteasome (Su9, Fig 3.1.4a) [9], but accumulated when attaching a tail that is not recognized (SP25, Fig 3.1.4a). Deleting the primary ubiquitin ligase that targets N-end rule substrates (ubr1Δ) to the proteasome caused buildup of substrate with the Su9 tail, while not affecting degradation of UBL substrate, indicating N-end rule substrates require ubiquitination for degradation. Deleting the gene encoding proteinase A (pep4Δ), which functions in the final step of autophagy, did not affect substrate abundance (Fig 3.1.4b) suggesting substrates are not degraded through the autophagy-lysosome pathway. Taken together, the YFP model substrate platform is an effective way to measure degradation by the proteasome in yeast.

Varying amino acid lengths of ER/K α-helix motifs were inserted between YFP and tail of N-end rule degron and UBL substrates to generate YFP spacing substates. The tail was the same as the 18 amino acid long tail attached to GFP substrates used in the in vitro studies, but is 19 amino acids in length due to insertion of a glycine/Gly/G residue

at position three. Tails retained a C-terminal 6xHis tag to maintain design consistency between in vitro and in vivo substrates. Substrates containing α-helices were integrated into the ORF of HO1 in S. cerevisiae and expressed from a constitutive TPI1 promoter. Correct integration was confirmed by selection with nourseothricin and sanger sequencing. Yeast strains used in this study are shown in Table 3.5.

Flow Cytometry

Cells were grown in synthetic complete medium at 25^{o}C to mid-log phase after 7-8 doublings and harvested for direct fluorescent measurement of RFP and YFP channels by an LSR Fortessa (BD biosciences) flow cytometer. Time courses of YFP fluorescence were measured to determine in vivo degradation rates by inhibition of protein synthesis through the addition of 125 μM cycloheximide and YFP fluorescence measurements were taken for 120 minute time courses. Degradation rates were calculated in the same way as in the in vitro experiments. The data were analyzed by FlowJo (FlowJo version 10.2). Cells were gated first along the FSC-A vs. SSC-A axes to eliminate dead cells. They were then gated against SSC-H vs. SSC-W and FSC-H vs. FSC-W axes to eliminate doublets. Finally, cells were gated to only include RFP-positive cells. YFP over RFP ratios of at least 10,000 cells were calculated and we report the median of those ratios for each experiment.

CONTRIBUTIONS

CD, BLS, and EC designed and conducted experiments and interpreted data, CD, BLS, EC, JK, HC, and SE constructed unique reagents for the studies, and AM conceived the study, designed experiments, and interpreted data. CD, BLS, and AM wrote the manuscript.

Chapter 4: Conclusions and Future Directions

SUMMARY OF DISSERTATION RESEARCH

Regulated protein degradation is an important process in preserving protein homeostasis. The primary regulated degradation machinery is the ubiquitin proteasome system. Substrates are targeted for degradation by the covalent attachment of ubiquitin chains to substrates at a lysine residue in the protein. However, ubiquitination is involved in other cellular processes as well. The proteasome can degrade any kind of protein targeted to it, but it does so selectively. Some protein substrates that are ubiquitinated escape degradation, while others are degraded efficiently. What's more is that there are multiple pathways that substrates can take to the proteasome. First, substrates with ubiquitin chains can bind directly to one of three known ubiquitin receptors on the proteasome and be degraded. Second, ubiquitinated substrates can bind extrinsic receptors in the form of UBL-UBA proteins, which bind ubiquitin substrates at their UBA domain, and bind the proteasome at their UBL domain on the same receptors as ubiquitin chains. Finally, some substrates can be degraded independent of ubiquitination and are targeted directly for degradation. Therefore, understanding the requirements for proteasome-mediated degradation, and how the interplay between these three pathways mediate and prioritize degradation is imperative.

My dissertation has aimed to address how the proteasome selects its substrates in two ways. In Chapter 2, I designed model substrates with either a ubiquitin targeting signal, a UBL targeting signal, or a ubiquitin-independent targeting signal to investigate how these three pathways compete. I then added a set of analogous competitors to each substrate to determine if they compete within their own pathways or with other pathways.

I found that ubiquitinated substrates compete with other ubiquitinated substrates for degradation, but not with UBL substrates or ubiquitin-independent substrates to a significant extent. Additionally, the UBL substrate did not compete with any of the three competitors, even with an analogous UBL competitor. Using kinetic modeling, I determined that substrates delivered through UBL domains may have priority over other substrates because they can access any of the three ubiquitin receptors, while ubiquitinated substrates targeted directly to the proteasome by direct binding are limited to Rpn10. Our results suggest that receptor binding availability is limiting, but tail insertion is not, because the ubiquitin-independent substrate, ODC, which binds directly in the pore-1 loops, competes only modestly with any of the three competitors, while the ubiquitinated substrate, which has limited receptor binding capacity, competes with a ubiquitinated competitor but not with UBL substrates that have access to more receptors.

It's possible that UBL-UBA shuttling factors, like Rad23 and Dsk2, function as an alternative path to the proteasome for high priority substrates, such as cell cycle regulators, under stress. Under proteotoxic stress, many proteins are being ubiquitinated and targeted for degradation, such as misfolded and damaged proteins. These substrates presumably bind and are degraded directly by the proteasome. However, some high priority substrates, such as cell cycle regulators may also need to be degraded for the cell to divide. It’s possible that these substrates bind to UBL-UBA shuttling factors and are targeted to the proteasome through these extrinsic receptors, possibly circumventing competition with misfolded and damaged proteins. In yeast strains lacking Cdc48 function, ubiquitinated proteins accumulate on proteasomes [99,100]. It has also been shown that Rad23 and Dsk2 increase ubiquitinated substrate occupancy on the proteasome in strains lacking Cdc48 function [99]. This may be because in strains lacking

Cdc48 function, proteasome occupancy is increased, and thus Rad23 and Dsk2 deliver other substrates to the proteasome. What's more, deletion of RAD23 and DSK2 in a cdc48 mutant strain leads to an increasingly severe growth defect [101], suggesting that Rad23 and Dsk2 may participate in alleviating cdc48 mutant growth defects. Based on our findings, it could be that Rad23 and Dsk2 function to deliver high priority substrates to the proteasome under increased load, and when they are deleted, these high priority substrates cannot be degraded, leading to toxicity. In addition to Cdc48 pathways, Rad23 may play an alternative role in delivering proteins with branched ubiquitin chains to the proteasome. This mechanism could explain why certain substrates have branched ubiquitin chains. For instance, if Rad23 exhibits a strong affinity for branched ubiquitin chains, it could serve as an efficient delivery system for proteins that require rapid degradation, such as regulatory proteins. This alternative pathway could bypass the usual pathway to the proteasome, offering a more streamlined route for proteasomal degradation.

My findings were surprising in two ways. First, for a substrate to be degraded, it must first bind the proteasome at a receptor, but then a disordered initiation region must engage the pore-1 loops. While there are many receptors for binding, there is only one entrance channel to the proteasome. Single molecule FRET-based biochemistry assays have tracked the kinetics of ubiquitin binding to receptors, and tail insertion into the pore. Ubiquitin binding is thought to be significantly faster than tail insertion [94]. It takes 1.6 seconds for the tail to insert, followed by a rapid conformational switch that takes 0.4 seconds. The ubiquitin chain is then removed within about 5 seconds, and the mechanical unfolding, translocation, and cleavage of the substrate takes an additional 11 seconds. Therefore, the data overwhelmingly suggest that the majority of substrate processing time is spent on deubiquitination and unfolding/translocation. Furthermore, some in vitro

competition assays have suggested that ubiquitin-chain interactions with receptors are short lived, and that substrates with better initiation regions competed more than substrates with poor initiation regions [10]. Therefore, based on the current state of the field, we initially thought that tail insertion would be the limiting step, not receptor binding.

However, our data clearly demonstrate that receptor binding availability is the primary source of competition among substrates, and that competition at the level of tail insertion is modest. While not what we initially thought, this makes sense given that the proteasome channel is large enough to accommodate more than one linear polypeptide chain. This can be supported by the evidence of some substrates initiating degradation at an internal initiation region, which must form a loop with a width of at least two polypeptide chains when entering the channel, suggesting that more than one polypeptide chain may fit in the entry channel [95]. Also, some proteasomes are doubly capped, meaning they may be able to degrade polypeptides in both directions simultaneously [96].

Second, the functions of UBL-UBA shuttling factors have been surprisingly unclear. Many studies have suggested that these factors serve as extrinsic ubiquitin receptors, and there is evidence that they are involved in degrading some well-known substrates. For example, Rad23 binding to the proteasome is regulated by phosphorylation. However, the physiological differences in function and importance between UBL-UBA shuttling factors and intrinsic ubiquitin receptors have remained unknown. My results in Chapter 2 demonstrate that UBLs do not compete with ubiquitinated substrates in binding to the proteasome, and that substrates targeted by UBLs are largely unaffected by cellular stress. This provides a surprising explanation for the functionality of UBL-UBA shuttling factors in cells: they may serve to deliver high-

priority substrates for degradation under cellular stress or increased proteasome load.

Rad23 and other UBL-UBA proteins could serve to open more accessibility to the proteasome by providing binding of ubiquitin chains to more than just Rpn10, thus decreasing competition of priority substrate degradation under stress. For example, Sic1, a Cdk1-Clb complex inhibitor, prevents premature cell cycle progression from G1 to S phase. Degradation of Sic1 by the proteasome relieves inhibition of Cdk1-Clb complexes and allows progression to S phase [97]. Sic1 degradation has been demonstrated to be mediated by direct binding to Rpn10, or by binding to Rad23 [98]. UBL-UBA shuttle factors, such as Rad23 and Dsk2, may serve as a backup route to the proteasome for high-priority substrates, such as Sic1, during stress.

In Chapter 3, I investigated how the spacing between the ubiquitin tag and initiation region affects the degradation efficiency of substrates. We designed model substrates with an N-terminal ubiquitin chain and a C-terminal short initiation region separated from the ubiquitin chain by varying lengths of alpha helices. We found that the proteasome has strict spacing requirements between the ubiquitin chain and the initiation region, likely due to the geometry of the proteasome receptor Rpn10, where ubiquitin chains bind, and the entrance channel where the pore-1 loops are located, where the initiation region binds. However, when the proteasome binding tag is switched to a UBL domain, the distance between the UBL and the initiation region must be longer, likely because UBL domains bind Rpn13, which is further from the entrance channel than Rpn10. These results are mostly consistent in vivo, indicating that there are strict requirements for spacing between the initiation region and the proteasome-targeting signal.

These results, however, are surprising. If the proteasome has such strict requirements for spacing, how then does it degrade such a diverse pool of proteins? It’s

possible that extrinsic factors, such as, for example Cdc48, an unfoldase, may process substrates before they are delivered to the proteasome. *In vitro*, Cdc48 can unfold and prepare a substrate for degradation without an initiation region [135]. Then, for example, if a substrate's initiation region is too short, such that it cannot reach the pore-1 loops, then Cdc48 may unfold the substrate, thus creating a longer initiation region that can reach the entry channel. One possibility is that Rad23 may serve as a spacing adaptor. Rad23's UBL domain is separated from its UBA domain by a flexible linker. This linker may add additional flexibility in the geometry requirements for substrates. Therefore, some substrates may require Rad23 for degradation to alleviate inadequate geometries.

My results demonstrate a hierarchy in proteasome substrate degradation, where substrates delivered by UBL domains may have a priority pathway and substrates must have the correct geometry to bind the proteasome simultaneously with their ubiquitin chain and initiation region.

FUTURE DIRECTIONS FOR PRIORITY PATHWAYS TO THE PROTEASOME

In Chapter 2, I demonstrate a hierarchy in proteasome substrates, suggesting that UBL domains may provide a priority pathway to the proteasome. In yeast, there are three UBL-UBA proteins (Rad23, Dsk2, and Ddi1), which have an N-terminal UBL domain, followed by a linker, and then one or two UBA domains. Ubiquitinated substrates can bind UBA domains, and then those substrate may be delivered for degradation by binding of the UBL domain to one of the three ubiquitin receptors on the proteasome. UBL-UBA proteins may be important for some proteasome-mediated degradation, because when they are dysfunctional, cells, especially neurons, are more likely to be damaged by stress or aging, which can lead to earlier neurodegeneration [66]. UBL-UBA proteins may also serve to delivery high priority substrates for degradation under stress conditions. For

example, Sic1 can be targeted for degradation by Rpn10 or Rad23. The Rad23 pathway may be more important when there is stress on the proteasome.

In Chapter 2, I demonstrate that UBL substrates do not compete much, even with themselves. What's more, we found that UBL substrates are not sensitive to proteotoxic stress caused by canavanine, or the accumulation of ubiquitinated species caused by MG-132 treatment. Biochemical assays have demonstrated that UBL domains can target substrates to any of the three ubiquitin receptors on the proteasome, while K48-linked ubiquitin chains can only target substrates to Rpn10 [27]. In Chapter 2, I build kinetic models to demonstrate that this observation is consistent with our findings. However, we did not directly test this hypothesis. One way to do this is to perform competition assays in yeast strain backgrounds with mutated proteasome receptors. For example, does UBL compete with itself or with ubiquitinated competitors more in a yeast strain where Rpn10 is the only functional receptor? Is the UBL substrate sensitive to canavanine or the accumulation of ubiquitinated species caused by MG-132 where Rpn10 is the only functional receptor? These experiments would be a direct way to test how receptor availability impacts the competition and stress sensitivity of substrates.

While our results are promising and provide insights into the dynamics of degradation mediated by UBL domains, we used a relatively artificial system. To simplify the experiment, our substrate had an N-terminal fusion of UBL to YFP. However, this is not how substrates are typically degraded. Substrates often bind the UBA domain of a UBL-UBA protein, which then targets them for degradation by binding the UBL domain to the proteasome. Therefore, the logical next step is to observe the degradation of a substrate that binds UBL-UBA proteins to mediate degradation to ensure that our artificial system reflects the true behavior of degradation of these substrates. Sic1, a Cdk1-Clb complex inhibitor, prevents premature cell cycle progression from G1

to S phase. Degradation of Sic1 by the proteasome relieves inhibition of Cdk1-Clb complexes and allows progression to S phase [97]. Sic1 degradation has been demonstrated to be mediated by direct binding to Rpn10, or by binding to Rad23 [98]. By testing the degradation of Sic1 in a strain with inactive Rpn10 vs. inactive Rad23 in the presence of canavanine and accumulated ubiquitin species will provide direct evidence of a Rad23 substrate. Another possibility is monitoring the degradation of Clb5 under stress conditions in a strain lacking UBL-UBA proteins. Clb5 has been shown to be stabilized in a strain lacking Cdc48 function likely because loss of Cdc48 function causes an accumulation of ubiquitinated misfolded proteins, thus clogging the UPS [101]. To elucidate the potential roles of Rad23 and other UBL-UBA proteins in degrading proteins under UPS stress, we could monitor Clb5 degradation kinetics under stress conditions. By examining the impact of UPS stress on Clb5 degradation, we can gain insights into how UBL-UBA proteins may facilitate proteasomal degradation under stress conditions for full length native high priority proteins.

Another possibility for the different competition dynamics between the ubiquitinated N-end rule substrate and the ODC and UBL substrates is a change in the free ubiquitin pool. The ubiquitinated competitor may use up most of the free ubiquitin pool, leading to reduced ubiquitination of the N-end rule substrate. The ODC and UBL model substrates, on the other hand, do not require ubiquitination and may remain unaffected. To explore this possibility, we blotted for ubiquitin and quantified the amount of free ubiquitin. We saw that the level of free ubiquitin did not change in the presence of ubiquitinated competitor, suggesting that loss of free ubiquitin is not a viable explanation for the observed competition dynamics. We could further test this model by observing competition dynamics in a strain overexpressing free ubiquitin. If overexpression of free ubiquitin leads to less competition between the ubiquitinated competitor and substrate,

then free ubiquitin may be the limiting step. However, if overexpression of free ubiquitin leads to no change in competition dynamics, then free ubiquitin is likely not the limiting factor affecting competition dynamics.

While there are some examples of Rad23-mediated degradation, the field lacks a complete understanding of the breadth of substrate specificity for Rad23-mediated degradation versus direct proteasome receptor binding. Do Rad23 UBA domains bind only specific types of ubiquitin chains, or can they bind any kind of ubiquitin chain? Testing Rad23 specificity for types of ubiquitin linkages and gaining a more complete picture of which substrates are targeted by Rad23 will provide insights into the importance and relevance of its priority pathway to the proteasome. Furthermore, there is some evidence for regulated Rad23-mediated degradation, as it has been demonstrated that phosphorylation of its serine residues may inhibit Rad23 UBL's interaction with the ubiquitin receptors on the proteasome [70], while overexpression leads to inhibition of degradation of substrates [71]. This may be important because Rad23 mediated degradation may be "switched on" under UPS stress to selectively target high priorirt substrates for degradation. On the other hand, under normal conditions, Rad23 may be "switched off" to allow degradation of typical substrates. Gaining a more complete picture of how Rad23 is regulated and its interaction with specific substrates may provide more relevant insights into its biological importance as a priority pathway to the proteasome.

FUTURE DIRECTIONS FOR SPACING BETWEEN UBIQUITIN TAG AND INITIATION REGION

In Chapter 3, I demonstrate that the spacing between a ubiquitin tag and a disordered initiation region must be precise to allow the ubiquitin chain to bind to one of the proteasome receptors while simultaneously allowing the initiation region to reach the

entrance channel to initiate degradation. However, the spacing requirements for a ubiquitinated substrate differ strikingly between in vitro and in vivo conditions.

In vitro, the optimal spacing was 19 amino acids, while in vivo, no alpha helical linker was the optimal spacing. One explanation for this difference is the design of the in vitro substrate versus the in vivo substrate. Figure 4.1 shows that the in vivo substrate had an 11 amino acid linker after the lysine residues where it is ubiquitinated, while the in vitro substrate only had a 6 amino acid linker. When comparing alpha-fold predictions [151] of the best degraded substrates in vivo and in vitro, the difference in linker length may explain the spacing difference because these two substrates seem to be spaced the same distance from the ubiquitin chain and initiation region (Figure 4.1, Right). Because the linker is longer in vivo, a shorter spacer may be required.

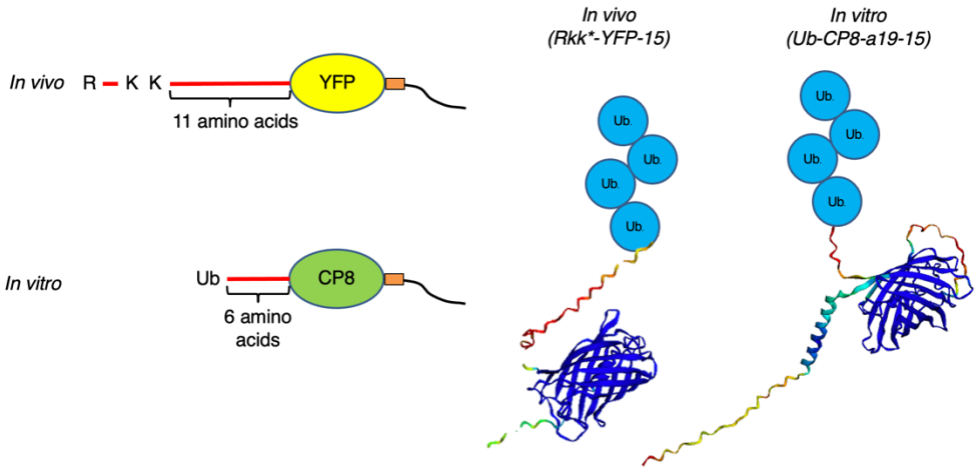

Figure 4.1: Differences in the *in vivo* and *in vitro* substrate design

Left: Substrate design for the *in vivo* and *in vitro* substrates. The *in vivo* substrate has an 11 amino acid linker after the lysine residues where it is ubiquitinated, while the *in vitro* substrate only has a 6 amino acid linker.
Right: Alpha-fold predictions of the two best degraded substrates *in vivo* and *in vitro* demonstrating that they possess about the same distance from ubiquitin chain to initiation region.

To test this explanation, we could design an in vitro substrate with a longer linker to match the length of the linker in the in vivo substrate. If the spacing requirements for the modified in vitro substrate are then like the in vivo results, it is likely that the linker length is the explanation for the discrepancy.

Another way to globally test if the structure of substrates impacts degradation on the proteome level, we could do a global study to determine if protein structures may help predict turnover.

Auxiliary factors *in vivo* may help alleviate the strict spacing requirements we observe for degradation of substrates that do not meet these requirements. Cdc48 has been demonstrated to unfold and prepare substrates for degradation, potentially exposing or lengthening the disordered initiation region [135]. For this reason, it's possible that Cdc48 may alleviate the strict spacing requirement of substrates. There are two ways we can address this question. First, *in vitro* assays may be performed whereby Cdc48 is pre-incubated with our model substrates, and then degradation assays performed. If Cdc48 loosens the spacing requirement, we'd expect to see less dependence on the correct alpha helix length on degradation rate. Second, *in vivo* assays may be performed in strains lacking Cdc48, such as temperature sensitive mutants. If Cdc48 functions to loosen spacing requirements, then strains lacking Cdc48 function would have stricter spacing requirements than wildtype.

FINAL REMARKS

The proteasome is a highly selective and precisely regulated protease that degrades proteins essential for cellular homeostasis. In this dissertation, I explored the molecular mechanisms by which the proteasome selects its substrates from a diverse protein pool.

I first investigated the interplay between different pathways to the proteasome, and revealed a hierarchy in degradation whereby substrates delivered by ubiquitin-like (UBL) domains may have priority access to the proteasome. This hierarchy is likely since UBL domains can bind to multiple receptors on the proteasome, while other ubiquitinated substrates can only bind to a single receptor. This hierarchy may be useful in designing therapeutics that could redirect the degradation of important or disease-causing proteins to the UBL pathway, ensuring efficient degradation even under stress conditions.

I next investigated how the spacing of the ubiquitin tag and disordered initiation region plays an important role in degradation. My findings reveal another layer to substrate selection by the proteasome, and provide important considerations when determining whether a given protein may be degraded by the proteasome.

Overall, my research provides new insights into how the proteasome selects its substrates in a diverse protein pool, and gives a deeper understanding of the proteasome's role in cellular homeostasis and disease. In Chapter 2, we demonstrated how substrates are prioritized, thus providing insights into how the proteasome selects some substrates over others. Many disease states are caused by mis regulation of protein degradation, leading to more of the disease causing protein. Understanding how the proteasome prioritizes substrates may help us design therapeutics which effectively reprioritize disease causing proteins by, for example, utilizing UBLs. Additionally, Chapter 3 demonstrates the need for substrates to have appropriate spacing between ubiquitin tags and disordered regions, providing another layer of detail to consider when predicting if protein targets can be effectively targeted for degradation by therapeutics. My research has laid the foundation for the development of new proteasome-based therapeutics, and I am excited to see how this research is translated into clinical practice in the future.

References

[1] C. Davis, B.L. Spaller, A. Matouschek, Mechanisms of substrate recognition by the 26S proteasome, Curr. Opin. Struct. Biol. 67 (2021) 161–169. https://doi.org/10.1016/j.sbi.2020.10.010.

[2] D. Finley, Recognition and Processing of Ubiquitin-Protein Conjugates by the Proteasome, Biochemistry-Us. 78 (2009) 477–513. https://doi.org/10.1146/annurev.biochem.78.081507.101607.

[3] M.H. Glickman, A. Ciechanover, The Ubiquitin-Proteasome Proteolytic Pathway: Destruction for the Sake of Construction, Physiol. Rev. 82 (2002) 373–428. https://doi.org/10.1152/physrev.00027.2001.

[4] I. Sahu, M.H. Glickman, Proteasome in action: substrate degradation by the 26S proteasome, Biochem. Soc. Trans. 49 (2021) 629–644. https://doi.org/10.1042/bst20200382.

[5] A.B. Abildgaard, S.K. Gersing, S. Larsen-Ledet, S.V. Nielsen, A. Stein, K. Lindorff-Larsen, R. Hartmann-Petersen, Co-Chaperones in Targeting and Delivery of Misfolded Proteins to the 26S Proteasome, Biomolecules. 10 (2020) 1141. https://doi.org/10.3390/biom10081141.

[6] R. Raynes, L.C.D. Pomatto, K.J.A. Davies, Degradation of oxidized proteins by the proteasome: Distinguishing between the 20S, 26S, and immunoproteasome proteolytic pathways, Mol. Asp. Med. 50 (2016) 41–55. https://doi.org/10.1016/j.mam.2016.05.001.

[7] D. Komander, M. Rape, The Ubiquitin Code, Annu Rev Biochem. 81 (2012) 203–229. https://doi.org/10.1146/annurev-biochem-060310-170328.

[8] S. Fishbain, T. Inobe, E. Israeli, S. Chavali, H. Yu, G. Kago, M.M. Babu, A. Matouschek, Sequence composition of disordered regions fine-tunes protein half-life, Nat. Struct. Mol. Biol. 22 (2015) 214–221. https://doi.org/10.1038/nsmb.2958.

[9] H. Yu, A.K.S. Gautam, S.R. Wilmington, D. Wylie, K. Martinez-Fonts, G. Kago, M. Warburton, S. Chavali, T. Inobe, I.J. Finkelstein, M.M. Babu, A. Matouschek, Conserved Sequence Preferences Contribute to Substrate Recognition by the Proteasome*, J Biol Chem. 291 (2016) 14526–14539. https://doi.org/10.1074/jbc.m116.727578.

[10] J.A.M. Bard, C. Bashore, K.C. Dong, A. Martin, The 26S Proteasome Utilizes a Kinetic Gateway to Prioritize Substrate Degradation, Cell. 177 (2019) 286-298.e15. https://doi.org/10.1016/j.cell.2019.02.031.

[11] Q. Guo, C. Lehmer, A. Martínez-Sánchez, T. Rudack, F. Beck, H. Hartmann, M. Pérez-Berlanga, F. Frottin, M.S. Hipp, F.U. Hartl, D. Edbauer, W. Baumeister, R. Fernández-Busnadiego, In Situ Structure of Neuronal C9orf72 Poly-GA Aggregates Reveals Proteasome Recruitment, Cell. 172 (2018) 696-705.e12. https://doi.org/10.1016/j.cell.2017.12.030.

[12] S. Albert, M. Schaffer, F. Beck, S. Mosalaganti, S. Asano, H.F. Thomas, J.M. Plitzko, M. Beck, W. Baumeister, B.D. Engel, Proteasomes tether to two distinct sites at the nuclear pore complex, Proc. Natl. Acad. Sci. 114 (2017) 13726–13731. https://doi.org/10.1073/pnas.1716305114.

[13] S. Asano, Y. Fukuda, F. Beck, A. Aufderheide, F. Förster, R. Danev, W. Baumeister, A molecular census of 26S proteasomes in intact neurons, Science. 347 (2015) 439–442. https://doi.org/10.1126/science.1261197.

[14] A. Turakhiya, Functional characterization of the role of ZFAND1 in stress granule turnover, Functional Characterization of the Role of ZFAND1 in Stress GranuleturnoverFunktionelle Charakterisierung Der Rolle von ZFAND1 Im Umsatz VonStressgranulaDoctoral Thesis for a Doctoral Degreeat the Graduate School of Life Sciences,Julius-Maximilians-Universität Würzburg,Section: Biomedicine. (n.d.).

[15] T. Tomita, A. Matouschek, Substrate selection by the proteasome through initiation regions, Protein Sci. 28 (2019) 1222–1232. https://doi.org/10.1002/pro.3642.

[16] A.H. de la Peña, E.A. Goodall, S.N. Gates, G.C. Lander, A. Martin, Substrate-engaged 26S proteasome structures reveal mechanisms for ATP-hydrolysis–driven translocation, Science. 362 (2018) eaav0725. https://doi.org/10.1126/science.aav0725.

[17] Y. Dong, S. Zhang, Z. Wu, X. Li, W.L. Wang, Y. Zhu, S. Stoilova-McPhie, Y. Lu, D. Finley, Y. Mao, Cryo-EM structures and dynamics of substrate-engaged human 26S proteasome, Nature. 565 (2019) 49–55. https://doi.org/10.1038/s41586-018-0736-4.

[18] E.J. Worden, C. Padovani, A. Martin, Structure of the Rpn11–Rpn8 dimer reveals mechanisms of substrate deubiquitination during proteasomal degradation, Nat. Struct. Mol. Biol. 21 (2014) 220–227. https://doi.org/10.1038/nsmb.2771.

[19] E.J. Worden, K.C. Dong, A. Martin, An AAA Motor-Driven Mechanical Switch in Rpn11 Controls Deubiquitination at the 26S Proteasome, Mol. Cell. 67 (2017) 799-811.e8. https://doi.org/10.1016/j.molcel.2017.07.023.

[20] M. Groll, L. Ditzel, J. Löwe, D. Stock, M. Bochtler, H.D. Bartunik, R. Huber, Structure of 20S proteasome from yeast at 2.4Å resolution, Nature. 386 (1997) 463–471. https://doi.org/10.1038/386463a0.

[21] A.M. Weissman, Themes and variations on ubiquitylation, Nat. Rev. Mol. Cell Biol. 2 (2001) 169–178. https://doi.org/10.1038/35056563.

[22] C.M. Pickart, MECHANISMS UNDERLYING UBIQUITINATION, Biochemistry. 70 (2001) 503–533. https://doi.org/10.1146/annurev.biochem.70.1.503.

[23] W. Li, Y. Ye, Polyubiquitin chains: functions, structures, and mechanisms, Cell. Mol. Life Sci. 65 (2008) 2397–2406. https://doi.org/10.1007/s00018-008-8090-6.

[24] S. Hatakeyama, K.I. Nakayama, U-box proteins as a new family of ubiquitin ligases, Biochem. Biophys. Res. Commun. 302 (2003) 635–645. https://doi.org/10.1016/s0006-291x(03)00245-6.

[25] S. Fang, A.M. Weissman, A field guide to ubiquitylation., Cell. Mol. Life Sci. : CMLS. 61 (2004) 1546–61. https://doi.org/10.1007/s00018-004-4129-5.

[26] Y. Saeki, Ubiquitin recognition by the proteasome, J. Biochem. 161 (2017) 113–124. https://doi.org/10.1093/jb/mvw091.

[27] K. Martinez-Fonts, C. Davis, T. Tomita, S. Elsasser, A.R. Nager, Y. Shi, D. Finley, A. Matouschek, The proteasome 19S cap and its ubiquitin receptors provide a versatile recognition platform for substrates, Nature Communications. (2020) 1–16. https://doi.org/10.1038/s41467-019-13906-8.

[28] M.E. French, C.F. Koehler, T. Hunter, Emerging functions of branched ubiquitin chains, Cell Discov. 7 (2021) 6. https://doi.org/10.1038/s41421-020-00237-y.

[29] C. Hoege, B. Pfander, G.-L. Moldovan, G. Pyrowolakis, S. Jentsch, RAD6-dependent DNA repair is linked to modification of PCNA by ubiquitin and SUMO, Nature. 419 (2002) 135–141. https://doi.org/10.1038/nature00991.

[30] Z. Zhang, S. Zhang, S.H.S. Lin, X. Wang, L. Wu, E.Y.C. Lee, M.Y.W.T. Lee, Structure of monoubiquitinated PCNA, Cell Cycle. 11 (2012) 2128–2136. https://doi.org/10.4161/cc.20595.

[31] K. Haglund, S. Sigismund, S. Polo, I. Szymkiewicz, P.P.D. Fiore, I. Dikic, Multiple monoubiquitination of RTKs is sufficient for their endocytosis and degradation, Nat. Cell Biol. 5 (2003) 461–466. https://doi.org/10.1038/ncb983.

[32] J.N. Dynek, T. Goncharov, E.C. Dueber, A.V. Fedorova, A. Izrael-Tomasevic, L. Phu, E. Helgason, W.J. Fairbrother, K. Deshayes, D.S. Kirkpatrick, D. Vucic, c-IAP1 and UbcH5 promote K11-linked polyubiquitination of RIP1 in TNF signalling, EMBO J. 29 (2010) 4198–4209. https://doi.org/10.1038/emboj.2010.300.

[33] B. Gerlach, S.M. Cordier, A.C. Schmukle, C.H. Emmerich, E. Rieser, T.L. Haas, A.I. Webb, J.A. Rickard, H. Anderton, W.W.-L. Wong, U. Nachbur, L. Gangoda, U. Warnken, A.W. Purcell, J. Silke, H. Walczak, Linear ubiquitination prevents inflammation and regulates immune signalling, Nature. 471 (2011) 591–596. https://doi.org/10.1038/nature09816.

[34] J.M. Boname, M. Thomas, H.R. Stagg, P. Xu, J. Peng, P.J. Lehner, Efficient Internalization of MHC I Requires Lysine-11 and Lysine-63 Mixed Linkage Polyubiquitin Chains, Traffic. 11 (2010) 210–220. https://doi.org/10.1111/j.1600-0854.2009.01011.x.

[35] E. Goto, Y. Yamanaka, A. Ishikawa, M. Aoki-Kawasumi, M. Mito-Yoshida, M. Ohmura-Hoshino, Y. Matsuki, M. Kajikawa, H. Hirano, S. Ishido, Contribution of Lysine 11-linked Ubiquitination to MIR2-mediated Major Histocompatibility Complex Class I Internalization*, J. Biol. Chem. 285 (2010) 35311–35319. https://doi.org/10.1074/jbc.m110.112763.

[36] N.A. Snyder, G.M. Silva, Deubiquitinating enzymes (DUBs): Regulation, homeostasis, and oxidative stress response, J. Biol. Chem. 297 (2021) 101077. https://doi.org/10.1016/j.jbc.2021.101077.

[37] Y. Li, D. Reverter, Molecular Mechanisms of DUBs Regulation in Signaling and Disease, Int. J. Mol. Sci. 22 (2021) 986. https://doi.org/10.3390/ijms22030986.

[38] J.C. Martinez, V.V. Filimonov, P.L. Mateo, G. Schreiber, A.R. Fersht, A Calorimetric Study of the Thermal Stability of Barstar and Its Interaction with Barnase, Biochemistry. 34 (1995) 5224–5233. https://doi.org/10.1021/bi00015a036.

[39] S. Huang, S. Murphy, A. Matouschek, Effect of the protein import machinery at the mitochondrial surface on precursor stability, Proc. Natl. Acad. Sci. 97 (2000) 12991–12996. https://doi.org/10.1073/pnas.230243097.

[40] M. Eilers, G. Schatz, Binding of a specific ligand inhibits import of a purified precursor protein into mitochondria, Nature. 322 (1986) 228–232. https://doi.org/10.1038/322228a0.

[41] S. Huang, K.S. Ratliff, M.P. Schwartz, J.M. Spenner, A. Matouschek, Mitochondria unfold precursor proteins by unraveling them from their N-termini, Nat. Struct. Biol. 6 (1999) 1132–1138. https://doi.org/10.1038/70073.

[42] S. Prakash, L. Tian, K.S. Ratliff, R.E. Lehotzky, A. Matouschek, An unstructured initiation site is required for efficient proteasome-mediated degradation, Nat. Struct. Mol. Biol. 11 (2004) 830–837. https://doi.org/10.1038/nsmb814.

[43] R. van der Lee, B. Lang, K. Kruse, J. Gsponer, N. Sánchez de Groot, M.A. Huynen, A. Matouschek, M. Fuxreiter, M.M. Babu, Intrinsically Disordered Segments Affect Protein Half-Life in the Cell and during Evolution, Cell Rep. 8 (2014) 1832–1844. https://doi.org/10.1016/j.celrep.2014.07.055.

[44] S.H. Lecker, A.L. Goldberg, W.E. Mitch, Protein Degradation by the Ubiquitin–Proteasome Pathway in Normal and Disease States, JASN. 17 (2006) 1807–1819. https://doi.org/10.1681/asn.2006010083.

[45] P. Venkatraman, R. Wetzel, M. Tanaka, N. Nukina, A.L. Goldberg, Eukaryotic Proteasomes Cannot Digest Polyglutamine Sequences and Release Them during Degradation of Polyglutamine-Containing Proteins, Mol. Cell. 14 (2004) 95–104. https://doi.org/10.1016/s1097-2765(04)00151-0.

[46] V. Bonet-Costa, L.C.-D. Pomatto, K.J.A. Davies, The Proteasome and Oxidative Stress in Alzheimer's Disease, Antioxid. Redox Signal. 25 (2016) 886–901. https://doi.org/10.1089/ars.2016.6802.

[47] A.F. Kisselev, T.N. Akopian, K.M. Woo, A.L. Goldberg, The Sizes of Peptides Generated from Protein by Mammalian 26 and 20 S Proteasomes IMPLICATIONS FOR UNDERSTANDING THE DEGRADATIVE MECHANISM AND ANTIGEN PRESENTATION*, J. Biol. Chem. 274 (1999) 3363–3371. https://doi.org/10.1074/jbc.274.6.3363.

[48] N. Shastri, S. Schwab, T. Serwold, PRODUCING NATURE'S GENE-CHIPS: The Generation of Peptides for Display by MHC Class I Molecules, Immunology. 20 (2002) 463–493. https://doi.org/10.1146/annurev.immunol.20.100301.064819.

[49] K.L. Rock, I.A. York, T. Saric, A.L. Goldberg, Protein degradation and the generation of MHC class I-presented peptides, Adv. Immunol. 80 (2002) 1–70. https://doi.org/10.1016/s0065-2776(02)80012-8.

[50] V.S. Lim, J.D. Kopple, Protein metabolism in patients with chronic renal failure: Role of uremia and dialysis, Kidney Int. 58 (2000) 1–10. https://doi.org/10.1046/j.1523-1755.2000.00135.x.

[51] J.L. Bailey, X. Wang, B.K. England, S.R. Price, X. Ding, W.E. Mitch, The acidosis of chronic renal failure activates muscle proteolysis in rats by augmenting transcription of genes encoding proteins of the ATP-dependent ubiquitin-proteasome pathway., J. Clin. Investig. 97 (1996) 1447–1453. https://doi.org/10.1172/jci118566.

[52] R.P. Bhole, P.R. Kute, R.V. Chikhale, C.G. Bonde, A. Pant, S.S. Gurav, Unlocking the potential of PROTACs: A comprehensive review of protein degradation strategies in

disease therapy, Bioorg. Chem. 139 (2023) 106720. https://doi.org/10.1016/j.bioorg.2023.106720.

[53] P. Wang, J. Zhou, Proteolysis Targeting Chimera (PROTAC): A Paradigm-Shifting Approach in Small Molecule Drug Discovery., Curr. Top. Med. Chem. 18 (2018) 1354–1356. https://doi.org/10.2174/1568026618666181010101922.

[54] S.J. Hughes, A. Ciulli, Molecular recognition of ternary complexes: a new dimension in the structure-guided design of chemical degraders, Essays Biochem. 61 (2017) 505–516. https://doi.org/10.1042/ebc20170041.

[55] Y. Leestemaker, H. Ovaa, Tools to investigate the ubiquitin proteasome system, Drug Discov. Today: Technol. 26 (2017) 25–31. https://doi.org/10.1016/j.ddtec.2017.11.006.

[56] K. Husnjak, S. Elsasser, N. Zhang, X. Chen, L. Randles, Y. Shi, K. Hofmann, K.J. Walters, D. Finley, I. Dikic, Proteasome subunit Rpn13 is a novel ubiquitin receptor, Nature. 453 (2008) 481–488. https://doi.org/10.1038/nature06926.

[57] Y. Shi, X. Chen, S. Elsasser, B.B. Stocks, G. Tian, B.-H. Lee, Y. Shi, N. Zhang, S.A.H. de Poot, F. Tuebing, S. Sun, J. Vannoy, S.G. Tarasov, J.R. Engen, D. Finley, K.J. Walters, Rpn1 provides adjacent receptor sites for substrate binding and deubiquitination by the proteasome., Science. 351 (2016) aad9421–aad9421. https://doi.org/10.1126/science.aad9421.

[58] P. Schreiner, X. Chen, K. Husnjak, L. Randles, N. Zhang, S. Elsasser, D. Finley, I. Dikic, K.J. Walters, M. Groll, Ubiquitin docking at the proteasome through a novel pleckstrin-homology domain interaction, Nature. 453 (2008) 548–552. https://doi.org/10.1038/nature06924.

[59] S. Elsasser, R.R. Gali, M. Schwickart, C.N. Larsen, D.S. Leggett, B. Müller, M.T. Feng, F. Tübing, G.A.G. Dittmar, D. Finley, Proteasome subunit Rpn1 binds ubiquitin-like protein domains, Nat Cell Biol. 4 (2002) 725–730. https://doi.org/10.1038/ncb845.

[60] B.L. Bertolaet, D.J. Clarke, M. Wolff, M.H. Watson, M. Henze, G. Divita, S.I. Reed, UBA domains of DNA damage-inducible proteins interact with ubiquitin., Nat. Struct. Biol. 8 (2001) 417–422. https://doi.org/10.1038/87575.

[61] J.S. Thrower, L. Hoffman, M. Rechsteiner, C.M. Pickart, Recognition of the polyubiquitin proteolytic signal, EMBO J. 19 (2000) 94–102. https://doi.org/10.1093/emboj/19.1.94.

[62] G.L. Grice, I.T. Lobb, M.P. Weekes, S.P. Gygi, R. Antrobus, J.A. Nathan, The Proteasome Distinguishes between Heterotypic and Homotypic Lysine-11-Linked Polyubiquitin Chains, Cell Rep. 12 (2015) 545–553. https://doi.org/10.1016/j.celrep.2015.06.061.

[63] F. Ohtake, H. Tsuchiya, Y. Saeki, K. Tanaka, K63 ubiquitylation triggers proteasomal degradation by seeding branched ubiquitin chains, Proc. Natl. Acad. Sci. 115 (2018) E1401–E1408. https://doi.org/10.1073/pnas.1716673115.

[64] C. Liu, W. Liu, Y. Ye, W. Li, Ufd2p synthesizes branched ubiquitin chains to promote the degradation of substrates modified with atypical chains, Nat. Commun. 8 (2017) 14274. https://doi.org/10.1038/ncomms14274.

[65] H.-J. Meyer, M. Rape, Enhanced Protein Degradation by Branched Ubiquitin Chains, Cell. 157 (2014) 910–921. https://doi.org/10.1016/j.cell.2014.03.037.

[66] S. Jantrapirom, L.L. Piccolo, M. Yamaguchi, Non-Proteasomal UbL-UbA Family of Proteins in Neurodegeneration, Int. J. Mol. Sci. 20 (2019) 1893. https://doi.org/10.3390/ijms20081893.

[67] H. Hiyama, M. Yokoi, C. Masutani, K. Sugasawa, T. Maekawa, K. Tanaka, J.H.J. Hoeijmakers, F. Hanaoka, Interaction of hHR23 with S5a THE UBIQUITIN-LIKE DOMAIN OF hHR23 MEDIATES INTERACTION WITH S5a SUBUNIT OF 26 S PROTEASOME*, J. Biol. Chem. 274 (1999) 28019–28025. https://doi.org/10.1074/jbc.274.39.28019.

[68] S. Elsasser, D. Chandler-Militello, B. Müller, J. Hanna, D. Finley, Rad23 and Rpn10 serve as alternative ubiquitin receptors for the proteasome., J. Biol. Chem. 279 (2004) 26817–26822. https://doi.org/10.1074/jbc.m404020200.

[69] G.A. Collins, A.L. Goldberg, Proteins containing ubiquitin-like (Ubl) domains not only bind to 26S proteasomes but also induce their activation, Proceedings of the National Academy of Sciences. 117 (2020) 4664–4674. https://doi.org/10.1073/pnas.1915534117.

[70] R.-Y. Liang, L. Chen, B.-T. Ko, Y.-H. Shen, Y.-T. Li, B.-R. Chen, K.-T. Lin, K. Madura, S.-M. Chuang, Rad23 Interaction with the Proteasome Is Regulated by Phosphorylation of Its Ubiquitin-Like (UbL) Domain, J Mol Biol. 426 (2014) 4049–4060. https://doi.org/10.1016/j.jmb.2014.10.004.

[71] L. Chen, K. Madura, Rad23 Promotes the Targeting of Proteolytic Substrates to the Proteasome, Mol. Cell. Biol. 22 (2002) 4902–4913. https://doi.org/10.1128/mcb.22.13.4902-4913.2002.

[72] B. Medicherla, Z. Kostova, A. Schaefer, D.H. Wolf, A genomic screen identifies Dsk2p and Rad23p as essential components of ER-associated degradation, EMBO Rep. 5 (2004) 692–697. https://doi.org/10.1038/sj.embor.7400164.

[73] Y. Murakami, S. Matsufuji, T. Kameji, S. Hayashi, K. Igarashi, T. Tamura, K. Tanaka, A. Ichihara, Ornithine decarboxylase is degraded by the 26S proteasome without ubiquitination, Nature. 360 (1992) 597–599. https://doi.org/10.1038/360597a0.

[74] H.-Y. Wu, S.-F. Chen, J.-Y. Hsieh, F. Chou, Y.-H. Wang, W.-T. Lin, P.-Y. Lee, Y.-J. Yu, L.-Y. Lin, T.-S. Lin, C.-L. Lin, G.-Y. Liu, S.-R. Tzeng, H.-C. Hung, N.-L. Chan, Structural basis of antizyme-mediated regulation of polyamine homeostasis, Proc. Natl. Acad. Sci. 112 (2015) 11229–11234. https://doi.org/10.1073/pnas.1508187112.

[75] M. Zhang, C.M. Pickart, P. Coffino, Determinants of proteasome recognition of ornithine decarboxylase, a ubiquitin-independent substrate, EMBO J. 22 (2003) 1488–1496. https://doi.org/10.1093/emboj/cdg158.

[76] M. Zhang, A.I. MacDonald, M.A. Hoyt, P. Coffino, Proteasomes Begin Ornithine Decarboxylase Digestion at the C Terminus*, J. Biol. Chem. 279 (2004) 20959–20965. https://doi.org/10.1074/jbc.m314043200.

[77] J. Takeuchi, H. Chen, P. Coffino, Proteasome substrate degradation requires association plus extended peptide, EMBO J. 26 (2007) 123–131. https://doi.org/10.1038/sj.emboj.7601476.

[78] G. Mannhaupt, R. Schnall, V. Karpov, I. Vetter, H. Feldmann, Rpn4p acts as a transcription factor by binding to PACE, a nonamer box found upstream of 26S proteasomal and other genes in yeast, FEBS Lett. 450 (1999) 27–34. https://doi.org/10.1016/s0014-5793(99)00467-6.

[79] Y. Xie, A. Varshavsky, RPN4 is a ligand, substrate, and transcriptional regulator of the 26S proteasome: A negative feedback circuit, Proc. Natl. Acad. Sci. 98 (2001) 3056–3061. https://doi.org/10.1073/pnas.071022298.

[80] D. Ju, Y. Xie, Identification of the Preferential Ubiquitination Site and Ubiquitin-dependent Degradation Signal of Rpn4*, J. Biol. Chem. 281 (2006) 10657–10662. https://doi.org/10.1074/jbc.m513790200.

[81] D. Ju, Y. Xie, Proteasomal Degradation of RPN4 via Two Distinct Mechanisms, Ubiquitin-dependent and -independent*, J. Biol. Chem. 279 (2004) 23851–23854. https://doi.org/10.1074/jbc.c400111200.

[82] J. Erales, P. Coffino, Ubiquitin-independent proteasomal degradation, Biochim. Biophys. Acta (BBA) - Mol. Cell Res. 1843 (2014) 216–221. https://doi.org/10.1016/j.bbamcr.2013.05.008.

[83] J.A.M. Bard, E.A. Goodall, E.R. Greene, E. Jonsson, K.C. Dong, A. Martin, Structure and Function of the 26S Proteasome., Annu. Rev. Biochem. 87 (2018) 697–724. https://doi.org/10.1146/annurev-biochem-062917-011931.

[84] H. Yu, A. Matouschek, Recognition of Client Proteins by the Proteasome., Annu Rev Biophys. 46 (2017) 149–173. https://doi.org/10.1146/annurev-biophys-070816-033719.

[85] B. Dahlmann, Role of proteasomes in disease, BMC Biochem. 8 (2007) S3-12. https://doi.org/10.1186/1471-2091-8-s1-s3.

[86] A. Varshavsky, The N-end rule pathway and regulation by proteolysis, Protein Sci. 20 (2011) 1298–1345. https://doi.org/10.1002/pro.666.

[87] V. Chau, J.W. Tobias, A. Bachmair, D. Marriott, D.J. Ecker, D.K. Gonda, A. Varshavsky, A Multiubiquitin Chain Is Confined to Specific Lysine in a Targeted Short-Lived Protein, Science. 243 (1989) 1576–1583. https://doi.org/10.1126/science.2538923.

[88] A. Bachmair, D. Finley, A. Varshavsky, In Vivo Half-Life of a Protein is a Function of its Amino-Terminal Residue, Science. 234 (1986) 179–186. https://doi.org/10.1126/science.3018930.

[89] R.S. McIsaac, B.L. Oakes, X. Wang, K.A. Dummit, D. Botstein, M.B. Noyes, Synthetic gene expression perturbation systems with rapid, tunable, single-gene specificity in yeast, Nucleic Acids Res. 41 (2013) e57–e57. https://doi.org/10.1093/nar/gks1313.

[90] K.A. Johnson, Chapter 23 Fitting Enzyme Kinetic Data with KinTek Global Kinetic Explorer, Methods Enzym. 467 (2009) 601–626. https://doi.org/10.1016/s0076-6879(09)67023-3.

[91] K.A. Johnson, Z.B. Simpson, T. Blom, Global Kinetic Explorer: A new computer program for dynamic simulation and fitting of kinetic data, Anal. Biochem. 387 (2009) 20–29. https://doi.org/10.1016/j.ab.2008.12.024.

[92] K.A. Johnson, Z.B. Simpson, T. Blom, FitSpace Explorer: An algorithm to evaluate multidimensional parameter space in fitting kinetic data, Anal. Biochem. 387 (2009) 30–41. https://doi.org/10.1016/j.ab.2008.12.025.

[93] J.J. Work, O. Brandman, Quantitative analysis of the ubiquitin-proteasome system under proteolytic and folding stressors, BioRxiv. (2019) 780676. https://doi.org/10.1101/780676.

[94] Y. Lu, B. Lee, R.W. King, D. Finley, M.W. Kirschner, Substrate degradation by the proteasome: A single-molecule kinetic analysis, Science. 348 (2015) 1250834. https://doi.org/10.1126/science.1250834.

[95] S. Fishbain, S. Prakash, A. Herrig, S. Elsasser, A. Matouschek, Rad23 escapes degradation because it lacks a proteasome initiation region, Nat. Commun. 2 (2011) 192–192. https://doi.org/10.1038/ncomms1194.

[96] S. Lokireddy, N.V. Kukushkin, A.L. Goldberg, cAMP-induced phosphorylation of 26S proteasomes on Rpn6/PSMD11 enhances their activity and the degradation of misfolded proteins, Proc. Natl. Acad. Sci. 112 (2015) E7176–E7185. https://doi.org/10.1073/pnas.1522332112.

[97] E. Schwob, T. Böhm, M.D. Mendenhall, K. Nasmyth, The B-type cyclin kinase inhibitor p40SIC1 controls the G1 to S transition in S. cerevisiae, Cell. 79 (1994) 233–244. https://doi.org/10.1016/0092-8674(94)90193-7.

[98] R. Verma, R. Oania, J. Graumann, R.J. Deshaies, Multiubiquitin Chain Receptors Define a Layer of Substrate Selectivity in the Ubiquitin-Proteasome System, Cell. 118 (2004) 99–110. https://doi.org/10.1016/j.cell.2004.06.014.

[99] H. Tsuchiya, F. Ohtake, N. Arai, A. Kaiho, S.Y.M. cell, 2017, In vivo ubiquitin linkage-type analysis reveals that the Cdc48-Rad23/Dsk2 axis contributes to K48-linked chain specificity of the proteasome, Elsevier. (n.d.). https://doi.org/10.1016/j.molcel.2017.04.024.

[100] R. Verma, R. Oania, R. Fang, G.T. Smith, R.J. Deshaies, Cdc48/p97 Mediates UV-Dependent Turnover of RNA Pol II, Mol. Cell. 41 (2011) 82–92. https://doi.org/10.1016/j.molcel.2010.12.017.

[101] R. Higgins, M.-H. Kabbaj, D. Sherwin, L.A. Howell, A. Hatcher, R.J. Tomko, Y. Wang, The Cdc48 Complex Alleviates the Cytotoxicity of Misfolded Proteins by Regulating Ubiquitin Homeostasis, Cell Rep. 32 (2020) 107898. https://doi.org/10.1016/j.celrep.2020.107898.

[102] D. Finley, X. Chen, K.J. Walters, Gates, Channels, and Switches: Elements of the Proteasome Machine, Trends Biochem. Sci. 41 (2016) 77–93. https://doi.org/10.1016/j.tibs.2015.10.009.

[103] F. Ohtake, H. Tsuchiya, The emerging complexity of ubiquitin architecture, J. Biochem. 161 (2017) 125–133. https://doi.org/10.1093/jb/mvw088.

[104] S. Prakash, A. Matouschek, Protein unfolding in the cell., Trends Biochem. Sci. 29 (2004) 593–600. https://doi.org/10.1016/j.tibs.2004.09.011.

[105] M. Schmidt, J. Hanna, S. Elsasser, D. Finley, Proteasome-associated proteins: regulation of a proteolytic machine, Biol. Chem. 386 (2005) 725–737. https://doi.org/10.1515/bc.2005.085.

[106] S. Elsasser, D. Finley, Delivery of ubiquitinated substrates to protein-unfolding machines, Nat. Cell Biol. 7 (2005) 742–749. https://doi.org/10.1038/ncb0805-742.

[107] A.M. Whiteley, M.A. Prado, S.A.H. de Poot, J.A. Paulo, M. Ashton, S. Dominguez, M. Weber, H. Ngu, J. Szpyt, M.P. Jedrychowski, A. Easton, S.P. Gygi, T. Kurz, M.J. Monteiro, E.J. Brown, D. Finley, Global proteomics of Ubqln2-based murine models of ALS, J. Biol. Chem. 296 (2021) 100153. https://doi.org/10.1074/jbc.ra120.015960.

[108] A.M. Whiteley, M.A. Prado, I. Peng, A.R. Abbas, B. Haley, J.A. Paulo, M. Reichelt, A. Katakam, M. Sagolla, Z. Modrusan, D.Y. Lee, M. Roose-Girma, D.S. Kirkpatrick, B.S. McKenzie, S.P. Gygi, D. Finley, E.J. Brown, Ubiquilin1 promotes antigen-receptor mediated proliferation by eliminating mislocalized mitochondrial proteins, ELife. 6 (2017) e26435. https://doi.org/10.7554/elife.26435.

[109] Q. Deveraux, V. Ustrell, C. Pickart, M. Rechsteiner, A 26 S protease subunit that binds ubiquitin conjugates., J. Biol. Chem. 269 (1994) 7059–7061. https://doi.org/10.1016/s0021-9258(17)37244-7.

[110] E. Sakata, S. Bohn, O. Mihalache, P. Kiss, F. Beck, I. Nagy, S. Nickell, K. Tanaka, Y. Saeki, F. Förster, W. Baumeister, Localization of the proteasomal ubiquitin receptors Rpn10 and Rpn13 by electron cryomicroscopy, Proc. Natl. Acad. Sci. 109 (2012) 1479–1484. https://doi.org/10.1073/pnas.1119394109.

[111] C.R.M. Wilkinson, M. Seeger, R. Hartmann-Petersen, M. Stone, M. Wallace, C. Semple, C. Gordon, Proteins containing the UBA domain are able to bind to multi-ubiquitin chains, Nat. Cell Biol. 3 (2001) 939–943. https://doi.org/10.1038/ncb1001-939.

[112] L. Chen, U. Shinde, T.G. Ortolan, K. Madura, Ubiquitin-associated (UBA) domains in Rad23 bind ubiquitin and promote inhibition of multi-ubiquitin chain assembly, EMBO Rep. 2 (2001) 933–938. https://doi.org/10.1093/embo-reports/kve203.

[113] H. Rao, A. Sastry, Recognition of Specific Ubiquitin Conjugates Is Important for the Proteolytic Functions of the Ubiquitin-associated Domain Proteins Dsk2 and Rad23*, J. Biol. Chem. 277 (2002) 11691–11695. https://doi.org/10.1074/jbc.m200245200.

[114] S. Raasi, I. Orlov, K.G. Fleming, C.M. Pickart, Binding of Polyubiquitin Chains to Ubiquitin-associated (UBA) Domains of HHR23A, J. Mol. Biol. 341 (2004) 1367–1379. https://doi.org/10.1016/j.jmb.2004.06.057.

[115] K. Zientara-Rytter, S. Subramani, The Roles of Ubiquitin-Binding Protein Shuttles in the Degradative Fate of Ubiquitinated Proteins in the Ubiquitin-Proteasome System and Autophagy, Cells. 8 (2019) 40. https://doi.org/10.3390/cells8010040.

[116] H. Takeuchi, S. Jin, J. Wang, G. Zhang, J. Kawanokuchi, R. Kuno, Y. Sonobe, T. Mizuno, A. Suzumura, Tumor necrosis factor-alpha induces neurotoxicity via glutamate release from hemichannels of activated microglia in an autocrine manner., J Biological Chem. 281 (2006) 21362–21368. https://doi.org/10.1074/jbc.m600504200.

[117] T. Inobe, S. Fishbain, S. Prakash, A. Matouschek, Defining the geometry of the two-component proteasome degron, Nat. Chem. Biol. 7 (2011) 161–167. https://doi.org/10.1038/nchembio.521.

[118] H. Yu, G. Kago, C.M. Yellman, A. Matouschek, Ubiquitin-like domains can target to the proteasome but proteolysis requires a disordered region, Embo J. 35 (2016) 1522–1536. https://doi.org/10.15252/embj.201593147.

[119] S. Sivaramakrishnan, B.J. Spink, A.Y.L. Sim, S. Doniach, J.A. Spudich, Dynamic charge interactions create surprising rigidity in the ER/K α-helical protein motif, Proc. Natl. Acad. Sci. 105 (2008) 13356–13361. https://doi.org/10.1073/pnas.0806256105.

[120] G.C. Lander, E. Estrin, M.E. Matyskiela, C. Bashore, E. Nogales, A. Martin, Complete subunit architecture of the proteasome regulatory particle, Nature. 482 (2012) 186–191. https://doi.org/10.1038/nature10774.

[121] K. Lasker, F. Förster, S. Bohn, T. Walzthoeni, E. Villa, P. Unverdorben, F. Beck, R. Aebersold, A. Sali, W. Baumeister, Molecular architecture of the 26S proteasome holocomplex determined by an integrative approach, Proc. Natl. Acad. Sci. 109 (2012) 1380–1387. https://doi.org/10.1073/pnas.1120559109.

[122] F. Beck, P. Unverdorben, S. Bohn, A. Schweitzer, G. Pfeifer, E. Sakata, S. Nickell, J.M. Plitzko, E. Villa, W. Baumeister, F. Forster, Near-atomic resolution structural model of the yeast 26S proteasome, (2012). https://doi.org/10.2210/pdb4b4t/pdb.

[123] P. Unverdorben, F. Beck, P. Śledź, A. Schweitzer, G. Pfeifer, J.M. Plitzko, W. Baumeister, F. Förster, Deep classification of a large cryo-EM dataset defines the conformational landscape of the 26S proteasome, Proc. Natl. Acad. Sci. 111 (2014) 5544–5549. https://doi.org/10.1073/pnas.1403409111.

[124] K. Paraskevopoulos, F. Kriegenburg, M.H. Tatham, H.I. Rösner, B. Medina, I.B. Larsen, R. Brandstrup, K.G. Hardwick, R.T. Hay, B.B. Kragelund, R. Hartmann-Petersen, C. Gordon, Dss1 Is a 26S Proteasome Ubiquitin Receptor, Mol. Cell. 56 (2014) 453–461. https://doi.org/10.1016/j.molcel.2014.09.008.

[125] Y.A. Lam, T.G. Lawson, M. Velayutham, J.L. Zweier, C.M. Pickart, A proteasomal ATPase subunit recognizes the polyubiquitin degradation signal, Nature. 416 (2002) 763–767. https://doi.org/10.1038/416763a.

[126] A.J. Boughton, L. Liu, T. Lavy, O. Kleifeld, D. Fushman, A novel recognition site for polyubiquitin and ubiquitin-like signals in an unexpected region of proteasomal subunit Rpn1, J. Biol. Chem. 297 (2021) 101052. https://doi.org/10.1016/j.jbc.2021.101052.

[127] T. Tomita, J.M. Huibregtse, A. Matouschek, A masked initiation region in retinoblastoma protein regulates its proteasomal degradation, Nature Communications. (2020) 1–8. https://doi.org/10.1038/s41467-020-16003-3.

[128] T.A. Groothuis, N.P. Dantuma, J. Neefjes, F.A. Salomons, Ubiquitin crosstalk connecting cellular processes, Cell Div. 1 (2006) 21–21. https://doi.org/10.1186/1747-1028-1-21.

[129] Y. Lee, D.H. Thompson, Stimuli-responsive liposomes for drug delivery, Wiley Interdiscip Rev Nanomed Nanobiotechnology. 9 (2017). https://doi.org/10.1002/wnan.1450.

[130] J.C. Christianson, Y. Ye, Cleaning up in the endoplasmic reticulum: ubiquitin in charge, Nat Struct Mol Biol. 21 (2014) 325–335. https://doi.org/10.1038/nsmb.2793.

[131] S. Elsasser, M. Schmidt, D. Finley, Characterization of the Proteasome Using Native Gel Electrophoresis, Methods Enzymol. 398 (2005) 353–363. https://doi.org/10.1016/s0076-6879(05)98029-4.

[132] Y. Saeki, A. Saitoh, A. Toh-e, H. Yokosawa, Ubiquitin-like proteins and Rpn10 play cooperative roles in ubiquitin-dependent proteolysis, Biochem Bioph Res Co. 293 (2002) 986–992. https://doi.org/10.1016/s0006-291x(02)00340-6.

[133] V. Su, A. Lau, Ubiquitin-like and ubiquitin-associated domain proteins: significance in proteasomal degradation, Cell. Mol. Life Sci. (2009) 2819–2833. https://doi.org/10.1007/s00018-009-0048-9.

[134] N.P. Dantuma, C. Heinen, D. Hoogstraten, The ubiquitin receptor Rad23: At the crossroads of nucleotide excision repair and proteasomal degradation, DNA Repair. 8 (2009) 449–460. https://doi.org/10.1016/j.dnarep.2009.01.005.

[135] M.M. Olszewski, C. Williams, K.C. Dong, A. Martin, The Cdc48 unfoldase prepares well-folded protein substrates for degradation by the 26S proteasome, Communications Biology. (2019) 1–8. https://doi.org/10.1038/s42003-019-0283-z.

[136] Z. Ji, H. Li, D. Peterle, J.A. Paulo, S.B. Ficarro, T.E. Wales, J.A. Marto, S.P. Gygi, J.R. Engen, T.A. Rapoport, Translocation of polyubiquitinated protein substrates by the hexameric Cdc48 ATPase, Mol. Cell. 82 (2022) 570-584.e8. https://doi.org/10.1016/j.molcel.2021.11.033.

[137] N.O. Bodnar, K.H. Kim, Z. Ji, T.E. Wales, V. Svetlov, E. Nudler, J.R. Engen, T. Walz, T.A. Rapoport, Structure of the Cdc48 ATPase with its ubiquitin-binding cofactor Ufd1-Npl4, Nat Struct Mol Biol. 25 (2018) 616–622. https://doi.org/10.1038/s41594-018-0085-x.

[138] E. Okeke, L. Chen, K. Madura, The Cellular Location of Rad23, a Polyubiquitin Chain-Binding Protein, Plays a Key Role in Its Interaction with Substrates of the Proteasome, J. Mol. Biology. 432 (2020) 2388–2404. https://doi.org/10.1016/j.jmb.2020.03.001.

[139] K.A. Donovan, F.M. Ferguson, J.W. Bushman, N.A. Eleuteri, D. Bhunia, S. Ryu, L. Tan, K. Shi, H. Yue, X. Liu, D. Dobrovolsky, B. Jiang, J. Wang, M. Hao, I. You, M. Teng, Y. Liang, J. Hatcher, Z. Li, T.D. Manz, B. Groendyke, W. Hu, Y. Nam, S. Sengupta, H. Cho, I. Shin, M.P. Agius, I.M. Ghobrial, M.W. Ma, J. Che, S.J. Buhrlage, T. Sim, N.S. Gray, E.S. Fischer, Mapping the Degradable Kinome Provides a Resource for Expedited Degrader Development, Cell. 183 (2020) 1714-1731.e10. https://doi.org/10.1016/j.cell.2020.10.038.

[140] M.C. Silva, F.M. Ferguson, Q. Cai, K.A. Donovan, G. Nandi, D. Patnaik, T. Zhang, H.-T. Huang, D.E. Lucente, B.C. Dickerson, T.J. Mitchison, E.S. Fischer, N.S. Gray, S.J. Haggarty, Targeted degradation of aberrant tau in frontotemporal dementia patient-derived neuronal cell models, Elife. 8 (2019) e45457. https://doi.org/10.7554/elife.45457.

[141] A.P. Russ, S. Lampel, The druggable genome: an update, Drug Discov Today. 10 (2005) 1607–1610. https://doi.org/10.1016/s1359-6446(05)03666-4.

[142] X. Sun, H. Gao, Y. Yang, M. He, Y. Wu, Y. Song, Y. Tong, Y. Rao, PROTACs: great opportunities for academia and industry, Signal Transduct. Target. Ther. 4 (2019) 64. https://doi.org/10.1038/s41392-019-0101-6.

[143] K.M. Sakamoto, K.B. Kim, A. Kumagai, F. Mercurio, C.M. Crews, R.J. Deshaies, Protacs: Chimeric molecules that target proteins to the Skp1–Cullin–F box complex for ubiquitination and degradation, Proc. Natl. Acad. Sci. 98 (2001) 8554–8559. https://doi.org/10.1073/pnas.141230798.

[144] D.P. Bondeson, B.E. Smith, G.M. Burslem, A.D. Buhimschi, J. Hines, S. Jaime-Figueroa, J. Wang, B.D. Hamman, A. Ishchenko, C.M. Crews, Lessons in PROTAC Design from Selective Degradation with a Promiscuous Warhead, Cell Chem Biol. 25 (2018) 78-87.e5. https://doi.org/10.1016/j.chembiol.2017.09.010.

[145] C.M. Pickart, S. Raasi, Controlled Synthesis of Polyubiquitin Chains, Methods Enzym. 399 (2005) 21–36. https://doi.org/10.1016/s0076-6879(05)99002-2.

[146] A.F. Carvalho, M.P. Pinto, C.P. Grou, R. Vitorino, P. Domingues, F. Yamao, C. Sá-Miranda, J.E. Azevedo, High-Yield Expression in Escherichia coli and Purification of Mouse Ubiquitin-Activating Enzyme E1, Mol. Biotechnol. 51 (2012) 254–261. https://doi.org/10.1007/s12033-011-9463-x.

[147] J.R. Cannon, K. Martinez-Fonts, S.A. Robotham, A. Matouschek, J.S. Brodbelt, Top-Down 193-nm Ultraviolet Photodissociation Mass Spectrometry for Simultaneous Determination of Polyubiquitin Chain Length and Topology, Anal. Chem. 87 (2015) 1812–1820. https://doi.org/10.1021/ac5038363.

[148] T. Sone, Y. Saeki, A. Toh-e, H. Yokosawa, Sem1p Is a Novel Subunit of the 26 S Proteasome from Saccharomyces cerevisiae, J. Biol. Chem. 279 (2004) 28807–28816. https://doi.org/10.1074/jbc.m403165200.

[149] D. Finley, E. Özkaynak, A. Varshavsky, The yeast polyubiquitin gene is essential for resistance to high temperatures, starvation, and other stresses, Cell. 48 (1987) 1035–1046. https://doi.org/10.1016/0092-8674(87)90711-2.

[150] G. Giaever, C.N. Genetics, 2014, The yeast deletion collection: a decade of functional genomics, Academic.Oup.Com. (n.d.). https://doi.org/10.1534/genetics.114.161620.

[151] J. Jumper, R. Evans, A. Pritzel, T. Green, M. Figurnov, O. Ronneberger, K. Tunyasuvunakool, R. Bates, A. Žídek, A. Potapenko, A. Bridgland, C. Meyer, S.A.A. Kohl, A.J. Ballard, A. Cowie, B. Romera-Paredes, S. Nikolov, R. Jain, J. Adler, T. Back, S. Petersen, D. Reiman, E. Clancy, M. Zielinski, M. Steinegger, M. Pacholska, T.

Berghammer, S. Bodenstein, D. Silver, O. Vinyals, A.W. Senior, K. Kavukcuoglu, P. Kohli, D. Hassabis, Highly accurate protein structure prediction with AlphaFold, Nature. 596 (2021) 583–589. https://doi.org/10.1038/s41586-021-03819-2.

Vita

Logan Spaller was born in Wilmington, North Carolina. He received a B.S. in Chemistry from the University of North Carolina at Chapel Hill in 2017. He receive his Ph.D. in Biochmistry from the University of Texas at Austin in 2023.

Permanent email: lspaller@utexas.edu

This dissertation was typed by Logan Spaller.